UNIVERSITÀ
DEGLI STUDI
DI TRIESTE

UNIVERSITÀ DEGLI STUDI DI TRIESTE

XXXIV CICLO DEL DOTTORATO DI RICERCA IN

Earth Science, Fluid-Dynamic and Mathematics. Interactions and Methods

Cultural Affairs and Missions Sector, Egyptian Ministry of Higher Education & Scientific Research

Investigation of groundwater occurrences and potential sources for groundwater pollution by joint application of geophysical and hydrochemical approaches: a case study of some urban cities at West Ismailia, Egypt

Disciplinary Sector: GEO/11 Applied Geophysics

Ph.D. student

HEBA MOHAMED MOHAMED IBRAHIM ELKOSIRI

Ph.D. program Coordinator

PROF. STEFANO MASET

Thesis Supervisor

PROF. EMANUELE FORTE

Thesis Co-supervisor

PROF. USAMA SAAD MASSOUD

ACADEMIC YEAR 2021/2022

ACKNOWLEDGEMENT

Abstract

Egypt is known to be one of the countries suffering from water poverty due to its limited share of the River Nile and the unmanaged liquid and solid waste disposal in the river, affecting its water quality. Despite the excreted efforts by the government to solve this problem, many parts of the country still suffer from clean water resources. This study chose the area west of Ismailia city due to its relevant socio-economic importance and the hydrogeological challenges it faces. This area's primary water source is the groundwater due to a lack of clean surface water resources. So, this study aims to characterize the principal groundwater aquifers in the investigated area by applying integrated geophysical techniques, including Vertical Electrical Sounding (VES) and Time Domain Electromagnetic (TEM). In addition, we Study the reasons for the water logging problem that threatens all the agricultural activities in the study area by applying Electrical Resistivity Tomography (ERT) near some lakes resulting from this waterlogging. Our final aim is to investigate the possible sources of contamination and deterioration in water quality by hydrochemical analysis.

In this concern, 35 VES and TEM data point stations were applied along five parallel profiles trending N-S through the study area. The VES and TEM data points were acquired nearly at the same sites to be suitable for joint inversion. VES data were collected by SYSCAL R2 instrument using Schlumberger array while the TEM data were collected by SIROTEM MK3 using the standard square single loop with 100 m length side. Then VES data was inverted by IPI2WIN 1-D while TEMIX XL4 inverted the TEM data. The Curupira program performed the joint inversion between both two methods.

In order to achieve our second purpose regarding the water logging problem, 11 ERT profiles were conducted through the study area, where 11 profiles were applied around one of the biggest lakes that resulted from this problem. In contrast, the last profile was applied far away from these lakes to compare the behaviour of ERT in both of them. The data was collected by the SYSCAL R2 instrument and then inverted using the RES2DINV program.

Hydrochemical analyses were applied to 15 water samples collected from some of the available water wells in the study area to study groundwater quality. These

samples were collected along two profiles directing N-S. The analyses were made in the "Central Laboratories of the National Water Research Centre (NWRC)".

From the VES and TEM data processing and interpretation, two aquifer systems were identified in the area, Pleistocene and Miocene aquifers; where the Pleistocene aquifer is the principal aquifer in the study area consisting of successive layers of gravel and sand and sand with many clay lenses of fluviatile origin. The upper surface of the Pleistocene aquifer could be detected at depths from 10 to 83 m below the ground surface, with a total thickness ranging from 129 m to 273 m. Its resistivity ranges between 4 to 95 Ωm. It is lying uncomfortably on the Miocene aquifer. Due to the subsurface structural complexity, a possible lateral seepage of saline water can occur from the Miocene aquifer into the Pleistocene one. The Miocene aquifer lies at depths ranging from 130 to 328 m below the ground surface. It is mainly composed of marine marly sandstone and limestone, showing relatively low resistivity values ranging from 6 to 22 Ωm. The groundwater within this aquifer is mainly saline.

From ERT data inversion and interpretation, three geoelectrical units were revealed. The middle unit, mainly composed of evaporitic loamy sand, is responsible for the water logging problem that threatens the study area.

The detailed hydrochemical analysis revealed that trace and heavy metals are present in deficient concentrations in all samples collected from the study area and have no effect on groundwater quality. About 75% of the collected samples are characterized by high TDS (>3000), thus exceeding the allowed limits approved by WHO and local authorities, except for the samples collected from Wadi El-Tumilat. As a result of this high salinity, this water is not suitable for drinking or domestic use.

Table of Contents

List of Figures

List of Tables

Chapter (1)

1.1. Preface

Sustainable development for any area of interest is mainly based on many factors and variables, from which the water resources are ones of the most important. Therefore, to design and establish new urban and agricultural developments or to extend existing development plans of urban areas, the first step to take into consideration is the provision of usable water resources.

River Nile is the main source of water in Egypt and it is the life artery that provides necessary water for most parts of the country. However, in the last few years, the demand for water in Egypt has increased by a quick rate due to the significant increase in Egypt's population and country aspirations to augment the food through advanced technology-based reclamation.

It is clear that Egypt is suffering from lack in its water resources due to two main reasons. First, its water share of the River Nile is limited, controlled by international agreements, and may be reduced in the future due to developments along the Nile River roots until the southern Egyptian borders with Sudan (e.g. dams, building new cities, agricultural projects). Second, the River Nile is subjected to violations and contamination due to unmanaged liquid and solid waste disposal in the river itself, which in turn affects the water quality and makes the purification process harder and more expensive. As a result, the Egyptian government followed the policy of constructing many water plants in the cities or parts suffering from shortage in water resources in order to provide them with the water needed for various uses (e.g. drinking, domestic, industrial and agricultural).

Despite all of the exerted efforts, there are many regions around the country that are still suffering from shortage in clean water resources due to decreasing in the

efficiency of water networks to support the over increasing demands, which leads to repeated cutoff in the water for many times per day. So, there is an urgent need to look for supplementary renewable fresh water resources (e.g. groundwater, desalinated seawater) to be used as supplementary means for water supplies.

1.2. Study Area

In this study, the area west to Ismailia city was chosen due to its relevant socio-economic importance and the hydrogeological challenges it faces. The study area is located between lat. 30° 21' 36" and 30° 37' 12" and long. 31° 58' 48" and 32° 6' 0" as shown in figure (1.1). It is bordered from the south by Cairo-Ismailia desert road, El-Salhiya city from the north, El-Salhiya Road from west and Ismailia city from east. Ismailia is considered one of the most important governorates in Egypt as it is the east gate for Egypt to Asia Continent and Arab countries. It is specified by the special geographical location as Suez Canal is managed from it, the great civilized and political history in addition to its high economic importance. This is due to its fish wealth and tourism in addition to the high-quality agricultural exports. All of these factors make Ismailia one of the most attractive governorates for local and international investments in different fields either industrial or agricultural. This returns to many reasons from which the most important is its good groundwater resources and soil potentialities to grow various crops. This in turn, leaded Ismailia to be in the first level for exporting fruits and vegetables which are highly demanded by name.

However, further developments in this vital part are somehow threatened by shortage in clean surface water supplies and depends mainly on groundwater resources. Also, this area is facing two main environmental challenges. At first, groundwater is subjected to contamination and deterioration in its quality due to

leakage from the poorly developed sewage system of the villages or excessive use of fertilizers. The second problem is water logging that constitutes the major threat for the green economy of this very productive area as shown in figure (1.2).

1.3. Objectives of the Study

The main objectives of our study are:

- Identification and characterization of groundwater aquifers in the area of interest, which will be achieved by integrated geophysical methods including Vertical Electrical Sounding (VES), Electrical Resistivity Tomography (ERT) and Time Domain Electromagnetic (TEM).

- Investigate the possible sources of contamination and deterioration in water quality by hydrochemical analysis for some water samples collected from the available water wells in the study area. By this step we can check the validity of groundwater for drinking and other uses.

- Study the reasons for the water logging problem by applying ERT near some lakes resulted from previous water logging.

- Based on the results of fore-mentioned approaches we were able to describe the present situation of groundwater aquifers, to identify the proper locations for drilling new water wells, and to assess the suitability of groundwater for drinking and other purposes.

- Finally, we can implement a Geographic Information System (GIS) database that incorporates all results and information obtained from this study that may boost the sustainable development plans of the considered cities and is a relevant outcome for monitoring and future studies.
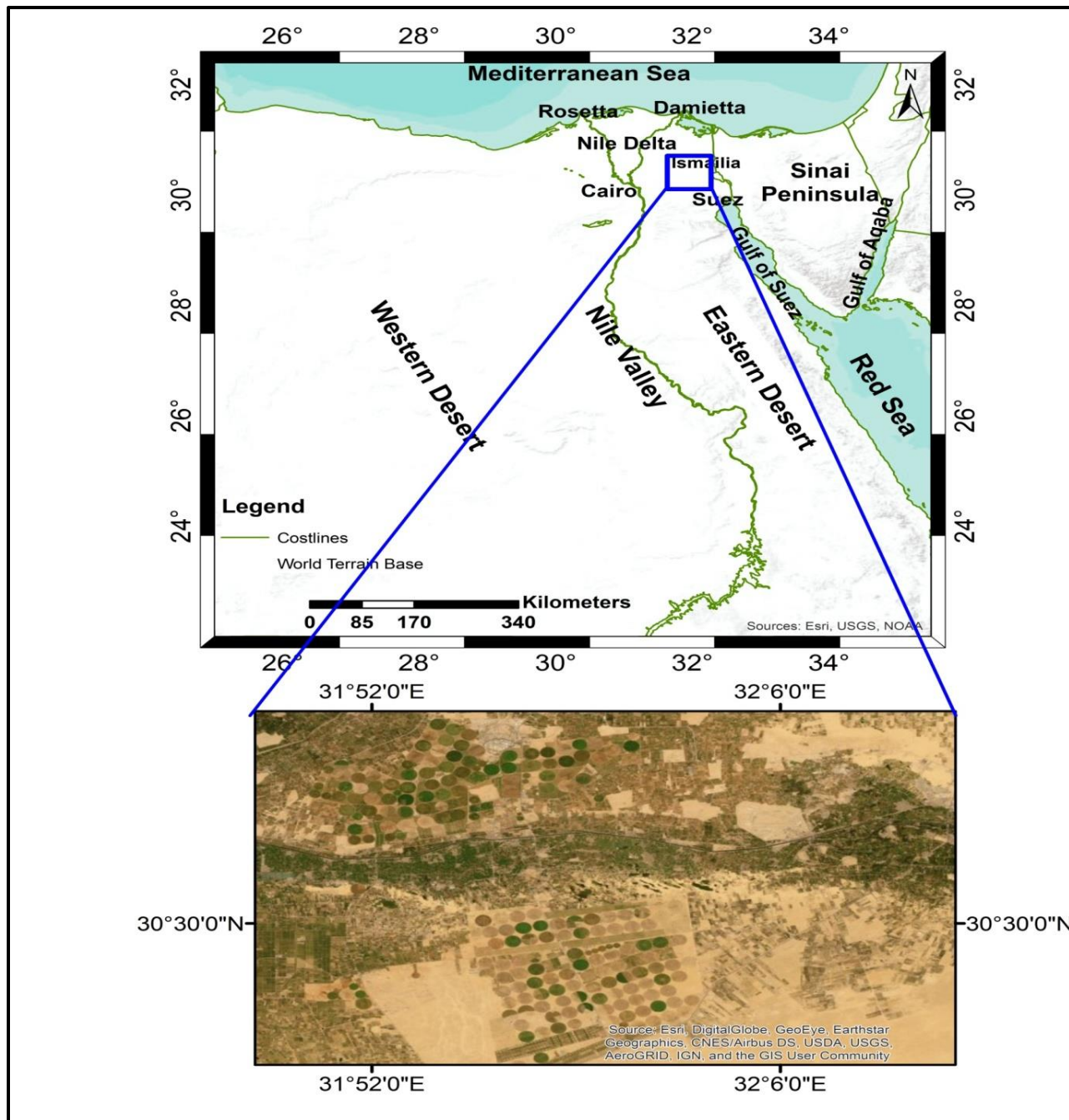
Fig. 1. 1: Location map of the study area.

Fig. 1. 2: An example of a water logging lake near Wadi El-Tumilat.

1.4. Previous Studies

There are many geological, geophysical and hydrological studies that have been performed in the east Nile Delta, generally, and particularly close to Ismailia, especially because of its great economic importance, as we mentioned before. From these studies we can list the following prominent ones, highlighting their main results:

Geriesh, (1994): This is one of the most important and comprehensive studies that were performed in the East Nile Delta. The main aim was studying the hydrogeological and hydrochemical characteristics of the quaternary aquifer in the whole basin of Suez Canal region. So, he was able to evaluate the groundwater origin, recharge history and potentiality to develop a reasonable management scheme for controlling the groundwater recharge. The studied area lies between Lat. 30° 20'- 31° 20' and long. 31° 20'- 32° 30' and covers the Nile Delta region from east with an area of about 5000 km². This was done by collecting 125

groundwater samples from productive wells for hydrochemical analysis, 62 rock samples from 8 wells to describe the main lithologies and for grain size analysis. Besides, detailed topographic and 24 vertical electrical soundings have been performed. This study has pinpointed that there are two main groundwater aquifers in the study area, namely: a main fluvial aquifer occupying the area of Um Gidam slopes and El-Salhiya plain; the deep horizon beneath Wadi El-Tumilat depression, characterized by fresh water and good overall hydraulic properties. Local fluvio-marine aquifer occupies the low land areas of the northern and eastern boundaries and Wadi El-Tumilat depression and characterized by brackish water and less favorable hydraulic properties. Groundwater flows from the recharging areas of Wadi El-Tumilat and the southern parts of the Nile Delta plain towards the Northern and Eastern Low lands.

El Rayes et al., (2004): This study aimed to assess the quality of water resources in Ismailia district and define the sources of water contamination in the area. In addition, it designs a suitable treatment model to protect the quality of water that used in drinking and domestic purposes. So, a total of 154 water samples were chemically analyzed, from which 120 samples represent groundwater and 34 samples are canal water. Major ions including Ca, Mg, Na, Cl, HCO_3 and SO_4 and some of minor and trace elements including NO_3, PO_4, Cd, Fe and Pb were analyzed. Moreover, the Total Coliform bacteria content was counted for some selected samples. It was found that nitrates, phosphates, bacterial content and trace metals have all high concentration levels in surface water and groundwater underlying the villages and the industrial zone of Ismailia. They concluded that the main sources of groundwater contamination in the study area are leakage from the poorly developed sewage system of the villages, leaching of fertilizers that are dissolved into irrigation water found in agricultural areas and discharge of

industrial liquid wastes of the industrial zone. Therefore, they proposed a new treatment technique to be designed using the artificial recharge method to improve the water quality in two selected sites within the study area. The proposed design was tested and calibrated using groundwater flow modeling techniques. The mathematical MODFLOW program was used to predict the resulted groundwater regime and the discharge efficiency of the proposed designs. The produced treated water by this design could reach about 50.000 m³/d, which is high enough to supply the surrounding villages of each site. The proposed treatment design is recommended to be applied for the whole area.

Abd El Hamid, et al., (2005): The main aim of this study was to investigate groundwater occurrences around the new communities in the East Nile Delta since groundwater is considered the second main source of water in Egypt and it is the main element required for land reclamation projects and development in these new communities. In this direction, a number of 53 vertical electrical soundings (VESs) using Schlumberger electrode array with maximum current electrode spacing AB= 1400m have been carried out, especially in the parts without water wells. In addition, raw data of 92 VESs from **Ezz El Din, 1993 and Abd El-Gawad, 1997** were reinterpreted. The geoelectric parameters obtained from VES interpretation were calibrated with the nearby wells of known lithological and hydrogeological information obtaining a resistivity range for the subsurface litho-facies leading to a reliable classification and characterization. The resistivity layers showed three main litho-resistivity zones with quite different hydrogeological conditions. Litho-resistivity zone (A) represents the detrital surface cover. Litho-resistivity zone (B) represents a dry zone. Litho-resistivity zone (C) represents a saturated zone. This aquifer is belonging to Quaternary age and characterized by considerable thickness and fresh water. From the constructed geoelectric cross-sections, it was found that

there are several faults that affect the water quality due to the leakage of saline water of the Miocene aquifer into the quaternary one.

Embaby et al., (2017): the main purpose of this work was the assessment of groundwater quality for drinking and irrigation purposes in El-Salhiya plain (East Nile Delta). So, 30 groundwater samples were collected from wells tapping the Quaternary aquifer in El-Salhiya plain where the total depth of these wells ranges from 5 to 90m. From the hydrochemical analysis it was found that Total Dissolved Solids (TDS) content of the groundwater samples varies between 642 mg/l to 4530 mg/l; indicating fresh to slightly saline water classes. Na^+, Cl^- and SO_4^{-2} show strong positive correlation with TDS. The main water type is mostly chloride sodium. According to the water quality index (WQI), about 70% of the examined groundwater samples fall in the class which is recommended for drinking, while 30% fall in the poor class, which must be treated before use. For irrigation purposes, only 17% of the groundwater samples are suitable for irrigation of moderately sensitive crops while 66% can be used to irrigate moderately salt tolerant crops. The remaining (17%) are only recommended to irrigate high salt tolerant crops. One of the main results of this study is that special management of salinity control is mandatory for agricultural development and plants with good salt tolerance should be considered for further uses.

So, our study is a continuation and improvement of all these previous works from which we extracted all the available data about the geological and hydrogeological situation. Also, we were able to evaluate how far the groundwater situation has been changed through time. Based on the results of these studies we validated our data better defining the current situation of the study area. The results obtained in this study are very interesting and helpful to develop future reclamation plans and promoting a sustainable development of the analyzed area.

Chapter (2)

Geological Setting

2.1. Introduction

This study focuses on the area west to Ismailia (Egypt) including Wadi El-Tumilat, El-Salhiya and the area north to Cairo-Ismailia Desert road as shown in chapter one. This area is characterized by highly productive agricultural lands and good groundwater resources. In this chapter we briefly discuss the general geological and hydrogeological characteristic of east Nile Delta, and specifically those of the area west to Ismailia.

2.2. Climate

In Ismailia and its vicinities, the summers are long, hot and arid with humidity not exceeding 60% while the winters are relatively cold, dry, and mostly clear. Over most of the year, the temperature typically varies from 9 to 35 °C and is rarely below and above 6 and 37 °C, respectively. The annual precipitation is not exceeding 50 mm/yr **(Environmental action plan of Ismailia, 2008)** which means that it has insignificant contribution to the groundwater aquifers recharge in the study area.

2.3. Geomorphology of East Nile Delta

To characterize groundwater aquifers in any place, the first step is to analyze the geomorphology and geology which are considered the keystone for any exploitation and reclamation plan.

The landscapes within the east Nile Delta were studied and discussed by many authors since a long time: **Shata (1970), El-Shazly et al. (1975) and Geriesh (1994)**.

In this part, a brief explanation about the main land features in the study area will be presented. Within the study area six main geological and geomorphologic features can be highlighted, as follows:

Gebel Mokattam-Gebel Ataqa Structural Table land.

As shown in figure (1.1), this tableland is mainly made of Limestone and outcrops south to our study area. It was striking out due to the late Eocene and younger uplift (Dahab et al., 2009).

These massive rocks are in general characterized by low primary porosity and act as a watershed area drained in north direction, i.e. to El Dakruri depression. On the other hand, secondary porosity is related to karst phenomena mainly developed along joints and fissures.

Gebel Shabrawit– Cairo Structural Ridges

This unit is located in the southern part of the study area at the boundary zone between Gebel Mokattam-Gebel Ataqa Structural Tableland in the south and Um Gidam slopes to the north as in figure (1.1). It extends east-west as a series of high elongated ridges with many domes and monoclines. It starts with Gebel Shabrawit (223 m) from east to Gebel Um Ragam (275 m) and Gebel Hamza (210 m) to the west (Geriesh, 1994).

These ridges are mainly built up from Miocene and Eocene limestone and sandstone with some scattered Oligocene gravely sand hills. As shown in figure (1.1), they are drained by a number of dry wadies in the north, north-east and north-west directions.

Um Gidam Gravelly Slopes

This unit covers the foot slopes of the previous geomorphologic unit and extends northward until it reaches the southern part of Wadi El-Tumilat depression as in figure (2.1). It is characterized by a varying altitude that reaches about 180 m to the south and about 30 m to the north and east directions (Geriesh, 1994).

These slopes are mainly made from gravely sand sheets of quaternary age dissected by several radial drainage lines running from the southern structural ridges to the north, north-west and north-east as in figure (2.1). These wadies are narrow in the southern parts and become gradually wider along the downstream reaches. These dry wadies were very important during the past pluvial periods as they played a role in recharging groundwater and transporting sediments to the northern and eastern low slope sides.

El-Tell El Kabir and El-Salhiya Plain

This plain is represented by the area extending from Um Gidam slopes in the south to the north of Wadi El-Tumilat depression until the southern reaches of El Manzala Lake (Fig. 2.1). Its altitude is varying between 40 m to the south to about 10 m to the north (Geriesh, 1994).

It is mainly occupied by gravely sand sheets belonging to Quaternary age. This gravel is characterized by coarse grain size which reaches up to 5 cm in diameter, thus indicating good hydraulic characteristics in terms of trasmissivity and porosity. The northern and eastern parts are occupied by a considerable number of elongated sand dunes, mostly parallel to the northern and eastern low lands.

Wadi El-Tumilat Depression

This wadi represents a morpho-tectonic depression that crosses the study area from west to east and separates between the previously mentioned two geomorphological units. It extends from the Nile Delta in the west to the Timsah and Bitter lakes in the east (Fig. 2.1) with an extension about 50 km long and about

7 km wide. It has a very gentle slope towards east with an altitude varying from 10 m to the west to about 2 m to the east. Along its southern boundary, elongated, parallel small sand dunes with water ponds in between are well distributed. These ponds are a result of the water logging problem that will be explained in details in next chapters. There are evidences suggesting that this wadi was one of the past Nile branches acting as a recharge source for the groundwater aquifers during its running period (Geriesh, 1994).
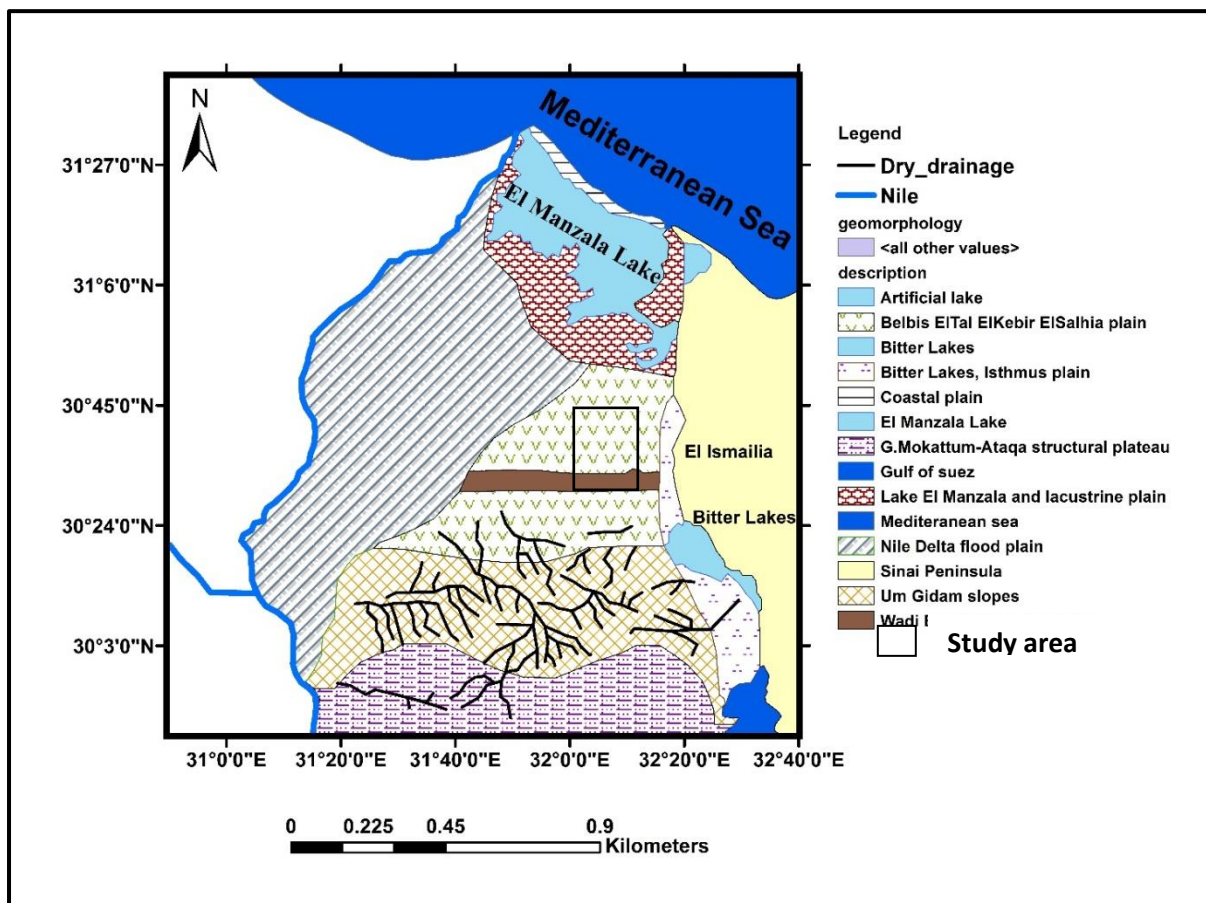
Fig. 2. 1: Geomorphological map of the eastern part of Nile Delta modified after (Dahab et al., 2009)

Isthmus Sandy Stretch

This sandy stretch extends from Gulf of Suez in the south to near El Sallah lagoons in the north. Such stretch was occupied, before the construction of the Suez Canal,

by a series of salty lakes. The traces of these lakes are well represented at El Ballah area. However, this strip of land has been much disturbed by the artificial Suez Canal and its digging products. Wind-blown sand sheets have accumulated along both banks of the Suez Canal.

2.4. Surface Geology

A better understanding of groundwater hydrochemistry in the area of interest requires a detailed study about its geology as groundwater is affected by hosting rocks, surficial soils, and tectonic structures. Geology of the eastern part of the Nile Delta was discussed by many authors since a long time, e.g. **Shukri and Ayouti (1956), Said and Beheri (1961), El Fayoumy (1968), Shata and E1 Fayoumy (1970), Bayoumy (1971), El Shazly et al. (1975), Zaghloul et al., (1977), and Abd El Gawad (1997).**

The study area is covered by Tertiary and Quaternary sediments with sporadic Mid-Tertiary basalt flows (Fig. 2.2). The deposits form a thick succession in the subsurface (~5000 m) with several formations having excellent hydraulic properties and acting as groundwater aquifers (Eltarabily, et al., 2017).The lithostratigraphic succession in the area east to Nile Delta can be compiled as shown in figure 2.3.

In the next section we will briefly discuss the main formations in the area east to Nile Delta.

Eocene
Three formations are distinguished of which Darat and Khaboba Formations belong to the Middle Eocene while Tanka Formation is mainly of Late Eocene age.
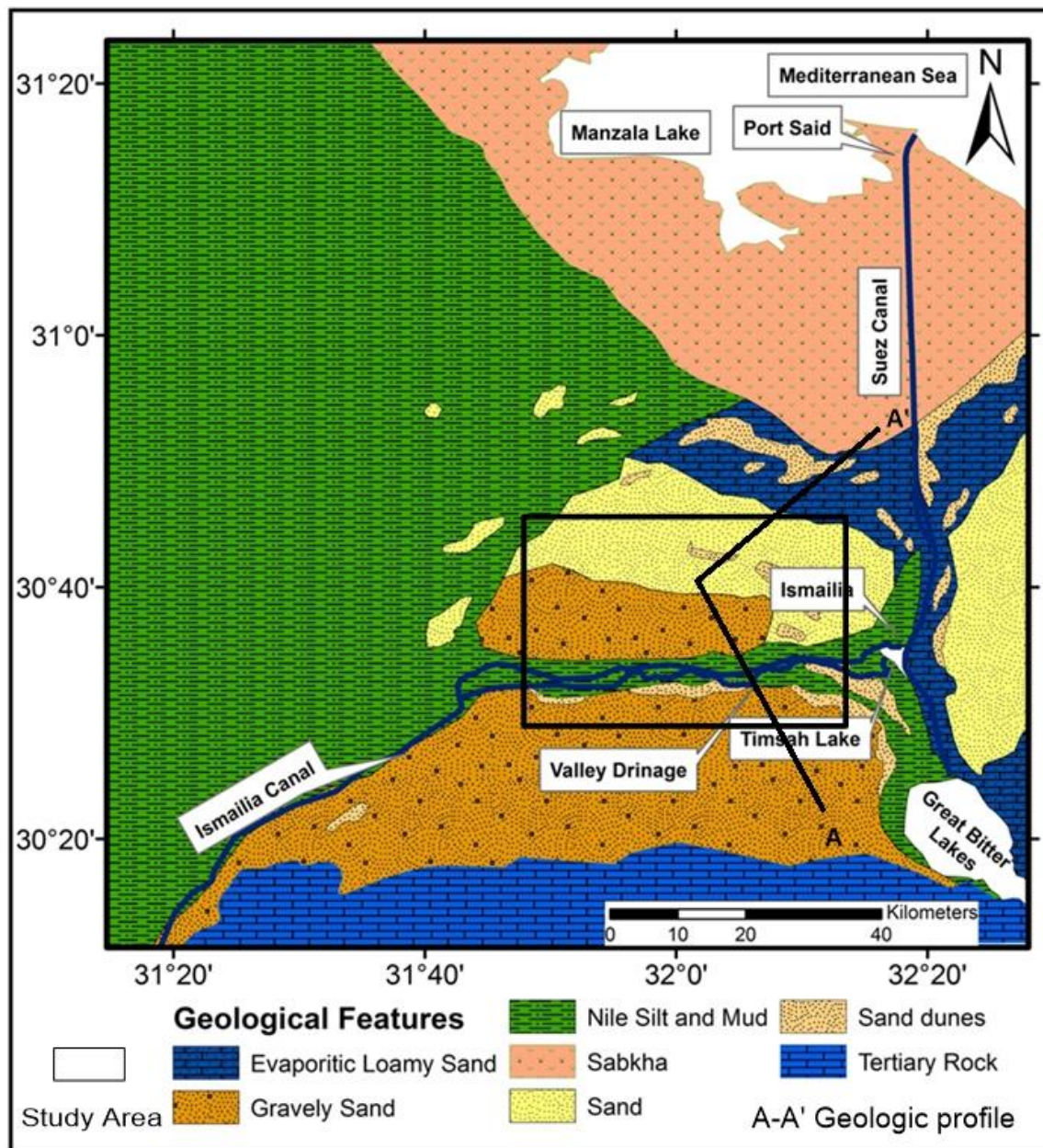
Fig. 2. 2: Geological map east to Nile Delta (Modified after Geriesh, 1994).
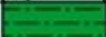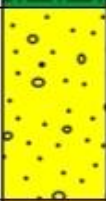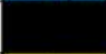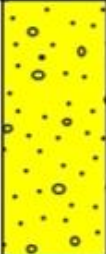
period	Epoch		H (m)	Lithology	Composition & Hydrogeological characteristics
Quaternary	Holocene		20		Nile Silt (aquitard)
	Pleistocene		300		Sand, gravels and rock fragments (aquifer)
Tertiary	Pliocene		250		Clay (aquitard)
	Miocene		285		Sand (aquifer)
					Fossiliferous limestone shale & marl
			35		Basalt
	Oligocene		350		Sand & gravel (aquifer)
	Eocene	Upper	120		Shaly, sandy limestone, sandy marl & clays
		Middle	200		White chalky limestone and marls

Fig. 2. 3: Simplified lithostratigraphic section of the east Nile Delta area, modified after Geriesh (1994).

- **Darat Formation**

It is mostly made of marl with fossiliferous chalky limestone of white color and smooth texture. It is exposed in three main localities: a) east of Gebel Ataqa with coarse texture; b) west of the Great Bitter Lake and the southern narrow strip of Gebel Iweibid, with light color and smooth texture in these two localities.

- **Khaboba Formation**

Mainly made of marl and fossiliferous limestone with lint bands. It is characterized by brown color and coarse texture, forming the marginal ridges of Gebel Ataqa and the southern limit of Gebel Iweibid.

- **Tanka Formation**

It is exposed to the south and west of Khaboba formation at Gebel Ataqa, forming the upper most horizons in Gebel Ataqa and Iweibid. It is mainly constituted by fossiliferous limestone with shale and it is characterized by light brown color with fine to medium texture.

Oligocene

Oligocene rocks are found with thickness ranging from 45 m at Gebel Iwiebied to 100 m at Gebel El Nassuri. They are mainly exposed in the area located between Cairo and Suez at Gebel Umm Raqm and Gebel Umm Qamar.

- **Gebel Ahmar Formation**

This is the main formation belonging to Oligocene age. It can be differentiated into three lithologic units:

Unit 1: This unit is exposed at Wadi Kahaliya, mostly constitutes of sands and flint gravels with fine texture.

Unit 2: Exposed at Gebel Umm Raqm and Wadi Yasara and characterized by coarse texture that is mainly composed of ferruginated red sandstones.

Unit 3: It is composed mostly of quartzitic and less ferruginated sandstone and flint gravels with medium texture. It is exposed on both sides of Wadi El-Gindali.

Mid-Tertiary Volcanics

These volcanics are mostly basalt sheets which are belonging to Late Oligocene - Early Miocene.

Miocene

It is represented by two formations of middle Miocene age, namely El Shatt Formation and Hommath Formation.

- **El Shatt Formation**

El Shatt Formation has been divided into the two following units:

Unit 1: It is mainly exposed at the eastern side of Suez Canal until the south of the Bitter Lakes. It is constituted of sandstones, clays and limestones, with more gypsum-anhydrite than the northern unit 2.

Unit 2: Exposed towards the east and northeast of the Bitter Lakes. It is mainly composed of sandstones, clays and limestones, with small and sometimes insignificant proportions of gypsum-anhydrite.

- **Hommath Formation**

It is mainly constituted by limestone with variable intercalations of clays and sand. It has been distinguished into two main units:

Unit 1: This unit is made by limestone with prominent intercalated sandstones.

Unit 2: Also, this unit is mainly made of limestone, but with prominent intercalated outcropping clays.

Pliocene

Deposits of this age are rarely recorded in the study area, but they are exposed between Cairo-Ismailia desert and agricultural roads with a maximum thickness equal to 28 m (Ezz El-Deen, 1993).They are made up by gravels and sands with less abundant clays and are mostly covered by small dispersed desert vegetation.

Quaternary

Quaternary rocks are widely distributed over the study area where two main formations of Quaternary age are well defined. They are divided based on the lithologic composition (Salem Z. E.-S. et al., 2021):

- **Mit-Ghamr formation**

It is the oldest formation (Late Pliocene–Pleistocene), mainly composed by thick beds of sands with clay and gravel inter-beds. It is characterized by quartz-rich sand that is medium to course-grained. Pebbles are found and consist of quartzite, chert and dolomite grains with shell fragments of gastropods and pelecypods, whereas the gravels are composed of flint and dolomites. It was suggested that the sediments of Mit-Ghamr formation were probably deposited under deltaic and/or coastal marine to fluvial conditions.

- **Bilqas formation**

Bilqas Formation is the youngest one (Late Pleistocene to Holocene) that is dominated by sand, silt and clay inter-beds where the sand is fine grained. However, the sediments are more calcareous in the northern part of the Nile Delta. These sediments were deposited in continental, fluviatile, lagoonal, and beach environments.

2.5. Structural framework

Folds and faults are the most relevant structural elements affecting the sedimentary succession of the study area. A considerable number of faults with different trends can be easily traced along the southern mountainous part in figure (2.3). The relationship between these faults was discussed by many authors since the beginning of last century, e.g. **El Shazly et al. (1975)**. Their studies can be summarized as follows;

1- The E-W faults are the oldest ones of Pre-Miocene origin.
2- The WNW-ESE faults are younger than the E-W ones and clearly affect the Miocene rocks.
3- NE-SW normal faults are the youngest dominant set, affecting the Quaternary sediments. The vertical displacement along these faults ranges

from few meters to hundred meters northeast direction which led to increase in thickness of the Quaternary aquifer by 3m/km in the northeast direction (Gad, 1995).

Regarding to the folds, the area under investigation is represented by two main types of folds; **the Late Cretaceous – Early Tertiary folds** (detected in Gebel Shabrawit, west of Bitter lakes and belong to the Syrian arc system) and the **Late Miocene folds** which are represented by the southern structural ridges (Fig. 2.4).

2.6. Subsurface geology

The subsurface geological setting of the area in which the study site is located is mainly composed by a sedimentary succession of Tertiary and Quaternary rocks.

Eocene
Carbonate facies of Eocene are mostly occupied the structural tableland with thickness ranging from 400 to 500 m. karsts conditions are prevailed.

Oligocene
It is mostly exposed along the foot-hill slopes of the Cairo-Gebel Shubrawit structural depressions and it is mainly constituted by sands and gravels (maximum thickness 80 m) and capped by Mid-Tertiary sediments. Oligocene sediments extend and slope generally northwards.
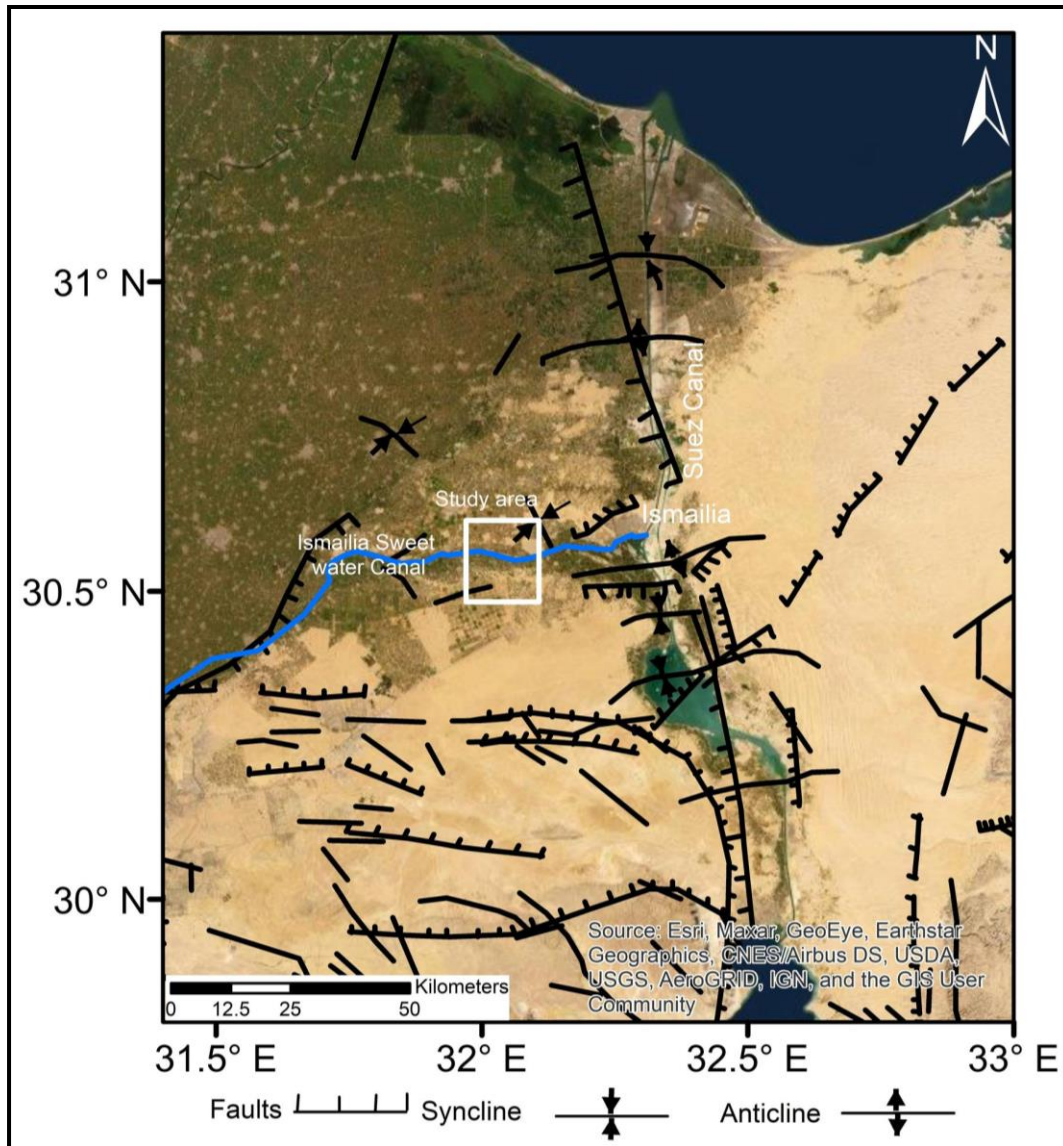
Fig. 2. 4: Structural map of the East Nile Delta modified after El-Dairy, (1980).

Miocene

Most of the faulted structural ridges are built up by Miocene facies that are all mainly constituted by marine sandy limestone. Near the south of Wadi El-Tumilat (Um Gidam slopes), the subsurface Miocene sediments have been recorded at depth of 140 m, whereas on its northern side (El-Salhiya Plain) the shallow wells (200 m depth) did not reach the Miocene sediments (Geriesh, 1994) as shown in figure 2.4 and 2.5. It may be expected that the groundwater which percolates through these sediments is probably saline.

Pliocene

Early Pliocene sediments recorded below the Isthmus stretch and the area north of Um Gidam slopes are mainly fluvio-marine and sandy clays (Geriesh, 1994). They represent an aquiclude horizon for the upper layers representing Pleistocene aquifer.
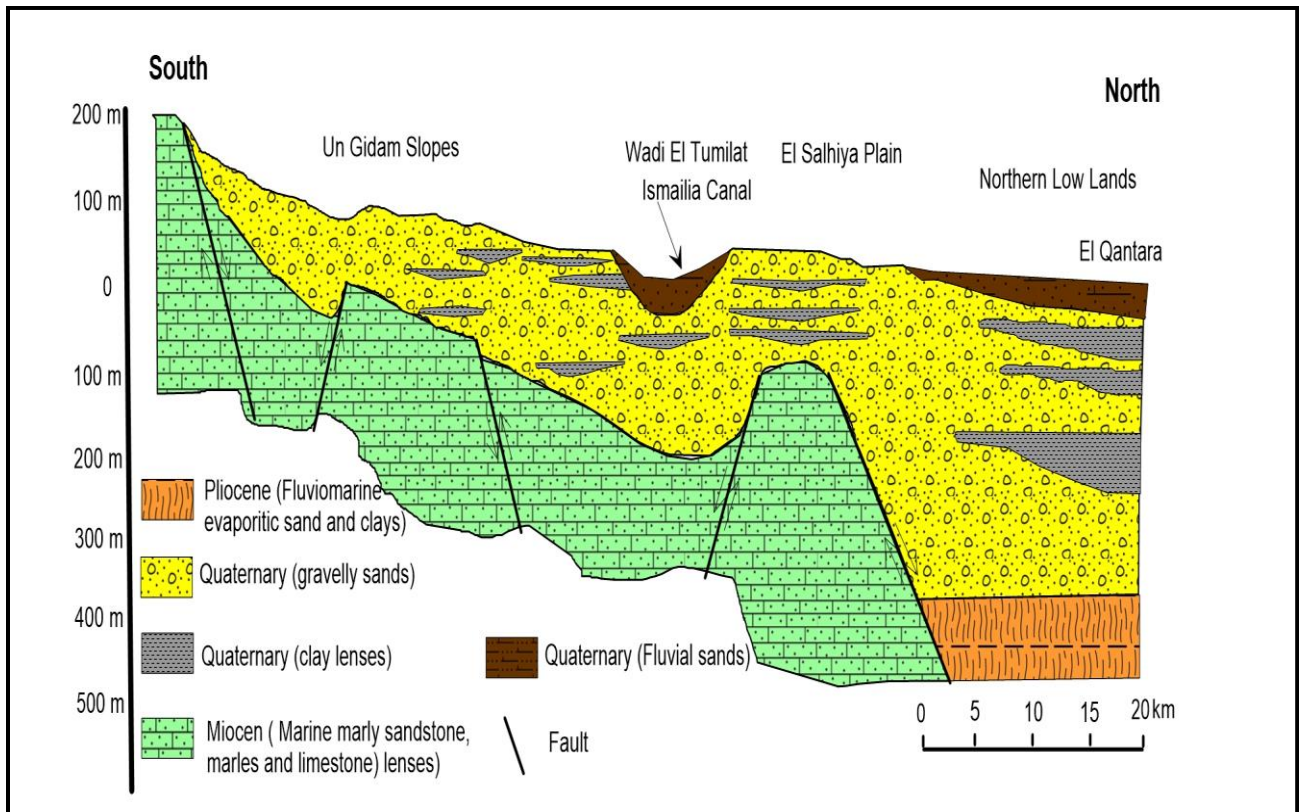
Fig. 2. 5: Geological section crossing the study area from South to North (A-A') modified after (Geriesh, 1994).
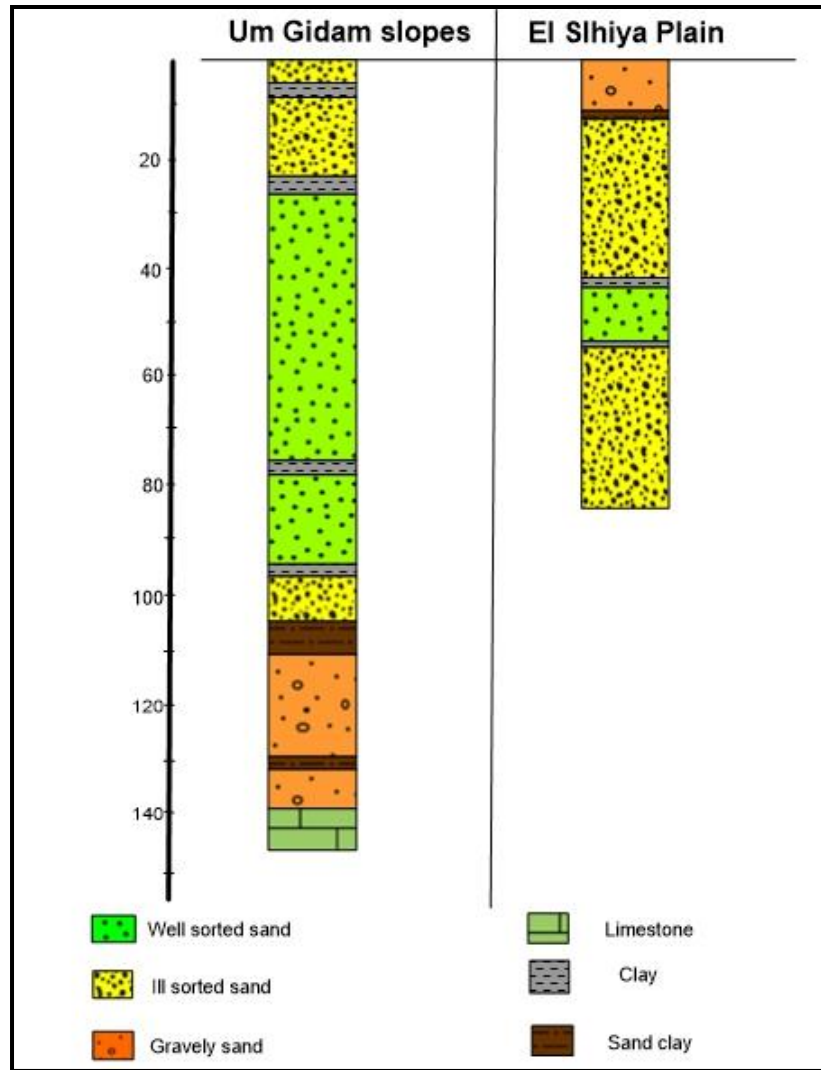
Fig. 2. 6: Representative lithostratigraphic sections for Um Gidam Slopes and El-Salhiya Plain areas modified after (Geriesh, 1994)

Early Pleistocene

Sediments of this age were deposited on the late Pliocene negative areas north to the structural ridges. They are mainly represented by thick gravelly sand and sand gravel and they are intercalated with clay beds north of Wadi El-Tumilat (El-Salhiya Plain). At El Qantara area, the thickness of these sediments reaches 10 to 80 m.

Late Pleistocene-Holocene

Late Pleistocene sediments are characterized by intercalations of gravelly sands, sand, slightly calcareous sandstones and clays. These sediments cover the area north to Um Gidam and the Isthmus stretch and overlying the early Pleistocene with a thickness ranging from 10 to 70 m and increasing north direction. These sediments represent the most important aquifer in the study area, mainly recharged by the surface water of the Nile Delta, Ismailia Canal, Suez Canal, Lake Manzala and the various drains found in the area.

Holocene sediments are represented by sand sheets particularly along the eastern side of the Isthmus stretch, and sand sheets west of El-Tell El Kabir and El-Salhiya plain (Shata et al., 1970). Sabkhas and salt marshes dominate the northern strip of El-Tell El Kabir and El-Salhiya plain. So, the groundwater in these sediments is mostly of leaky nature and its salinity level reflects the nature of the neighboring salt sources.

2.7. Hydrogeology

Based on the previous hydrogeologic studies, e.g. **El-Dairy (1980), Geriesh (1994), Gad (1995), El-Hadad (2002) and Salem, et al. (2021)**, three main aquifers can be identified in the study area (respectively of Quaternary, Miocene & Oligocene ages). The distribution and the thickness of these aquifers are mainly affected by the geomorphological features in the study area and will be discussed in the light of this.

Um Gidam Slopes and Wadi El-Tumilat

These slopes are mainly occupied by sands and gravels belonging to early Pleistocene and overlying uncomfortably the Miocene sediments. The surface of Um Gidam slopes regionally in a northward direction towards Wadi El-Tumilat and in the eastward direction towards the Isthmus stretch. As a results of this

sloping, both of Wadi El-Tumilat and the Isthmus stretch are considered natural drainage areas.

According to the wells drilled on these slopes which reach about 150m, the subsurface lithology is mainly composed by gravely sand with intercalations of sand and clay as shown in the lithological section in figure (2.5). Deep drilling in these slopes indicated that the main aquifer has Pliocene- early Pleistocene age. It is unconfined and mainly hosted within sands and gravels with groundwater of salinity not exceeding 1.000 ppm. This aquifer is underlain by another one of Miocene age with high salinity that reaches 10.000 ppm. As a result of faulting, where the early Pleistocene aquifer comes opposite to the Miocene one (Fig. 2.4), there may be a possibility of lateral seepage of saline water of the Miocene confined aquifer into the Pleistocene one.

Water table depth in Um Gidam is mainly controlled by ground elevation as it occurs at deep level in the southern portion of the slopes and becomes shallower in northward direction towards Wadi El-Tumilat and in westward direction towards the Nile Delta basin. The groundwater flows from south to north, i.e. towards Wadi El-Tumilat which acts as a natural drainage. The salinity of the water in this depression is rather low, especially in the areas surrounding Ismailia Canal. In the reaches of the Suez Canal to the east, the salinity of water becomes higher.

Isthmus Stretch
The geological succession in this part is composed of alternating sandstone and clay beds with occasional sandy limestone, conglomerate and marly layers belonging to Miocene age. Here, sandstone and conglomerates constitute the main water bearing units where the water is almost found under partially confined conditions. The water of this aquifer is of connate type and it has low exploitation

potentialities due to the abundance of anhydrite-gypsum within the succession and the continuous leaching processes.

The main Miocene aquifer is overlain by a subsidiary leaky aquifer in the topsoil layer (3 m thick) which is composed of clayey sand. The water in this layer is provided by leakage from the irrigation and drainage system (on the western side of the Suez Canal) and from local precipitation (on the eastern side) within this Isthmus stretch. The Suez Canal acts as a natural drain for this water.

Underlying this Miocene aquifer, relatively less saline water horizons were recorded in the Oligocene sandy geological units. The groundwater in these Oligocene horizons has a hydraulic pressure lifting it to nearly 16 m above the present sea level with lower salinity than that existing in the overlying Miocene aquifer. This Oligocene aquifer seems to be recharged from the heavy precipitation during the past wet periods, as well as from the upward leakage from the underlying Eocene and Cretaceous aquifers (possibly through fault lines).

Quaternary aquifer
Quaternary aquifer is the most important water-bearing deposit of the east Nile Delta. The saturated thickness of the Quaternary aquifer increases gradually in the north-west direction to reach about 900 m. It is recharged by the seepage of freshwater from the Damietta Branch and Ismailia Canal, the percolation of return irrigation water especially in the newly reclaimed lands with sandy soil, the infiltration of excess water storage in the overlying aquitard and the inter-aquifer flow, in particular between the Nile Delta and Miocene aquifers. It is mainly composed of fluviatile and fluvio-marine graded sand and gravel with clay intercalations of limited extension. The basal portion of this aquifer is formed of dark plastic clay. It rests directly with unconformity surface on the Miocene hard limestone as recognized in the north and south of Wadi El-Tumilat (Fig. 2.4). The

groundwater flow is directed from south to north with very low hydraulic gradient ($\approx 2\text{x}10^{-4}$) (Gad, 2015).

The Quaternary and the Miocene aquifers are hydraulically connected, but in some places they are separated by a semi-permeable layer which is highly controlled by deep-seated faults (Gad, 1995). These faults cause the saline groundwater of Miocene aquifer to move upward along the fault planes and to mix with the groundwater of the quaternary aquifer. The groundwater in the quaternary aquifers is unconfined in the western part and it begins to be under semi-confined conditions in the eastern part due to the presence of capped and underlying clay beds.

Along Wadi El-Tumilat, the quaternary aquifer is overlaid by a localized aquifer (named Wadi El-Tumilat aquifer). The thickness of this aquifer increases gradually from few meters at west to about 20 m at east (Geriesh, 1994) with increasing in the ratios of the fine-grained size and evaporitic content of its constituents in the same direction. As a result, the eastern parts of the aquifer are less permeable than its western parts and the former may act as an aquitard layer capping the main quaternary aquifer and forming a leaky aquifer system with it (El Shamy, 1992).

Chapter (3)

Methodology

In this chapter we briefly discuss the theoretical bases for those geophysical techniques applied in this study, namely: Vertical Electrical Sounding (VES), Transient Electromagnetic Sounding (TEM), and Electrical Resistivity Tomography (ERT).

3.1. Electrical Resistivity

Electrical resistivity (ER) methods are considered as one of the most common and helpful geophysical techniques applied in shallow subsurface investigations, especially in groundwater studies **(e.g. Christensen and Sørensen 1998; Sørensen et. al., 2005; Massoud, 2005)**. It is well known that the resistivity of a rock is very sensitive to its water content. In turn, water resistivity is very sensitive to its ionic content. Depending on this approach, different stratigraphic units in a geologic section can be mapped based on their resistivity contrast. The electrical resistivity of the soil/rock can be considered as a proxy for the spatial and temporal variation of many physical and mechanical properties (i.e. structure, water content, or fluid composition).

ER method is non-destructive, accurate and cost-effective tool for describing the subsurface properties at various scales. It has been deployed in various applications like groundwater exploration, landfill and solute transfer delineation, agronomical management by identifying areas of excessive compaction or soil horizon thickness and bedrock depth, and assessing the soil hydrological properties.

3.1.1. Basic electrical theory

The principle behind electrical geophysical methods is that because different geologic materials have different electrical properties they can be identified and characterized based on these properties. The main object of the electrical surveys is to determine the subsurface electrical resistivity (which is the inverse of the electrical conductivity) distribution by making measurements on the ground surface.

The basic concept of electrical resistivity is simple. A direct or low-frequency alternating current is injected into the earth through two metal electrodes (current electrodes). Because earth materials offer resistance to the passage of the electric current, some voltage loss is expected to occur as the current flows from one electrode to the another though the geologic materials. The voltage loss (voltage difference) that occurs as the electric current moves through the ground is measured at other two electrodes (potential electrodes) commonly placed between the current electrodes (except in case of Dipole-Dipole electrode configuration), as shown in figure (3.1). The subsurface apparent resistivity can be calculated from the injected current, the measured voltage difference values, knowing the geometrical distribution of all the electrodes.

Reynolds (1997) has indicated that ground resistivity is connected to various geological propertied such as the mineral and fluid content, porosity and degree of water saturation in the soil/rock**.**
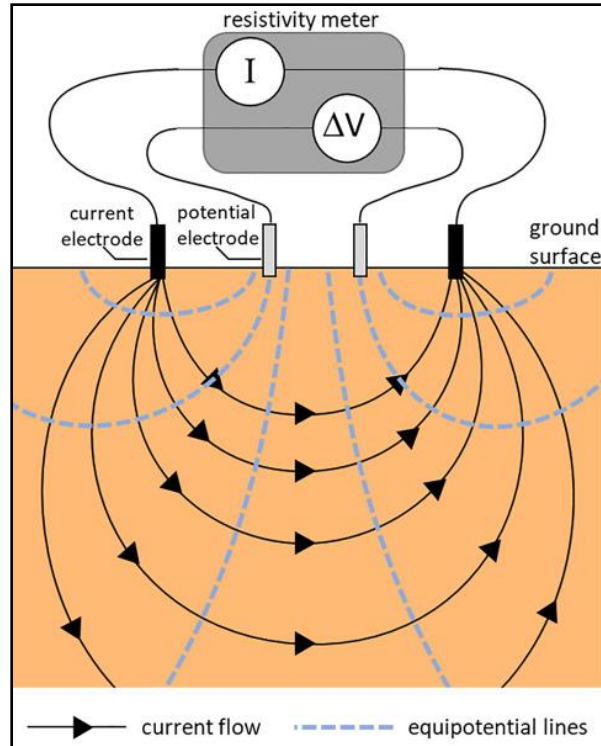
Fig. 3. 1: Basic concept of resistivity measurements.

The physical base of this method is the Ohm's Law which states that, for an electrical conductor, the current with intensity (I) is equal to the voltage (V) across it divided by a constant, which is the resistance (R), where the resistance is measured in Ohm, the current is in Amperes and voltage in Volts. This can be written as:

$R = V/I$ .... (3.1)

Equation (3.1) can be alternatively written in terms of the electrical resistivity (ρ), electric field strength (E) and current density (J) as:

$\rho = E/J$ .... (3.2)

Being $\rho = \frac{1}{\sigma}$.Ohm's Law, as written above, describes a conductor which has no dimensions. In considering the flow of electric current on the Earth, we must consider the flow of electric current in a finite volume. Let consider a cylinder

(Fig. 3.2) of length **L** and cross-section **A** that carries a current **I**. The resistance is proportional to the length and inversely proportional to the cross-sectional area (A) of the resistive material.

R α L/A ……………………………………*(3.3)*
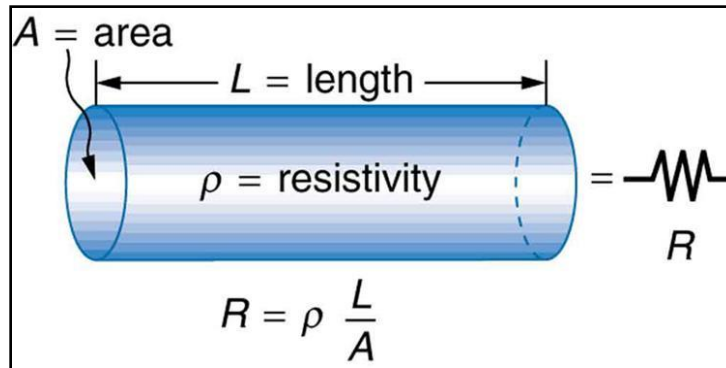
Fig. 3. 2: Flow of electric current in a uniform conductor.

The constant of proportionality is the electrical resistivity (ρ). Therefore, equation (3.3) can be written as:

R = ρL/A   or   ρ=RA/L …………………*(3.4)*

Resistivity is measured in Ohm*meter. The electrical conductivity (σ) of a material is defined as the inverse of its resistivity (ρ) and is measured in Siemens/meter (S/m). Therefore:

σ =1/ρ …………………………………… *(3.5)*

All the previous formulas are strictly valid only for perfect electrical conductors (a.k.a. ohmic materials), like some metals. Most of the rocks are instead insulators (i.e. dielectric materials) but when they contain water which always has a certain amount of dissolved ions, they can be considered as conductors following the Ohm's Law.

3.1.2. Rock types and resistivity

The measured resistivities in Earth's materials are mainly controlled by the movement of charged ions in pore fluids. Although pure water is not considered as a good conductor of electricity, groundwater generally contains dissolved solids that significantly improve its ability to conduct electricity. Hence, porosity and fluid saturation tend to dominate electrical resistivity measurements. In addition to pores, fractures within rocks can lead to low resistivities if filled with air.

The resistivity of geological materials exhibits one of the largest ranges of all physical properties (Fig. 3.3), with 24 orders of magnitudes from $1.6 \times 10^{-8} \Omega m$ for native silver to $10^{16} \Omega m$ for pure Sulphur (Reynolds, 1997).
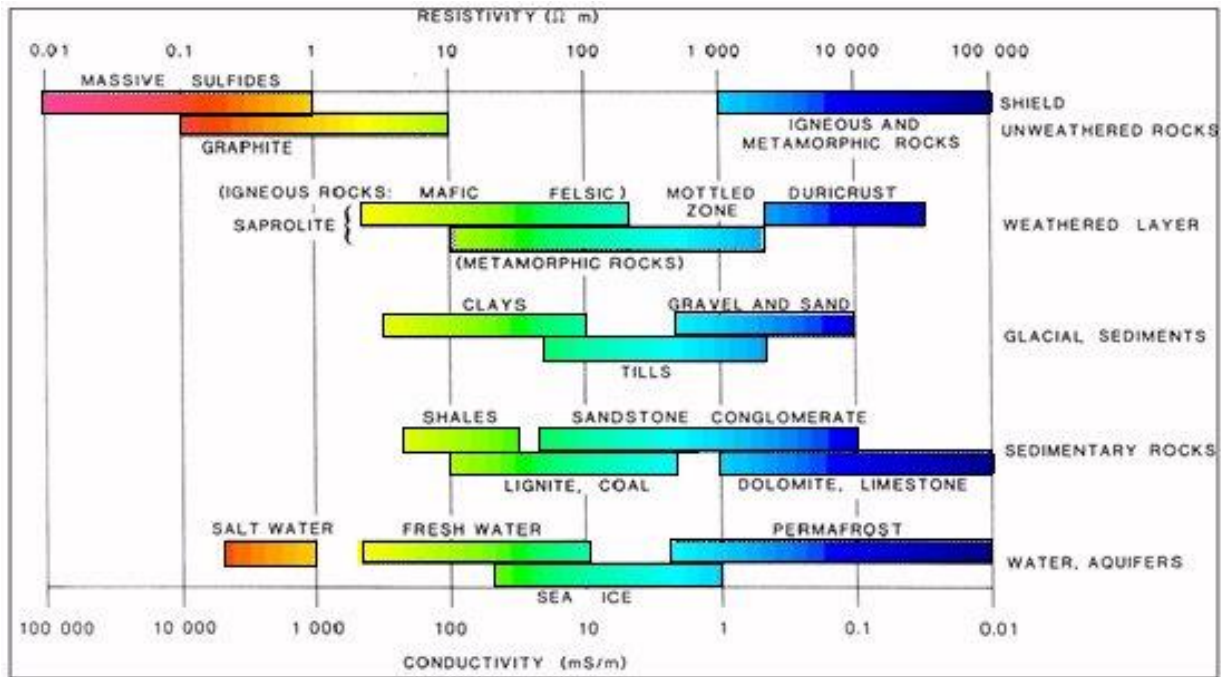
Fig. 3. 3: Approximate electrical resistivity ranges for different types of rock, soil and water.

3.1.3. Electrical resistivity modes

Electrical resistivity surveys can be carried out in two main ways:

1-Vertical Electrical sounding (VES): is applied to determine resistivity variations with depth. It has a 1S approximation and can be applied when horizontal or near horizontal interfaces exist. The application of the VES procedure is based on the fact that as the distance between the current electrodes increases, the depth up to which the current penetrates also increases. The position of the measurement is taken at the mid-point between the electrode array (Parasnis, 1997). The technique is extensively used in geotechnical surveys to determine the overburden thickness and in hydrogeology to define vertical discontinuities of porous strata.

2- Horizontal Electrical Profiling (HEP): It measures lateral variations in resistivity i.e. intrinsically considers a 2D approximation. The current and potential electrodes are maintained at a fixed separation and progressively moved along a profile, so a pseudo resistivity section (or profile) can be obtained. This method is employed in mineral prospecting to locate faults or shear zones and to detect localized bodies of anomalous conductivity, as well as in many other geological, hydrogeological, engineering and archaeological applications. The method is often referred as Electrical Resistivity Tomography (ERT).

3.1.4. Electrode configuration

All the arrays of electrodes used to obtain the apparent resistivity are variants of the four-electrode scheme. The most commonly used electrode configurations are Wenner, Schlumberger, dipole-dipole, pole-dipole and pole-pole arrays as shown in figure (3.4). The selection of a specific array depends on the application and the desired resolution. A comparison between these standard arrays is shown in table (3.1).
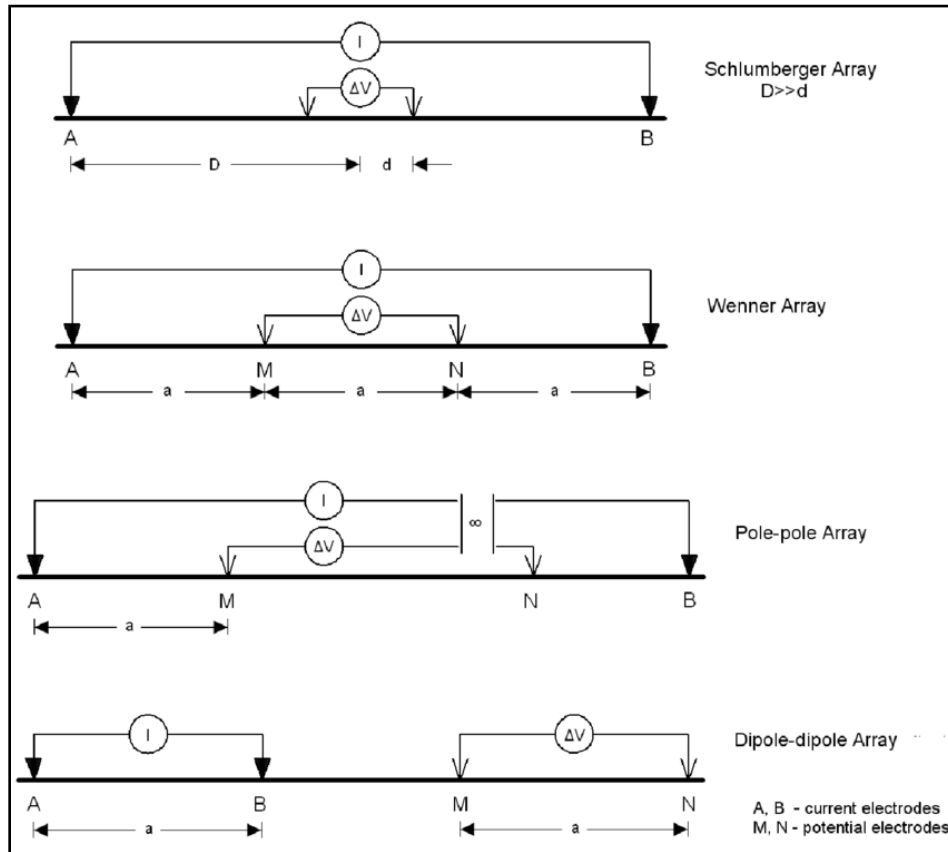
Fig. 3. 4: Most frequently electrode arrays.

Table. 3. 1: Performance comparison between Wenner, Schlumberger and Dipole-dipole arrays (after Reynolds, 1997)

Criteria	Wenner	Schlumberger	Dipole-dipole
Vertical resolution	Good	Moderate	Poor
Depth penetration	Poor	Moderate	Good
Suitability to VES	Moderate	Good	Poor
Suitability to HEP	Good	Unsuitable	Good
Sensitivity to orientation	Yes	Yes	Moderate
Sensitivity to lateral Inhomogeneity	High	Moderate	Moderate
Interpretational aids	Good	Good	Moderate

3.2. Electrical Resistivity Tomography

2-D Electrical Tomography is one of the new developments used in mapping areas with moderate and complex geology (Griffiths & Barker, 1993). It is of great advantage that it measures the resistivity variation in both vertical and horizontal directions, on the contrary to the resistivity sounding method which measures only the resistivity along the vertical direction (Loke, 1999). A typical 1-D resistivity-sounding survey usually consists of 10 to 20 readings, while 2-D resistivity surveys involve about 100 to 1000 measurements, or even more.

3.2.1. Measurement procedures

Carrying out a 2-D resistivity survey needs a large number of electrodes, 25 or more, connected to a multi-core cable. A laptop microcomputer and an electronic switching unit automatically select the relevant four electrodes for each measurement. Various electrode arrays, such as Wenner, dipole-dipole, and Schlumberger, among the others can be used. Figure (3.5) shows a possible sequence of measurements for the Wenner electrode array for a system of just 20 electrodes where "a" is the constant spacing between electrodes.
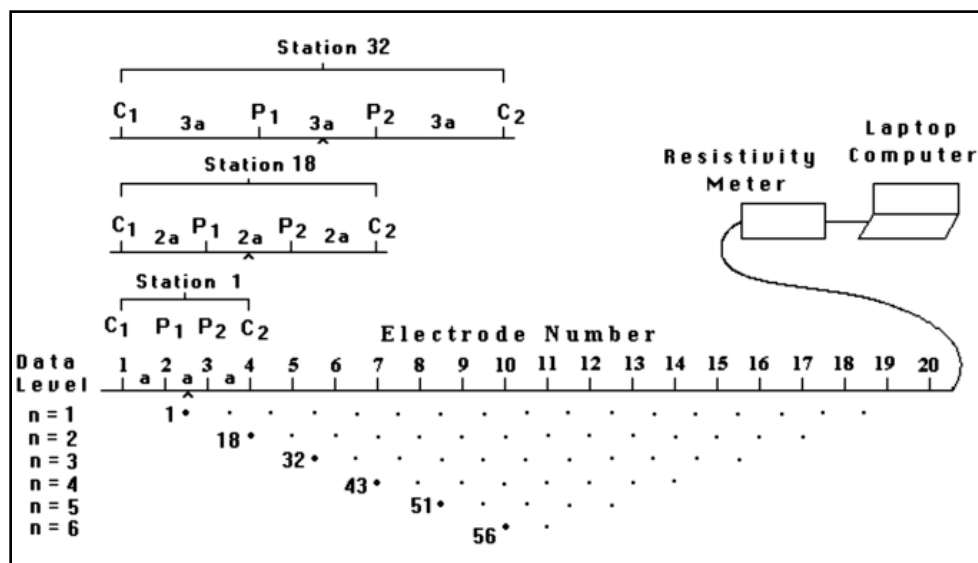
Fig. 3. 5: Arrangement of electrodes for a 2-D resistivity survey (Loke, 2001).

45

3.2.2. Data processing

The field data, in the form of resistivity profiles, have been processed and inverted using the RES2DINV software. This program is designed to process the data and construct two-dimensional real resistivity models of the subsurface. It was designed to invert large data sets (with about 200 to 5000 datum points) gathered by the system with many electrodes, according to the flow chart shown in figure (3.6). The program supports both finite-element and finite difference forward modelling techniques. It can be used for surveys using Wenner, dipole-dipole, pole-pole, Schlumberger and Wenner-Schlumberger arrays. It also supports other non-conventional arrays.
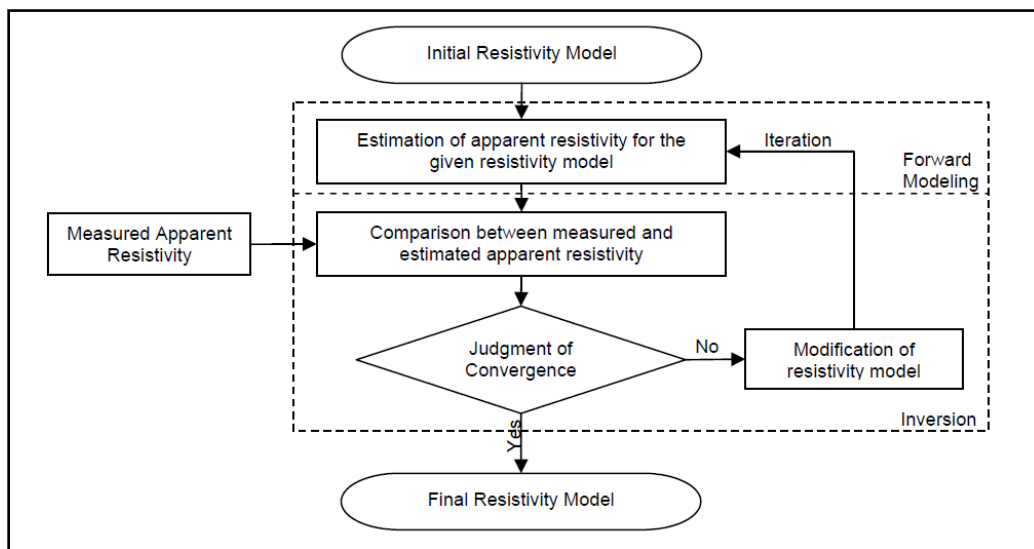
Fig. 3. 6: Flow chart of the resistivity inversion process.

3.2.3. Electrical Resistivity Meter

In this study, resistivity data was collected using **SYSCAL R2Resistivity Meter** (IRIS Instruments, Orleans, France) shown in figure (3.7). The SYSCAL R2 is a high-power fully automatic resistivity meter for DC resistivity surveys typically applied to groundwater exploration, environmental studies, civil engineering, structural geology investigation and mineral exploration.

It generates the current and measures its intensity, voltage, and standard deviation between repeated measurements which are then stacked to reduce random noises. It computes and displays the apparent resistivity for common electrode arrays such as Schlumberger and Wenner soundings and profiling.

This resistivity meter encompasses a controlled source of electric current and a unit for measuring the potential differences due to the current passing through the earth. To generate the current into the ground, it needs a converter, which transforms the 12 V of a battery to reach 800 V.

Fig. 3. 7: SYSCAL R2 resistivity meter and its components.

3.3. Transient Electromagnetic (TEM) Method

Among all the geophysical methods, the electromagnetic techniques have the broadest range of instrumental systems matched to various applications. Electromagnetic survey techniques have been successful applied in exploring groundwater and mapping groundwater contamination and depth to saltwater intrusion with fresh water, among the other applications **(e.g. Massoud et al., 2010; Khalil et al., 2012; Metwaly et al., 2014)**.

EM techniques can be broadly divided into two main groups: Time –Domain (TEM), which makes measurements as a function of time (a.k.a. Continuous Wave), and Frequency- Domain (FEM), which uses one or more frequencies (a.k.a. Pulse Transient). EM method is based on electromagnetic induction, so it does not require direct contact with the ground like in the electrical resistivity method. Therefore, EM field acquisition is usually made much faster than electrical methods. It can also be used on land, airborne, seaborne and down-hole.

3.3.1. Induction theory

The basis of electromagnetic methods is the induction law. Michael Faraday discovered the phenomenon of electromagnetic induction in 1832. The complete system of laws of electromagnetism was formulated by James Clerk Maxwell in 1864.

The EM induction process is summarized as follows:

- An EM transmitter outputs a time-varying electric current into a transmitter coil. The current in the transmitter coil generates a magnetic field of the same frequency and phase (The Primary Field).

- Lines of force of this magnetic field penetrate the subsurface conductors in the earth. Accordingly, an electromotive force (EMF) or voltage is set up within the conductor according to Faraday's law.

- In response to the induced EMF, eddy (secondary) current will flow in the conductor in planes perpendicular to lines of the primary magnetic field from the transmitter, as shown in figure (3.8).

- Current flow within the conductor generates a secondary magnetic field whose lines of force at the conductor are opposing to the primary magnetic field.

- The receiver coil, placed at some distance from the transmitter coil, is therefore energized by two fields: the primary field from the transmitter and the secondary field from the induced currents in the ground.

- The induced currents occur throughout the subsurface, and the corresponding secondary magnetic fields are functions of the transmitter frequency, power, geometry and the distribution of all electrical properties in the subsurface.

- The induced currents and the accompanying secondary magnetic field can be measured either while the primary field is transmitting (FDEM) or after the primary field has been switched off (TDEM).
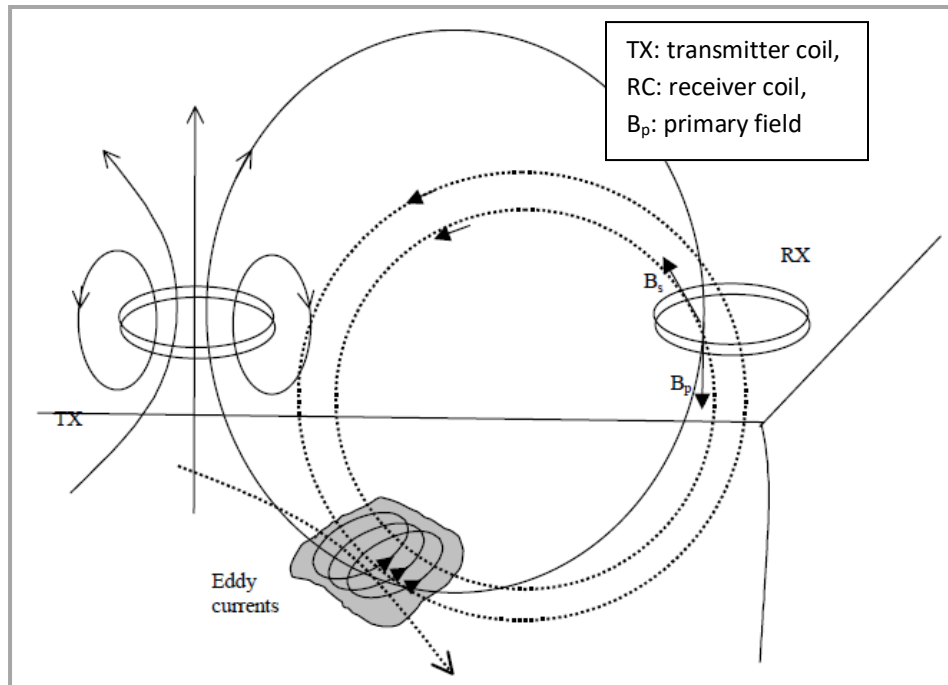
Fig. 3. 8: Electromagnetic induction process (Klein and Lajoie 1980).

3.3.2. Basic concept of TEM

The transient electromagnetic method (TEM) is an inductive method that utilizes a strong direct current passed through a loop commonly laid on the ground surface. The flow of this current in the surface loop will create a magnetic field that spreads out into the ground in the form of a primary magnetic field. When the applied current is abruptly terminated, the primary magnetic field is decayed with time. Suppose a conductor is present in the subsurface. In that case, the decay of the primary magnetic field with time, according to Faraday's law, will induce **eddy currents** that flow in the subsurface conductor. The rate of change of these currents and their respective secondary magnetic field characteristics depend on the subsurface conductor's size, shape, location and conductivity.

These **eddy currents** will initially flow at the surface of the conductor which is known as the "early-time stage" of the transient process. The zone immediately within the conductor experiences an inward diffusion of the eddy current which is

called the "intermediate-time stage" of the transient process. This process's final or "late-time" stage is reached when the induced current distribution is invariant with time. The only change observed is a decrease in the overall amplitude with time, as shown in figure (3.9).

3.3.3. Transmitter and receiver waveforms

The transmitter current waveform consists of positive going and negative going pulses between them. There is an *off-time* period, as shown in figure (3.10). The *off-time* always equals the *on-time*. The TEM signal is measured only during the transmitter off-time period, i.e. in the absence of the primary field. The output voltage of the receiver coil is shown schematically in the figure. In order to measure the characteristic decay of a voltage, the receiver is set to contain many narrow time gates (depending upon the instrument), each opening sequentially to measure (and record) the amplitude of the decaying voltage at successive times equal to the number of time gates.
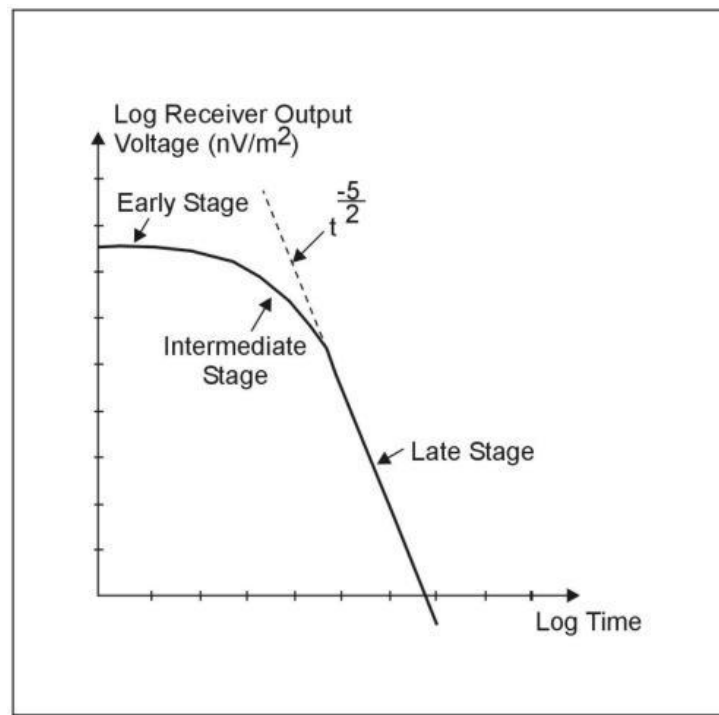
Fig. 3. 9: Stages of the induced voltage at the receiver coil.
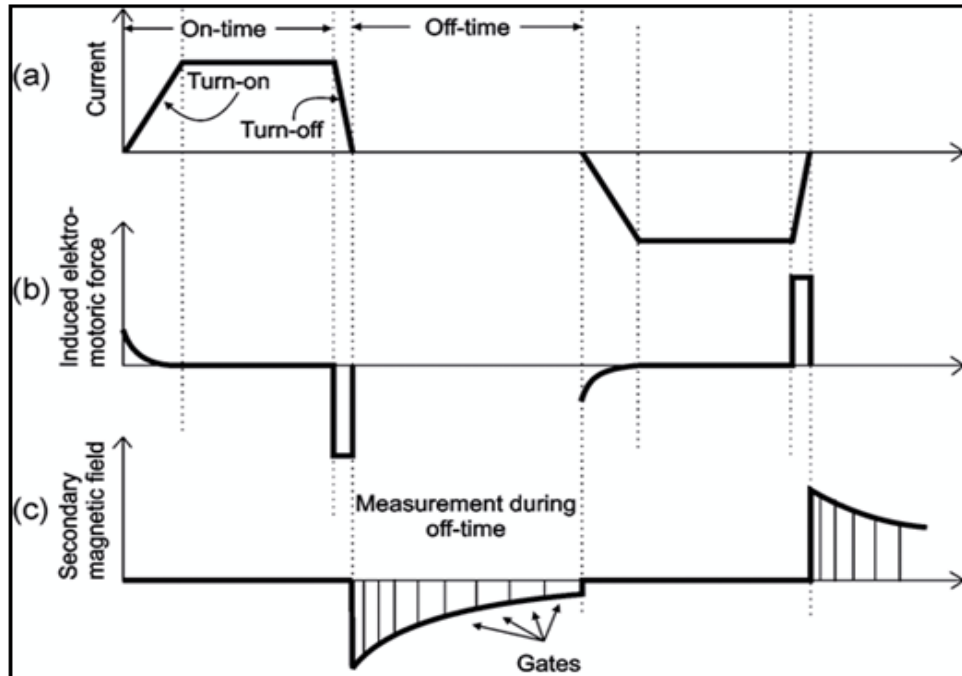
Fig. 3. 10: Schematic diagram showing the typical transmitted and received signals for EM systems (after Swift, 1990).

This feature offers a significant advantage over frequency-domain electromagnetic (FDEM) measurements, which are generally very sensitive to transmitter/receiver coil spacing variations since the FDEM receiver measures while the transmitter current is flowing. On the other hand, FDEM equipment can exploit smaller loops located at shorter distances than TDEM because by lowering the current frequency it is possible keeping constant all the other parameters, reach deeper layers,

3.3.4. TEM resistivity sounding

The basic principles of TEM resistivity sounding are relatively easily to understood and describe.

- Electric current flows through the transmitter loop and generates a **static** primary magnetic field.

- The transmitter current is then **switched off** and the primary magnetic field immediately falls to zero. This change in magnetic field induces a

secondary electric current in the Earth. Immediately after the transmitter current is turned off, the current loop can be thought of as an image the transmitter loop in the ground (Fig. 3.11).

- The secondary electric current distribution can be approximated as a horizontal **loop of current** and generates a secondary magnetic field.

- Over increasing times the secondary electric currents spread out (diffuse) in a pattern that is similar to a smoke ring. The secondary currents move deeper as time increases, and thus give information about progressively deeper structures.

- The velocity (Vz) with which the ring expands away from the transmitter at a time (t) is given by: $V_Z = 2\sqrt{\pi\sigma\mu t}$. Where, σ is the conductivity and μ is the magnetic permeability of the medium (Nabighian, 1979).
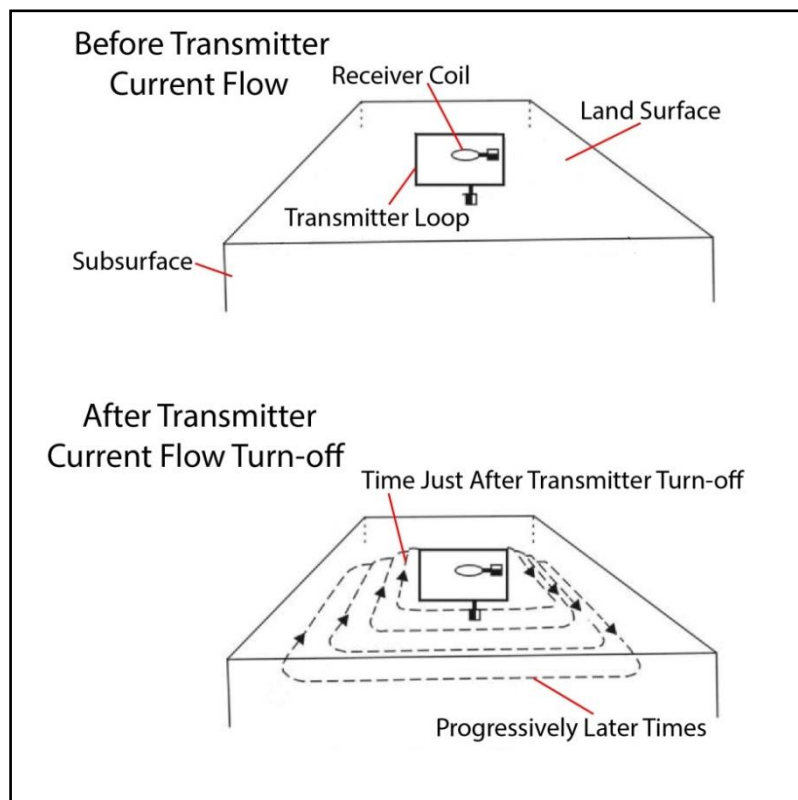
Fig. 3. 11: Transient current flow into the ground.

3.3.5. Apparent resistivity from induced voltage

The response recorded at the receiver is generally a complex function of conductivity and time. However, during the late-time stage, the mathematics simplifies considerably, and it can be shown that during this time, the response varies quite simply with time and conductivity as:

$$e(t) = \frac{k_1 M \sigma^{3/2}}{t^{5/2}} \dots\dots\dots\dots(3.6)$$

*K_1= constant, M = product of current (amps) * area (m²), t =time in seconds, σ = conductivity of half-space (Siemens/m), and e(t) = output voltage from a single turn receiver coil of 1 m² area (Ward and Hohmann, 1987).*

Output apparent resistivity can be estimated from the following relation, where K_2 is a constant.

$$\rho_a(t) = \frac{k_2 M^{2/3}}{e(t)^{2/3} t^{5/3}} \dots\dots\dots\dots(3\text{-}7)$$

3.3.6. Sources of noise

Noise sources for TDEM soundings can be divided into four categories:

- Circuit noise (usually so low in modern receivers as to rarely cause a problem).
- Radiated and induced noises.
- Presence of nearby metallic structures.
- Soil electrochemical effects (induced polarization).

The radiated noise consists of signals generated by radio, radar transmitters and thunderstorm lightning activity. The response from metallic structures can be orders of magnitude higher compared to the ground response. The most important source of induced noise is the intense magnetic fields from 50- to 60-Hz power lines. The significant signals induced in the receiver from these fields can overload

the receiver if the gain is set to be unduly high and consequently cause severe errors. The treatment is to reduce the receiver gain so that overload does not occur. Another alternative solution is repositioning the measurement array further away from the power line.

A relatively infrequent effect, but one which can arise, particularly in clayey soils, is that of induced polarization. Quick termination of the transmitter current can charge up the minute electrical capacitors in the soil interfaces. These capacitors consequently discharge and produce flowing currents similar to the transmitter eddy currents but in the opposite direction. Since these sources of reverse current are localized near the transmitter loop, using the offset configuration usually decreases the errors caused by them to small values. The net effect is to decrease the amplitude of the transient response (hence increasing the apparent resistivity), where the effect is very intense, to cause the transient response to become negative over some range of the measurement duration.

3.3.7. TEM resistivity meter

TEM measurements were conducted in the present study using **SIROTEM MK3** instrument made by Geo Instruments, Australia. This instrument detects underground conducting materials by transmitting electrical pulses along loops of cables spread on the Earth's surface. Also, it is considered unique to have the transmitter and receiver in a single robust, portable console unit shown in figure (3.12).

Fig. 3. 12: Console unit of SIROTEM MK3 resistivity meter.

Chapter (4)

Field Survey, Data Processing and Interpretation

The main focus of this chapter is characterizing the principal groundwater aquifers in the study area by applying electrical resistivity and transient electromagnetic techniques. After carrying on the field measurements, the collected data was processed and interpreted. Final results are presented in the form of textual and integrated graphical displays to clarify our conclusion and addressing the main objects of this study.

4.1. Working Plan

In the present study, the following stages are followed:

• VES and TEM measurements were acquired nearly at identical sites within the studied area to be suitable for carrying out the joint inversion. These measuring stations were arranged along five by seven, parallel, NS-EW trending profiles (35 data point stations).

• The VES and TEM data were first inverted into resistivity-depth multi-layer models. Then, joint inversion of VES and TEM data were performed to obtain a joint model for each site that combines both datasets.

• The joined models were used for the construction of three geoelectric cross-sections to represent the lateral variation in geoelectric properties of the subsurface medium from south to north of the area of interest.

• Groundwater occurrences in the study area are manifested by developing contour maps showing the resistivity distribution, as well as thickness and depth to the upper surface of the aquifers.

• As far as the environmental part of the study, an high resolution 2-D resistivity tomography survey was conducted along eleven profiles beside one of the largest lakes resulted from water logging problems, and hydrochemical analysis of some water samples have been done (described in details in Ch. 5).

• At the end of this study, conclusions and some recommendations are provided and shall be communicated to decision makers and stakeholders to be considered in the future development plans of the city to optimize water exploitation.

4.2. Data Acquisition

4.2.1. VES data

In the present study, resistivity measurements were conducted at first by applying Vertical Electrical Sounding (VES). The survey was conducted at 35 stations arranged in form of a grid of 5 by 7 points, trending from Cairo-Ismailia Desert road in the south until El-Salhiya city in the north and from El-Kasasin in the west to Abu Suweir in the east (Fig. 4.1). The study area is about 10 by 14 km with fixed stations inter-spacing of about 2 km in both directions. Resistivity data were measured using *SYSACAL-R2* resistivity meter by applying the standard Schlumberger electrode configuration with current electrodes (AB) spacing varying logarithmically from 2 up to 1000 meters.

As we discussed in chapter two, the topography of the investigated area is mainly characterized by changing in the elevation along the profiles going from south to north (Fig. 4.2). So, to study the effect variation in the ground elevation on the depth of groundwater aquifers, the configuration of the measurements grid for the study area has been made in order to fulfil this requirement, as shown in figure (4.1).

4.2.2. TEM data

In this work, the ***SIROTEM MK3*** instrument was used for collecting the TEM survey. TEM data have been recorded exactly at the same locations of VES data (Fig. 4.1). At some stations, the field measurements were repeated two or three times with different acquisition parameters. The common single-squared loop configuration with a loop side length of 100 m has been employed, where the same loop was used for transmitting and receiving the signals. In the present study, the measurement duration ranges from 0.2 to 28.6 msec.
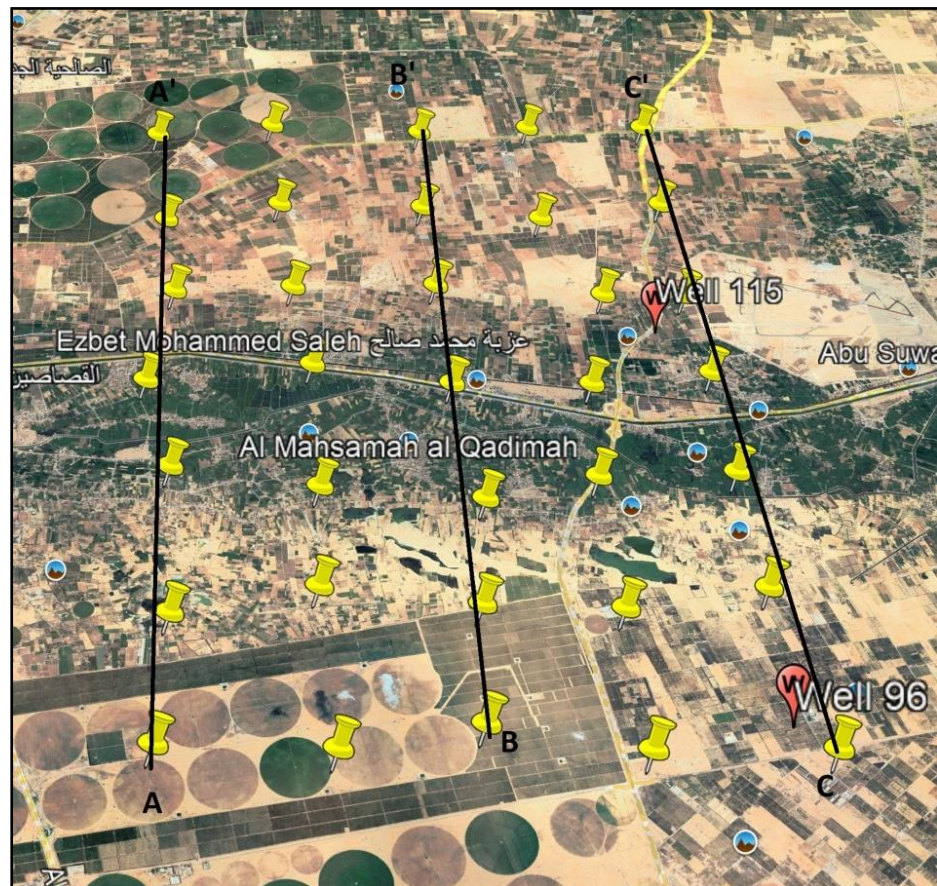
Fig. 4. 1: Location map of the measured VES-TEM data sites.
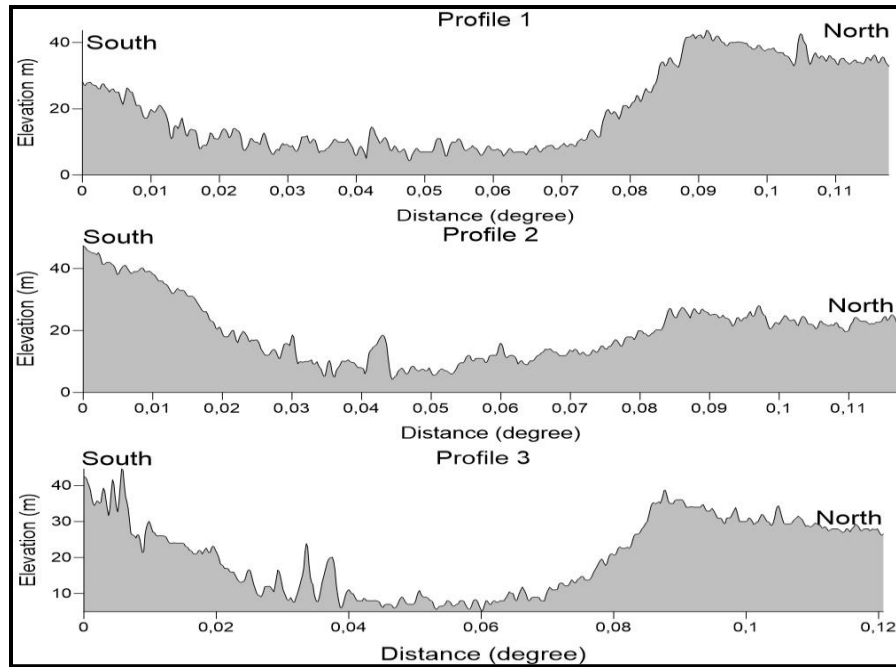
Fig. 4. 2: Elevation profiles across the study area.

4.3. Precautions during the field survey

The proper selection of the measuring locations during the field work is very important to avoid fundamental sources of noise. The following list describes the most common noise sources in VES-TEM data:

1. The VES-TEM locations were selected to be as far away as possible from external electrical fields resulting from electrical cables or high potential lines.

2. In resistivity method, the contact of electrodes was checked with each reading as in case of very dry soil the resistance of current electrodes becomes anomalously high and the applied current may fall to zero and the measurement will fail. In such case, to improve electrodes contact with the ground, some water needs to be added around current electrodes. Fortunately, we didn't need to perform special events as the conductivity of

the shallowest layer was in general very high, so there was a good electric contact between the electrodes and the ground.

3. As the TEM method is inductive and no electrodes are fixed into the ground, it is more sensitive to both external and internal noise sources. So, we tried to improve the signal/noise ratio by increasing the number of stacking and lowering the gain factor in highly noise sites.

4. The VES array was expanded along a straight line to avoid introducing errors in the geometric factor value which is used to calculate the apparent resistivity.

5. The TEM data was measured, at the same site, after the VES data collection thus avoiding the electromagnetic coupling between the current sources of both methods.

4.4. Qualitative Interpretation of the Sounding Curves

4.4.1. VES curves

In the resistivity sounding mode, the half current electrode spacing (AB/2) is increased at successive intervals and the value of the appropriate apparent resistivity (ρ_a) is measured. The measured apparent resistivity values are plotted against the half-current electrode spacing on logarithmic graphs to give the resistivity sounding curve. It is worth mentioning that, during the data acquisition, the readings were plotted directly on log-log plots in the field to follow up and check the behaviour of the resistivity sounding curve in real time. Unlike a theoretical curve, the field sounding curve comprises several overlapping segments. The segmented curve is processed and reduced to a continuous curve prior to its 1D interpretation **(Kunetz 1966; Zohdy et. al., 1973).**

Then, resistivity sounding curves are qualitatively interpreted before the subsequent inversion and detailed quantitative interpretation. Qualitative interpretation is used to give a general view about the vertical and lateral (i.e. between one VES and the others) variations of the electrical properties, and to shed light on the geological and hydrogeological conditions of the area under investigation. The qualitative interpretation of the apparent resistivity curves, although somewhat crude compared to the one performed on inverted data, is quite helpful to keep abreast of daily measurements during the fieldwork and as a preliminary quality control step. It includes a comparison of the relative changes in the apparent resistivity and approximated thickness values of the different layers detected from the sounding curves. Also, it gives information about the number of layers and their continuity throughout the area or in a certain direction and reflects the degree of homogeneity or heterogeneity of the individual layer.

Figure (4.3 a, b and c) shows some exemplary resistivity sounding curves obtained at the study area.

From the first insight for the resulted curves of the applied VES that were measured in the study area, three main patterns can be distinguished for all of them. These patterns are consistent with the main subsurface condition of the study area. So, based on the geoelectric properties, the study area was divided into three major parts:

1. Um Gidam plateau in the southern part with elevations ranging from 30-40 m. Two profiles, directing E-W, including 10 VES-curves, were conducted at the plateau. Here, we took VES-curve no.5 as representative for the whole VES-curves in this area, as shown in figure (4.3 a) since most of the remaining VES-curves are characterized by a very similar trend. The

apparent resistivity values for the first logarithmic cycle of the measured curve show different features due to the heterogeneity and rapid variations characterizing the surface and near-surface layers. Most of the sounding curves exhibit a Q-type curve with a similar descending behaviour for AB/2> 100.

2.   Wadi El-Tumilat, in the middle part of the study area, includes three profiles with elevations not exceeding 2 m. Here, most of the curves show a combined type (H-K and K-H) with the same descending behaviour, except for the last profile (VES 21-25), which is conducted at the borders with El-Salhiya, as shown in figure (4.3 b and c).

3.   El-Salhiya Plateau to the north, where the elevations raise again reaching more than 45 m. Here all the curves are of K- type, as shown in figure (4.3 d).

From this first analysis, we concluded that Wadi El-Tumilat is characterized by a peculiar situation that is responsible for the presence of combined VES curve types.
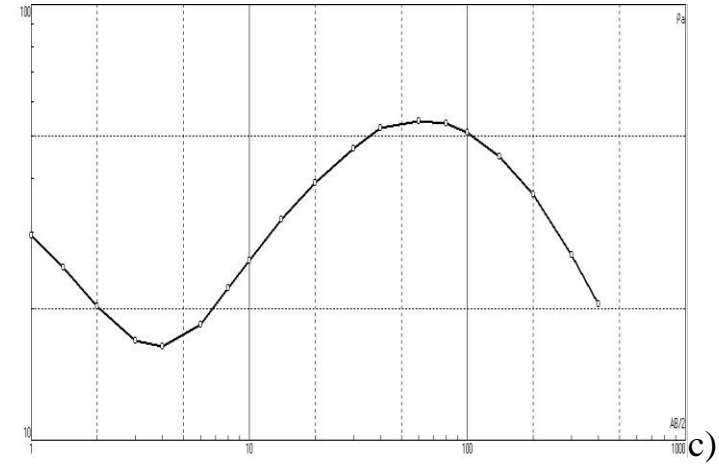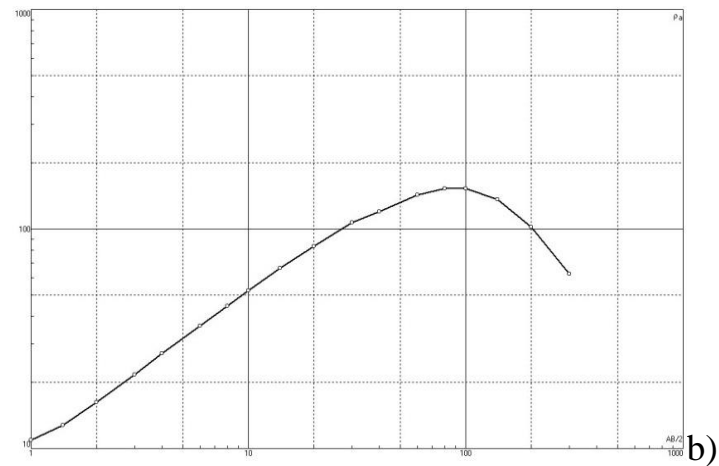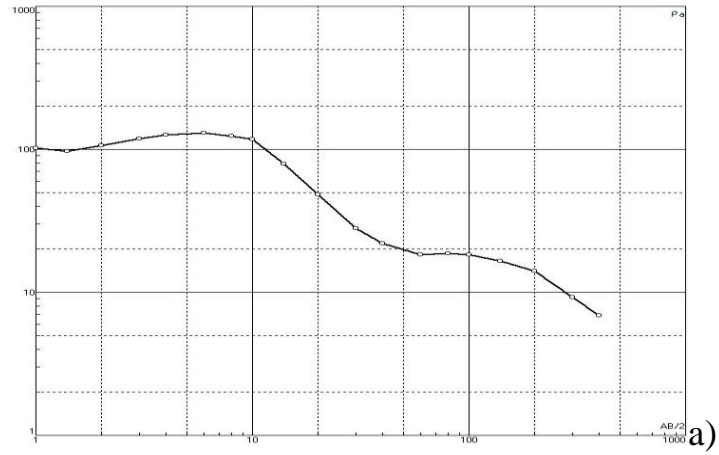
Fig. 4. 3: Exemplary resistivity curves obtained at (a) VES No. 5, (b) VES No. 16 and (c) VES No. 31.

4.4.2. TEM curves

Figure (4.4) shows the results of the TEM sounding at the measuring point No. 12. The left panel shows the quantity measured by the receiver coil which is the voltage decay as a function of time through a transient response after switching-off of the primary magnetic field. The values are plotted logarithmically in nano Volt (nV) normalized by the transmitter current in Ampere (A) and the coil area in square meter (m2). The normalized voltage quantities show a wide dynamic range of the voltage over six decades. The slope of the curve changes gently between 1.0 and 2.0 sec. and shows another broad change between 4.0 and 8.0 sec. The right panel shows the calculated apparent resistivity values corresponding to the normalized voltage. Generally, the resistivity curve shows low to moderate values which are greatly correlated with the conductive, water-bearing, lithologic section in the investigated area. Despite of the electrically conductive medium dominated in the studied area, the resistivity curve shows relative variations, where the values show firstly a gradual decrease through the time interval 0.5 -1.5 sec., an increase though the time range 1.5-6.0 sec. , then another decrease which is continuing down further until the end of the recording time. Although the qualitative interpretation gives an idea about the resistivity variations, it cannot estimate the depths at which the resistivity changes occur. So, the data modeling and inversion are necessary.
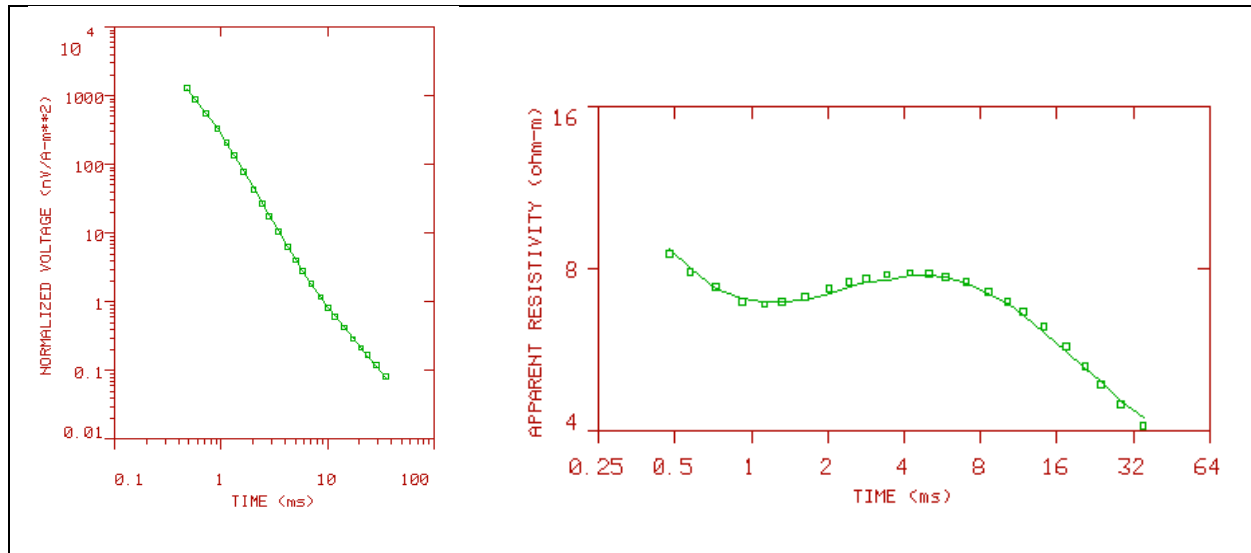
Fig. 4. 4: Results of the TEM sounding at measuring point No. 12.

4.5. Quantitative Interpretation of VES and TEM data

4.5.1. VES data inversion

By performing VES curves inversion, we can obtain a model of true resistivities and layer thicknesses.

Here, ***IPI2Win 1-D program (2000)*** was used for VES data inversion. This program is designed for automated and interactive semi-automated inversion of VES data for any array configurations adopted in geoelectrical prospecting. IPI2Win 1-D is further used for 1-D interpretation of VES curves along a single profile. With this program, the interpreter is able to choose from a set of equivalent solutions giving the best fitting in both geophysical and geological data.

To build the initial model that is introduced for the inversion process for our data, we depended on the priori information we got from reviewing geological and hydrogeological studies conducted in the study area. Figure (4.5) shows some field curves, multi-layer models and the calculated model responses obtained from the inversion process of VES data. The RMS mis-fit errors for all the inverted VES

data have very low values ranging from 0.935 to 1.76 %, which is a good indication for accuracy and robustness of the obtained models, even they have to be indeed carefully evaluated and checked for their geological reliability.

The final output of the quantitative interpretation is a set of multi-layer models; each of them describes the geoelectric parameters of the subsurface layers at its respective site (see the appendix).

a)

b)
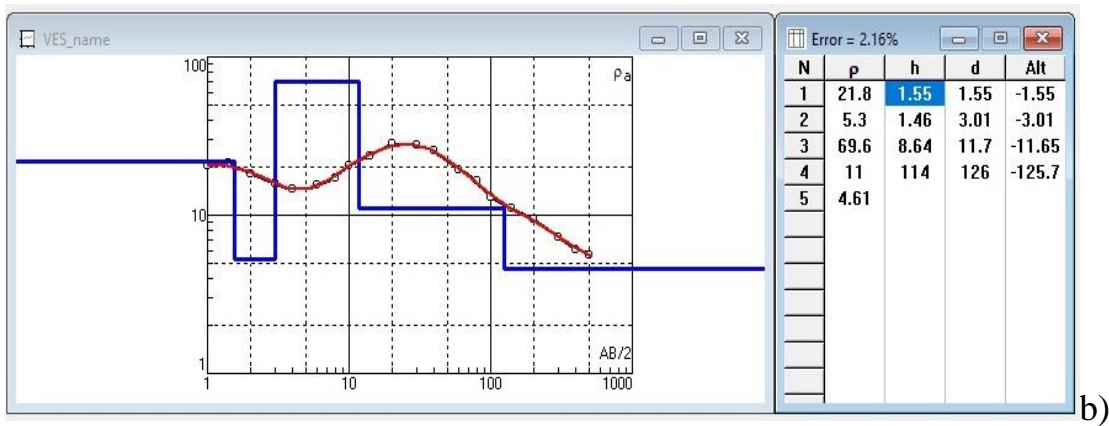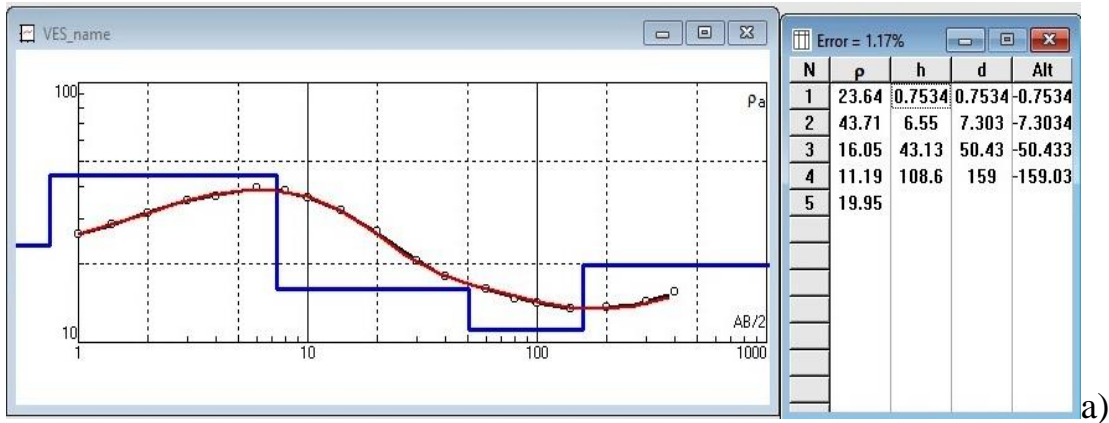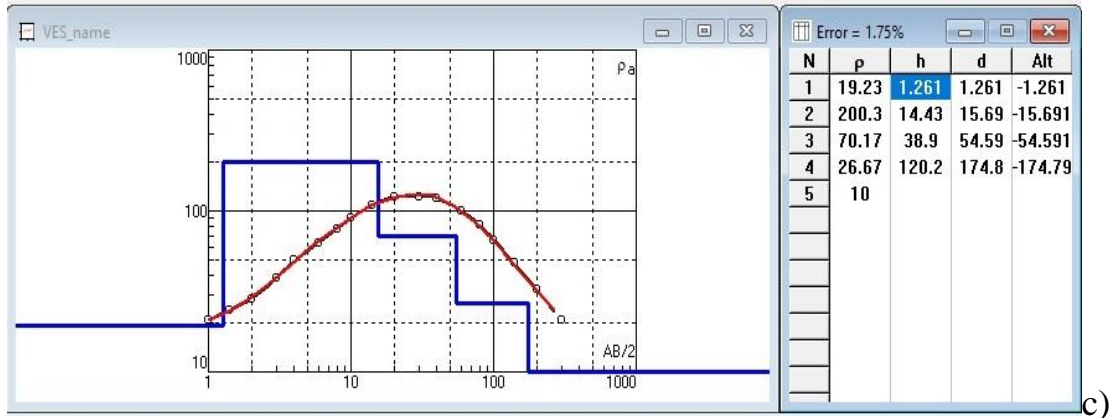
Fig. 4. 5: Multi-layer model obtained from data inversion at VES No. (a) 1, (b) 15, (c) 32.

4.5.2. TEM Data Analysis

In this study, inversion of the TEM data was performed by *TEMIX XL 4* software. To obtain more constrained results, the obtained VES models were used as initial models for inversion of the comparable TEM data, as the VES-TEM data sets were measured at approximately identical locations and almost at the same time. Figure 4.6 a and 4.6 b shows two examples of the TEM models obtained from the TEM data inversion. The final output of the TEM data inversion is a set of multi-layer models describing the geoelectrical parameters of the subsurface layers (see the appendix). For sounding 3, a six-layer model fits with the data with a mean misfit error of 2.59% while for sounding 19, the model consists only of five layers with 2.8% mean misfit error.

DATA SET: 3-122 **% ERROR:** 2.5891 **DATA BASE: ISMAILIA.TEX**

Point cursor at segment - hold left button and move RES: 0.3477 DEP: 364.192
+ add layer − delete layer rePlot Quit editing

LAYER #:	1	2	3	4	5	6 NEXT LYR
RESIST.:	42.7672	3.6884	16.4653	5.7593	1.7181	1.0324
DEPTH:	14.7439	36.7608	100.156	152.0509	276.6541	--INF-

a)

DATA SET: 19-38 **% ERROR:** 2.8411 **DATA BASE: ISMAILIA.TEX**

Point cursor at segment - hold left button and move RES: 0.071 DEP: 240.795
+ add layer − delete layer rePlot Quit editing

LAYER #:	1	2	3	4	5 NEXT LYR
RESIST.:	48.6409	129.5064	14.9119	2.249	1.0668
DEPTH:	9.418	34.65	139.6228	217.8278	--INF-

b)

Fig. 4. 6: Exemplary multi-layer model obtained from TEM data inversion at station No. 3 (a) and 19 (b).

4.6. Geoelectrical Cross-sections

Based on the available geological and hydrogeological information, the obtained multi-layer models from both VES and TEM methods were used for constructing three geoelectrical cross-sections (A-A`, B-B` and C-C`) crossing the study area

69

from S-N as shown in figure (4.1). These sections were constructed at first by using the VES models and then by means of the TEM models trying to correlate both methods. Here, we describe only the first cross-section (A-A') for each method, while the global interpretation is provided later on section 4.7.4.
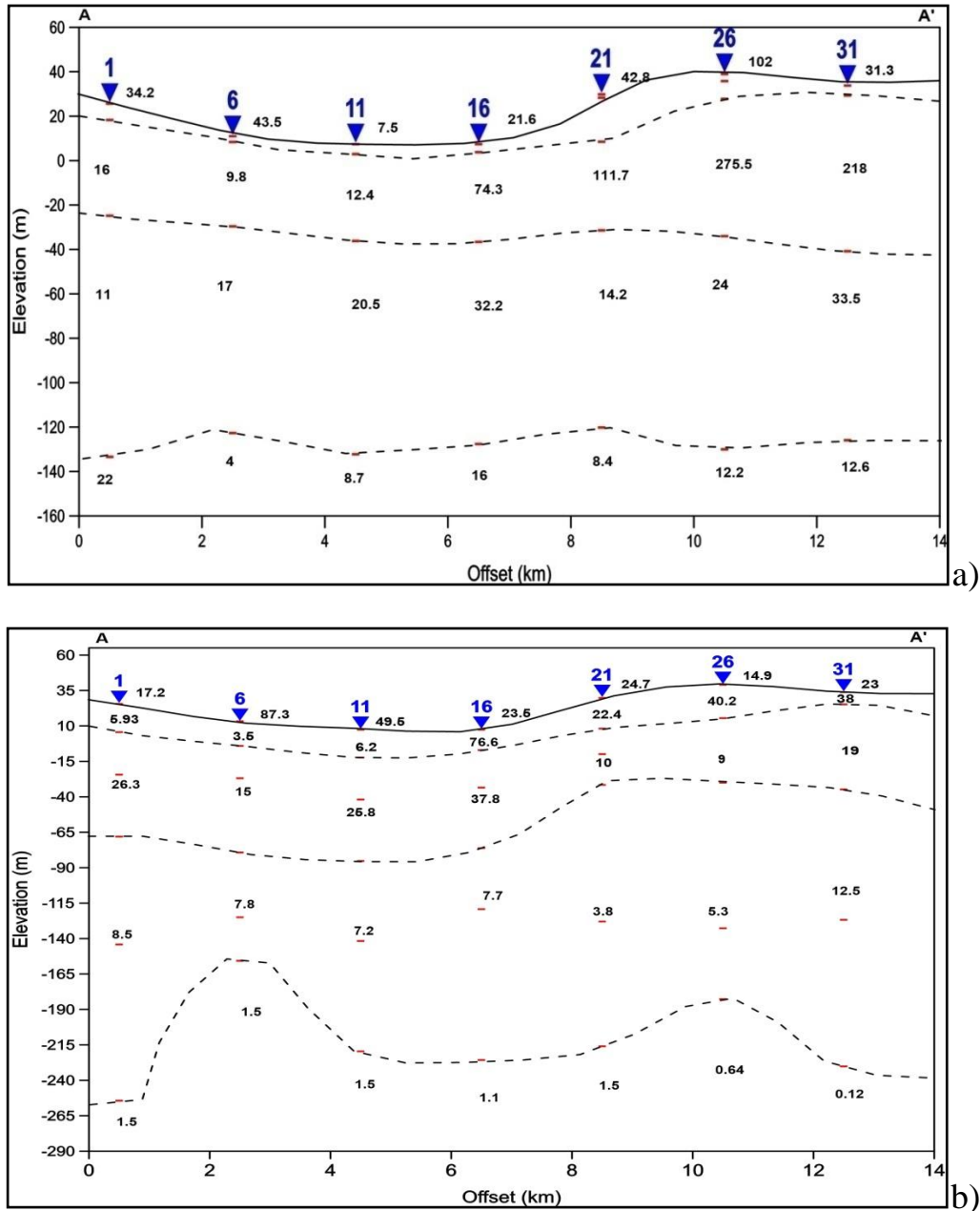
Fig. 4. 7: Geoelectrical cross-section A-A` obtained by (a) VES and (b) TEM models.

Actually, we are not going to describe these sections, individually, in detail as our main focus is the sections resulted from the joint inversion process. Now, we will just correlate between VES and TEM sections to reveal points of similarity and discrepancy, further explaining why the joint inversion process is important.

Inspection of these sections (Fig. 4.7) revealed that VES inversion includes five geoelectrical layers in most of the built models and six layers just for few locations. Meanwhile the inversion of TEM data resulted in geoelectrical models composed by six layers in most of the locations, while just some of them exhibit only five layers, as shown in the figure 4.7b.

In the above geoelectrical cross sections, the first 2- 3 layers of inverted VES models are integrated into one surface-heterogeneous layer as these first few meters of the subsurface are mainly made by the overburden which is typically laterally not homogeneous. This is based on the fact that DC resistivity data are very sensitive for the top most layers. Which means that it has the capability to identify near surface layers of relatively small thickness. In contrary, the TEM method is more sensitive to greater depths and cannot distinguish thin layers, but rather, it tends to compile the uppermost 10-15 m into just one single layer.

The Pleistocene aquifer occupies the middle part of the VES, and TEM geoelectric cross-sections comprise two geoelectrical levels but actually very close in term of resistivity value.

The Miocene aquifer is correlated to the last (lowermost) layer in both VES and TEM sections. This interpretation is justified taking into account the knowledge of subsurface lithology derived from available boreholes and other geological information of the area.

The differences are significant and meaningful when analysed in the light of the principle of operation of each technique. This can be clarified in the following points:

1. In DC resistivity measurements, the electric current flows through the subsurface layers vertically or horizontally (based on the type of survey we use) (or inclined near to vertical). Then, the current lines intersect a number of interfaces before giving the measured voltage response. Accordingly, the calculated apparent resistivity values (ρ_a) can be considered as a volumetric average of resistivities of a set of layers defined by the current pathways and geometry of the used array. In TEM soundings and immediately after transmitter current is turned off, this current flow moves outward and downward diminishing amplitude with time, like smoke rings. Then the measured response at the receiver unit is affected by the vertical, as well as, the lateral variation in the resistivity values.

2. The sensed volume of the ground is different in DC and TEM soundings. In the DC sounding, a large volume of the ground contributes in the measured response, while the ground volume in TEM sounding is slightly wider than the loop area.

3. The TEM method is mainly sensitive to conductive media as the induction process is strong only in low resistivity media. In addition, it is mainly sensitive to vertical changes in layer characteristics, which are clear in the cross section (fig. 4.7).

So, to combine the advantages of each method, get more constrained results, and to overcome the limitations of inverting each of them separately, we applied a joint inversion considering at the same time both datasets.

4.7. Joint Inversion

4.7.1. Introduction

Electric resistivity and time domain electromanetic techniques are commonly used in studies concerning shallow geology and characterization of groundwater aquifers e.g. thickness, depth, electrical conductivity and locating the best sites for drilling new wells (Fitterman and Stewart, 1986). However, the 1D models resulted from the individual inversion of each method are often ambiguous and do not reflect the real geological setting. Limitations of both methods in resolving subsurface structures were discussed by many scholars (Albouy et al., 2001). While VES method is effective in investigating shallow depths and has a good sensitivity for both conductive and resistive layers, TEM can well define the interface between resistive and conductive layers and has a greater sensitivity to deeper structures. These differences are in fact related to the different physical basis, as VES is a galvanic method, while TEM is based on the principle of electrical induction.

One of the main problems that arise from interpreting each method separately is the non uniqueness of the obtained models by data inversion. When a layer of intermediate resistivity lies between two layers with different resistivities, then the sounding curves may be matched by a model with only two layers. As the layers of the suggested model are usually kept to the minimum number needed to produce a reasonable fit between model and data (Albouy et al., 2001). This results in suppression the identity of the intermediate layer. Another situation arises if there is a thin layer of lower resistivity between two thicker layers, the geometry of this layer may not be uniquely defined by the model. This model equivalence effect means that soundings can be interpreted only in terms of the product of layer thickness and conductivity (inverse of resistivity) for such a relatively conductive

layer. This situation corresponds to a salt water aquifer lying between an unsaturated or fresh water saturated aquifer, and resistive basement or in the case of an electrically conductive clay aquitard separating two fresh water aquifers. Although VES and TEM soundings have important applications in the characterization of aquifers, the suppression and equivalence principles of DC and EM sounding interpretation clearly affect the ability to delineate certain classes of aquifers. The two techniques also have fundamental differences in the way they characterize subsurface structures. DC currents flow perpendicular to the layers' boundaries inside resistive layers and parallel inside conductive layers, while EM currents flow parallel for any resistive or conductive layers but are negligible in resistive layers. Therefore, integration between the two methods is the best option to reduce the ambiguities and limitations arising from the separate inversion of each single dataset. Because different types of data contain complementary information about the subsurface, it is expected that the non-uniqueness of the inverse problem is reduced (but not resolved) when data are inverted jointly. By the use of joint inversion, one can get use of the advantages of each method as VES method is good in defining resistive structures at shallow depths while TEM is more sensitive to conductive structures at deeper depths.

The use of joint inversion is already well known in many different field of geophysics (e.g. Raiche et al., 1985; Bortolozo, 2011, Bortolozo et al., 2015a, 2015b). There are many different approaches for joint inversion like Jupp-Vozof algorithm (Jupp and Vozof, 1975) and Price's (1977) CRS (Controlled Random Search) algorithm.   Some researchers such as Albouy et al. (2001) and Schmutz et al. (2000), showed how the joint inversion reduced the uncertainty of the inverted parameter(s) determination, becoming a great tool to constrain the geophysical and, in turn, the geological models.

4.7.2. Joint Inversion of VES-TEM data

In the current work, the VES and TEM sounding data were measured at approximately the same point locations, as previously described and shown in figure (4.1). When working with VES/TEM joint inversion, the first procedure to be applied is the static shift correction, which is essential to remove any static shift (if found) from the data. This guarantee the development of a joint model that can fit with both datasets without introducing spurious trends and errors related to different data ranges.

In this study, the algorithm implemented and developed by Bortolozo and Porsani (2012) was applied to convert VES data to time scale (s) as for TEM ones. This program is based on the equations proposed by Meju (2005) to covert VES and TEM data to equivalent scales. So, both of the two methods can be analysed in the same graph without any type of transformation as the equations are empirical and combine both numerical modeling and statistical analysis of a large set of field studies.

In our case, most of the apparent resistivity curves exhibit a small vertical shift relative to the overlapping TEM curves. In addition, the VES sounding curves show a reasonable degree of correlation with the TEM curves, thus confirming that they are suitable for the joint inversion.

VES and TEM data were jointly inverted by exploiting the **Curupira** program (Bortolozo and Porsani, 2012). The final output of VES-TEM joint inversion was a set of models; each of them describing the subsurface geoelectrical parameters at each specific site. The inversion of the data is done using the Price's (1977) CRS (Controlled Random Search) algorithm. The CRS is a very suitable global search algorithm when dealing with electric and electromagnetic methods (while it is not

ideal for other geophysical joint inversion). The geoelectrical parameters obtained from the inverted models and the squared misfit values are presented in the appendix.

In this section we provide and critically discuss the results of three representative examples of joint inversions for the study area obtained in Um gidam in the south (location 3), Wadi El-Tumilat (location 14), and El-Salhiya in the north (location 27).

- *Joint inversion of VES and TEM data at site 3*

The dataset of VES and TEM (3) used to construct this joint model were applied in the southern part of the study area in Um Gidam, at the elevation of 33.5 m. Fig. (4.8) shows the results of the individual VES and TEM inversions, as well as the joint inversion of both datasets. For a better comparison between the individual and joint inversions, Curupira program was used for running both the individual and joint inversions. Figure (4.8) shows different panels each comprises data and model response curves, geoelectric model (individual or joint) and geological profile resulted from the inversion. It is important to remember that not all geoelectric layers presented can be straight forwardly interpreted as a geological layer: in some cases, two (or more) geoelectrical layers correspond to one geological layer, while when the resolution or the measured parameter contrast of geophysical data are not sufficient, two (or more) geological layers correspond to one geophysical one.

The computed data misfit of the VES inversion shown in fig. 4.8(a) is about 1.2% and the geoelectric model is made of five layers interpreted as four geological layers. The topmost geological layer of the profile combines two geoelectrical layers with resistivity ranging between 58 Ωm and 333 Ωm and a thickness of 9.5

m. Normally, the top-most soil layer presents a wide range of resistivity, since it can be composed of different sediments whose composition and grain size are often not homogeneous. Such a layer is also subjected to many variations in composition due to human activities and weathering, as well as by pedogenic processes. The second layer is interpreted as well sorted sand with thickness of 28 m and mean resistivity of 13 Ωm. The third layer is correlated to gravel and sand with 120 m of thickness and 18 Ωm of mean resistivity.

It is obvious that these two latter geoelectrical layers can be actually interpreted as only one geological layer, since they exhibit nearly the same resistivity. However the data fitting is worst when performing this procedure, so we chose to include an extra geoelectrical layer thus minimizing the computed data misfit. The last geoelectrical layer has a mean resistivity value equal to 4 Ωm.

For the TEM inversion shown in fig. 4.8(b), the obtained model is made of six geoelectrical layers corresponding to four main geological layers. The top-most two geoelectrical layers are interpreted as only one geological layer that is presented as well-sorted sand with resistivity ranging from 5 to 16 Ωm and a thickness of 37.5 m. Comparing the top most part of the resulted geological section with the one resulted from the VES inversion, we can notice that the surficial soil layer appears at the top of VES model and not on the TEM. This occurs because of the different vertical resolution of the two methods being the VES more sensitive and resolutive in the shallower part, while the TEM is more sensitive with increasing depth. Based on that, we can notice that TEM data reached the Miocene aquifer at the depth of about 154 m and it is mainly represented by limestone, while in VES we just touched its upper surface. Therefore the joint inversion between the two methods is definitely the best solution, since it optimizes the resolution from one side and the penetration depth from the other.

Figure 4.8c shows the results of the joint inversion. We can notice that the error is 2.9% in case of DC joint inversion and 1.5% in TEM joint inversion. The result of the joint inversion is a geoelectrical model of six layers which were interpreted with five geological layers, as shown in figure 4.9c. The topsoil is 12m thick and has a mean resistivity of 87 Ωm. The second layer is also about 12m thick and mainly made of clay with resistivity value of 2.4 Ωm. The third and fourth layers represent the Pleistocene aquifer with resistivity ranging from 10 to 13 Ωm and a total thickness of 176 m, while the Miocene aquifer can be reached at a depth of about 200 m.

- *Joint inversion of VES and TEM data at site 14*

In this section the joint inversion of VES and TEM data for site 14 is taken as representative for Wadi El-Tumilat (4.9). The DC inversion resulted in five geoelectrical layers; the misfit is equal to 0.94%. In this example, the geoelectrical model is interpreted as a geological model with only four layers. In the TEM inversion, the misfit error is about 1.7% for the model constituted by six geoelectrical layers. This model was interpreted as a geological model having four layers. The VES is able to highlight the soil layer above the evaporitic loamy sand while TEM can only resolve the combination of both of them.

In the case of joint model, the adjusted misfit errors are equal to 1.7% and 2% for VES and TEM data, respectively. The resulted geoelectric model is made of six layers that were interpreted as five geological layers, with a maximum depth of 328 m. Here, the Pleistocene aquifer lies at a depth of 55 m and its resistivity ranges from 13 to 44 Ωm, while the Miocene aquifer is close to the maximum reached depth.
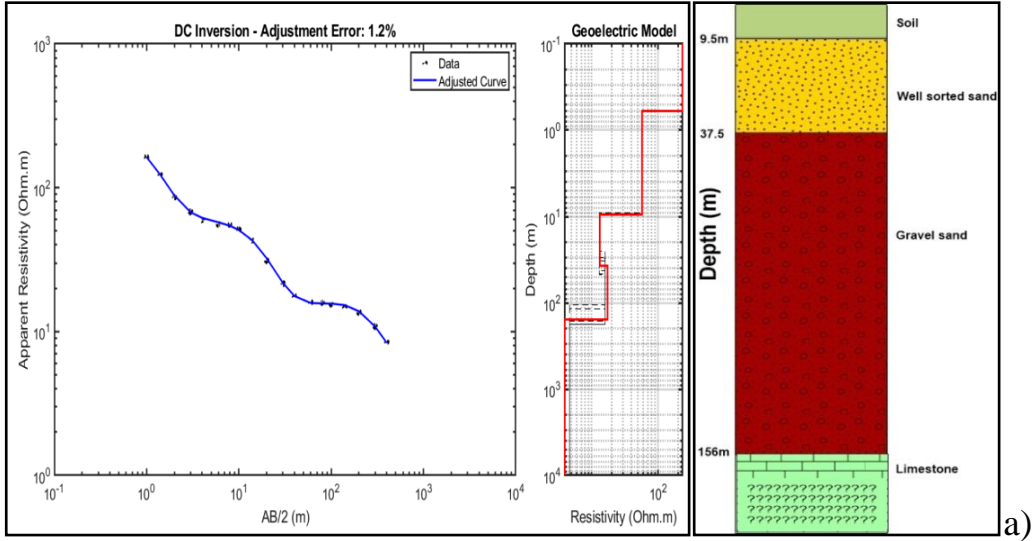
a)
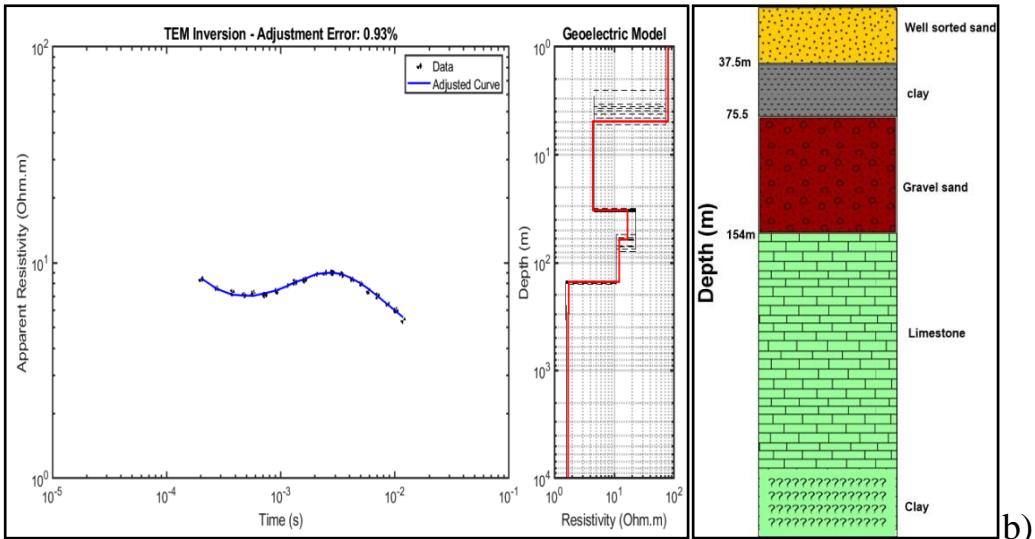
b)
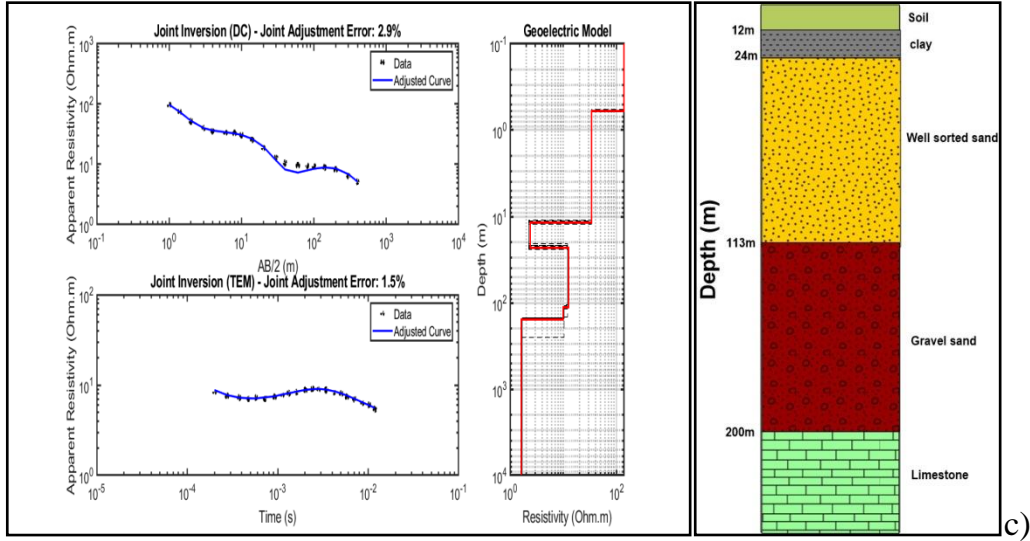
Fig. 4. 8: Results of joint inversion of dataset (3) and interpreted geological models (right side). a) VES individual inversion. b) TEM individual inversion. c) VES and TEM (3) joint inversion.

Fig. 4. 9: Results of joint inversion of dataset (14) and interpreted geological models (right side). a) VES individual inversion. b) TEM individual inversion. c) VES and TEM (14) joint inversion.

- *Joint inversion of VES and TEM data at site 27*

This dataset represents the northern part of the investigated area. For individual DC inversion, the error was 1.1% and the resulted model consists of five geoelectrical layers. Corresponding to five geological layers (4.10). The Pleistocene aquifer starts at a depth of 30 m, while the Miocene one at 194 m. TEM individual inversion resulted also in a five layers geoelectrical model with 0.55% misfit error. This model was interpreted as a four layers geological model where the first layer

81

is related to well-sorted sands that contain the Pleistocene aquifer. In the joint inversion, misfit error for VES and TEM data are equal to 2% and 3.7%, respectively. The resulted six layers geoelectrical model was related to six geological layers. The Pleistocene aquifer was encountered at a depth of 32 m, while the Miocene aquifer was reached at 270 m.
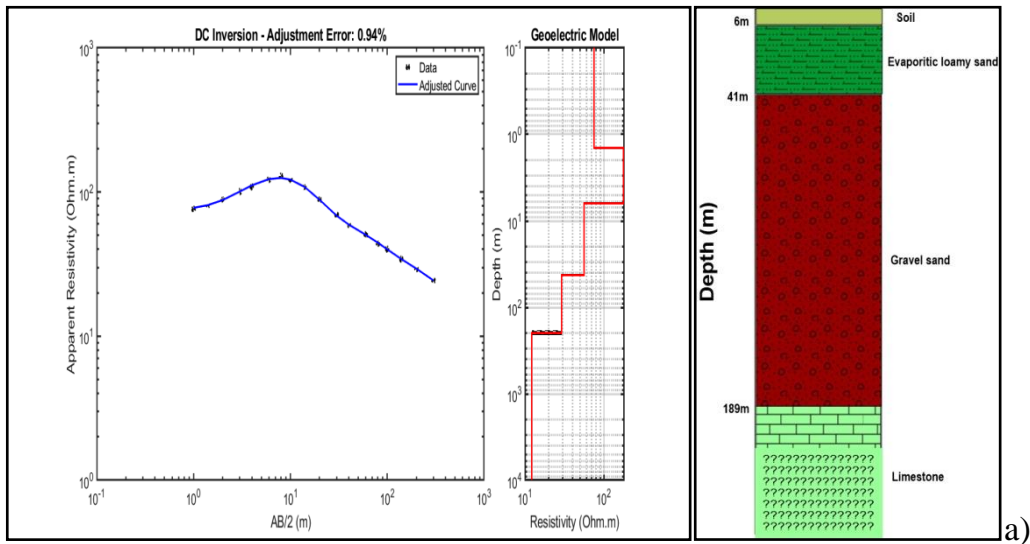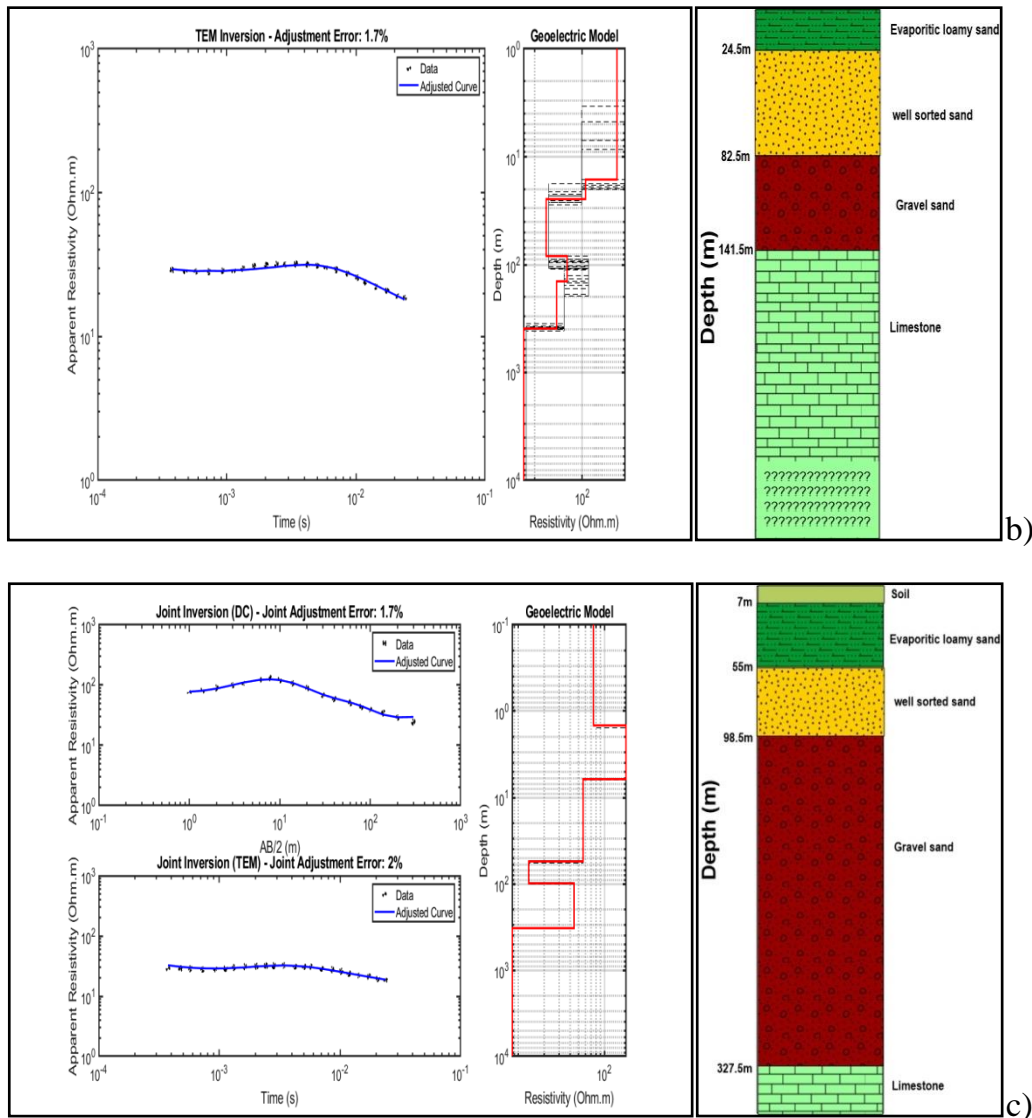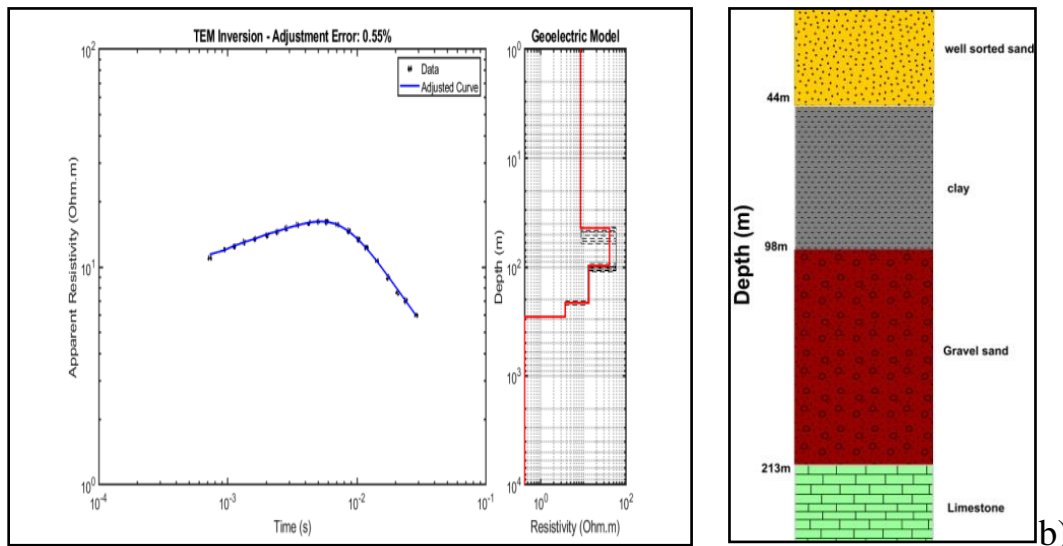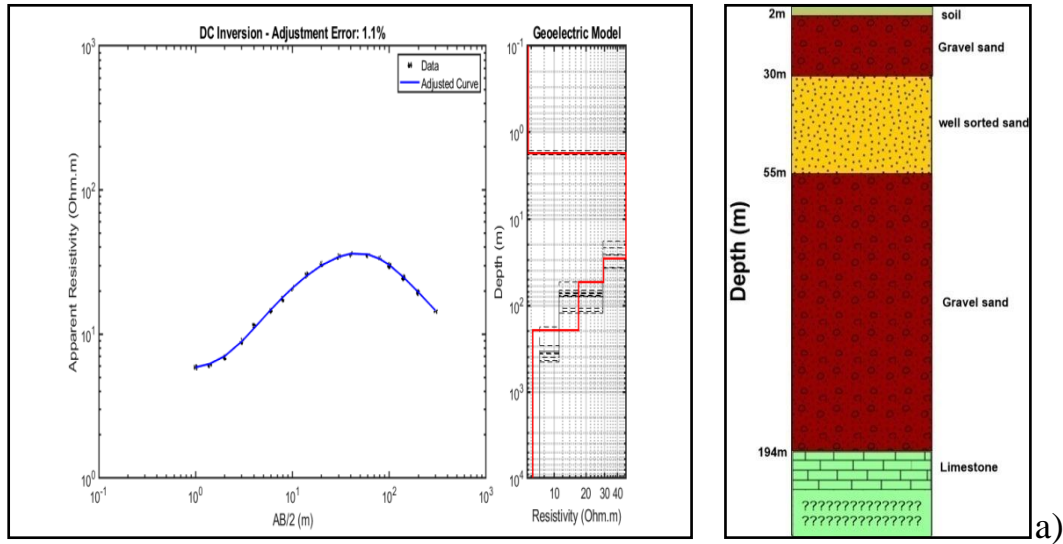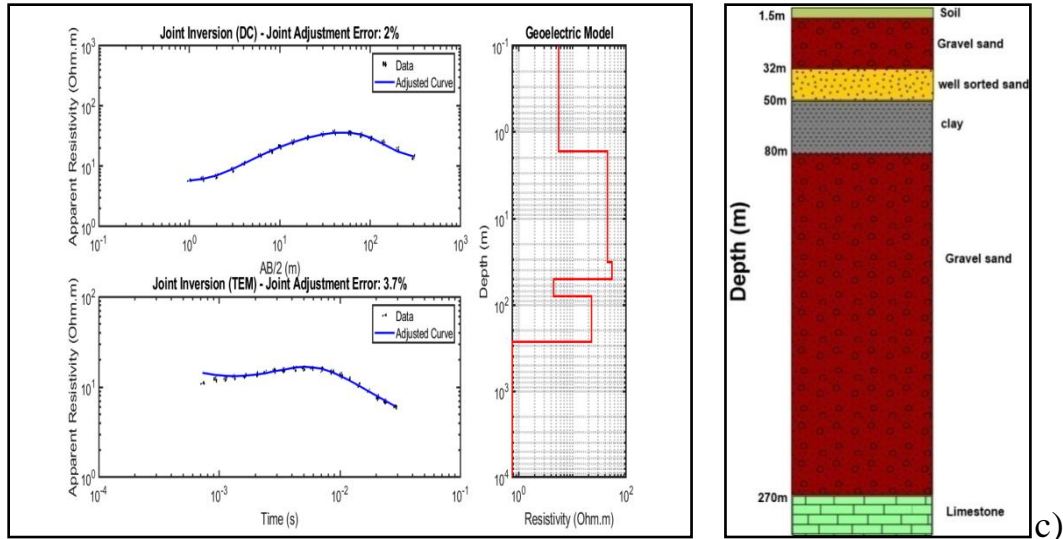

a)

b)

Fig. 4. 10: Results of joint inversion of dataset (27) and interpreted geological models (right side). a) VES individual inversion. b) TEM individual inversion. c) VES and TEM (27) joint inversion.

4.7.3. Geoelectrical cross sections from joint models

The multi-layer models obtained from joint inversion of VES and TEM data collected at each survey station have been used to construct three geoelectrical cross-sections S-N crossing the study area (A-A`, B-B` and C-C`) as shown in figure (4.1). Figure 4.11 (a, b and c) shows the 2D variation in geoelectric properties of these cross sections.

Inspection of the three geoelectrical cross-sections revealed that six geoelectrical layers can be identified. The most important conclusions deduced from these sections are:

- The uppermost two layers exhibit different resistivity values (from 1.2 to 134.2 Ωm) due to different weathering conditions close and far from the surface. Close to the surface there are Quaternary sand and gravel, while Wadi El-Tumilat is covered by fluvial sand and mud.

- The Pleistocene aquifer is equivalent to the fourth and fifth geoelectrical layers based on their resistivities. It has resistivity ranging from 4.9 to 94.8 Ωm. It attains a minimum thickness of 129 m at VES 23 and a maximum thickness of 273 m at ves14. It is mainly made of gravel sand and sandstones that are intercalated by many clay lenses.

- The Miocene aquifer comprises only the last geoelectrical layer and it is mainly made of limestone as shown in fig. 4.13. It shows resistivity values ranging from 0.7 to 22 Ωm. The upper surface of this layer lies at depths ranging from 130 to 327.6 m from the ground surface, while the bottom of this unit cannot be detected.

- Comparing these geoelectrical and geological cross sections representative for the study area (Fig. 4.12), we can see that there is a very good matching. The Miocene limestone is dislocated by a series of grabens and horsts which can be clearly detected in the three geoelectrical cross sections.

a)

Um Gidam-South — **El-Salhiya-North**

Um Gidam-South — **El-Salhiya-North**
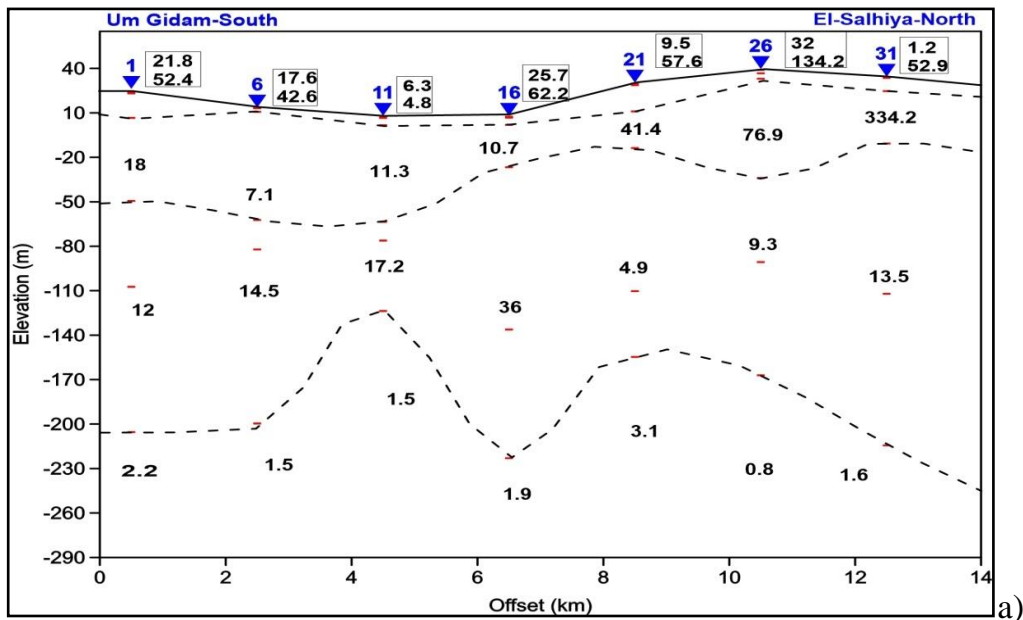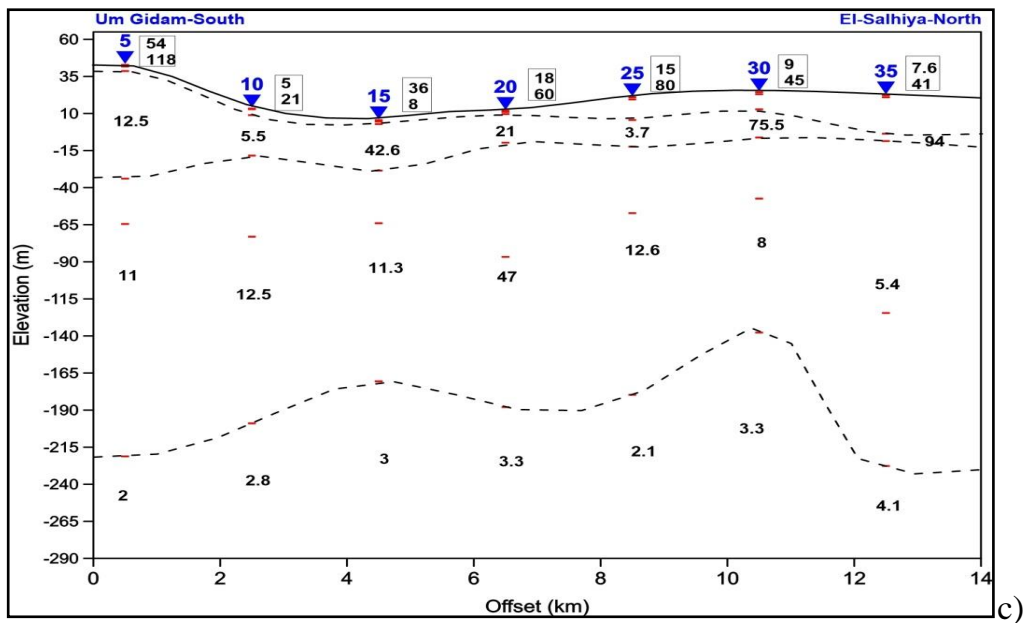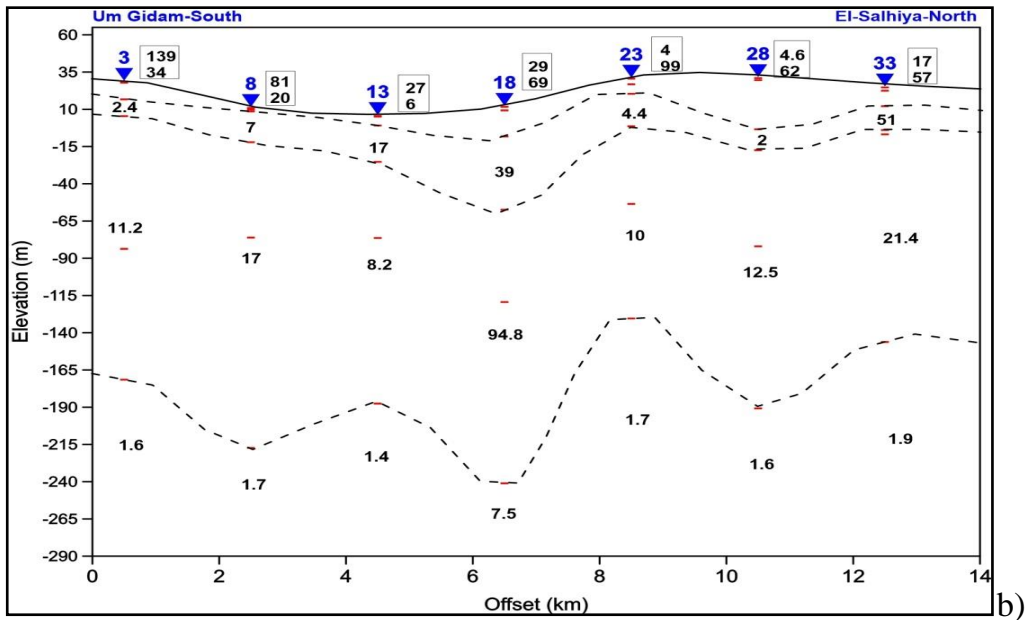
Fig. 4. 11: Geoelectrical cross-sections constructed by VES-TEM joint models; (a) A-A', (b) B-B' and (c) C-C'.
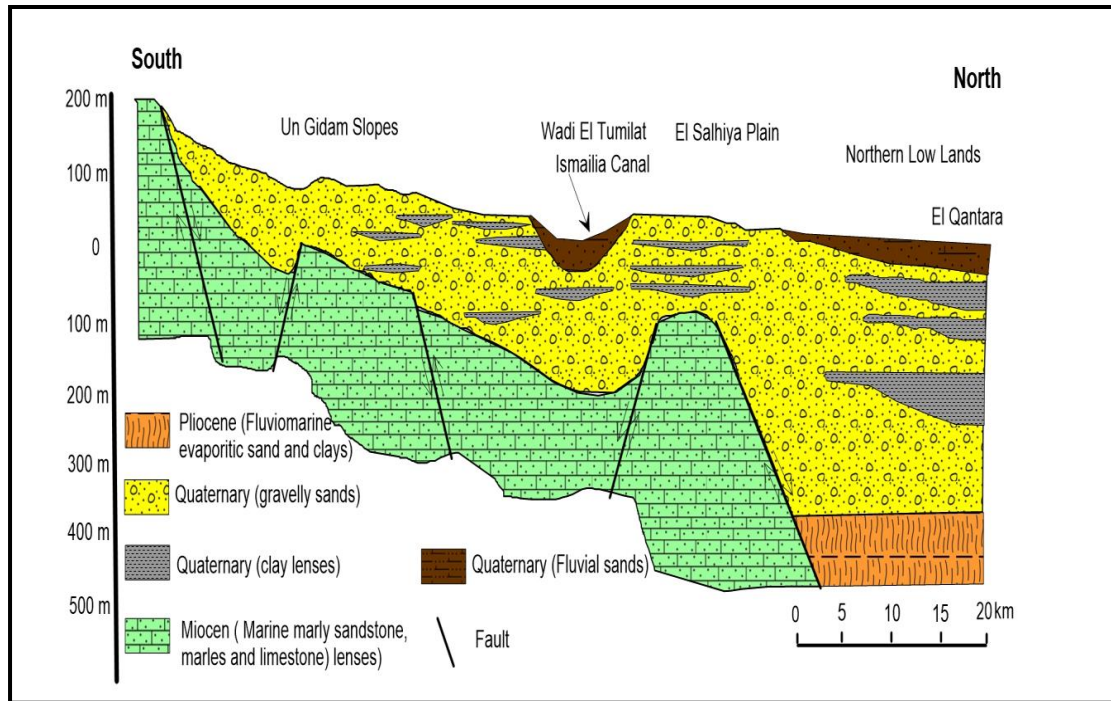
Fig. 4. 12: Geological section crossing the study area from South to North (A-A') (modified after Geriesh, 1994).

4.8. Water–bearing formations

From the geophysical survey conducted in the study area, two main aquifer systems were detected namely: a shallow Pleistocene aquifer and a deeper aquifer of Miocene age.

4.8.1. Pleistocene Aquifer

It is considered the main water aquifer in the study area. It is made by successive layers of gravel and sand and sand with many clay lenses of fluviatile origin, where it overlies uncomfortably the limestone Miocene sediments. It is a highly productive aquifer; with the majority of productive wells in the study area tap this aquifer. As a result of faulting, where the early Pleistocene aquifer comes opposite to the Miocene one (Fig. 4.12), possible lateral seepage of saline water can occur from the Miocene aquifer into the Pleistocene one.

The Pleistocene aquifer is mainly recharged from the Nile Delta aquifer in addition to other secondary feeding sources as seepage water from the nearby canals (i.e. Ismailia Canal), as well as surface infiltration from irrigation water.

Since the main objective of this study is to characterize the main aquifers in the investigated area, we prepared three contour maps showing the areal distribution of geoelectrical parameters of the aquifers; they are described in the following sections.

4.8.1.1.   *Depth of the aquifer surface*

The top surface of the Pleistocene aquifer can be detected at depths ranging from 10 to 83 m as shown in fig. (4.13). Inspection of the depth map showed that there are no general trends for the depth of the upper surface of the aquifer, which reflects the complexity of the subsurface structure of the study area, as shown in fig. (4.12). This could be due to a series of graben and horst faults affecting the depths of both aquifers. As a result, in some parts the Pleistocene aquifer is facing the Miocene aquifer because of the fault slip which increases the opportunity of water infiltration from the saline Miocene aquifer to the Pleistocene one. This agrees with the whiteness of the local farmers who confirmed that some nearby wells having similar depths produce fresh water while others produce brackish/saline water.
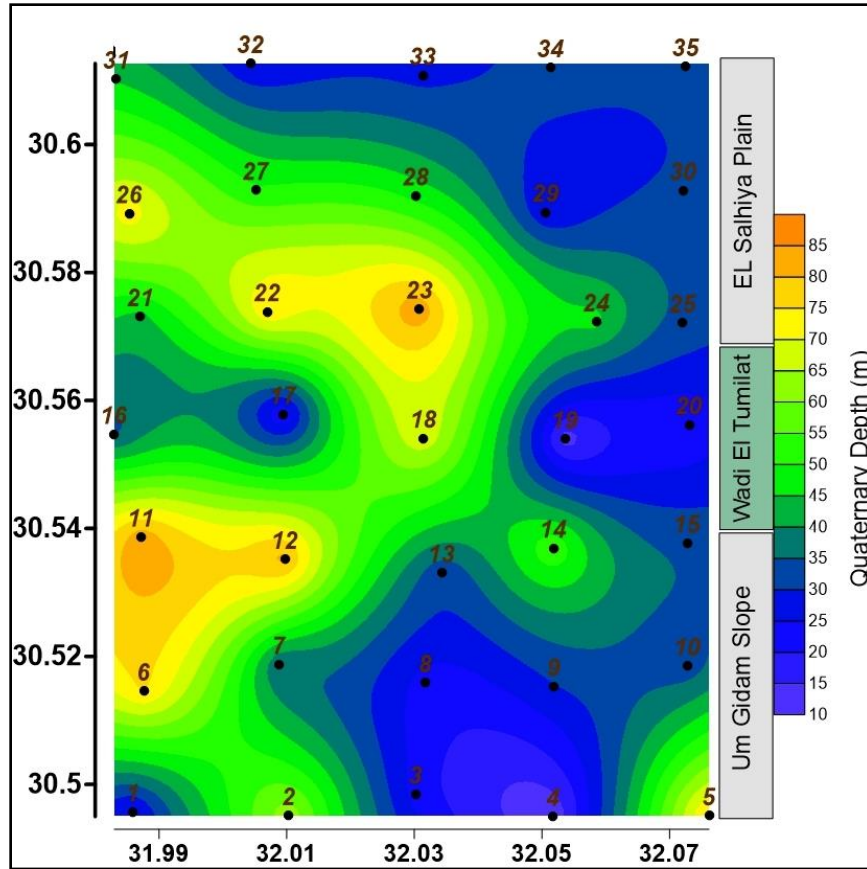
Fig. 4. 13: Contour map of the depth to the top surface of Pleistocene aquifer.

4.8.1.2. Thickness of the Pleistocene aquifer

The thickness of the Pleistocene aquifer shows no particular trends or peculiar directions for increasing or decreasing thickness, but it agrees with the structure complexity of the study area. The aquifer attains it minimum thickness of 129 m at station no. 23 and the maximum thickness of 273 m at station No. 14, as shown in figure (4.14). As a result, the Pleistocene aquifer is considered to be thick enough in the study area to act as a long-acting water resource as the large thickness means high water content in this high porosity gravel sand aquifer.
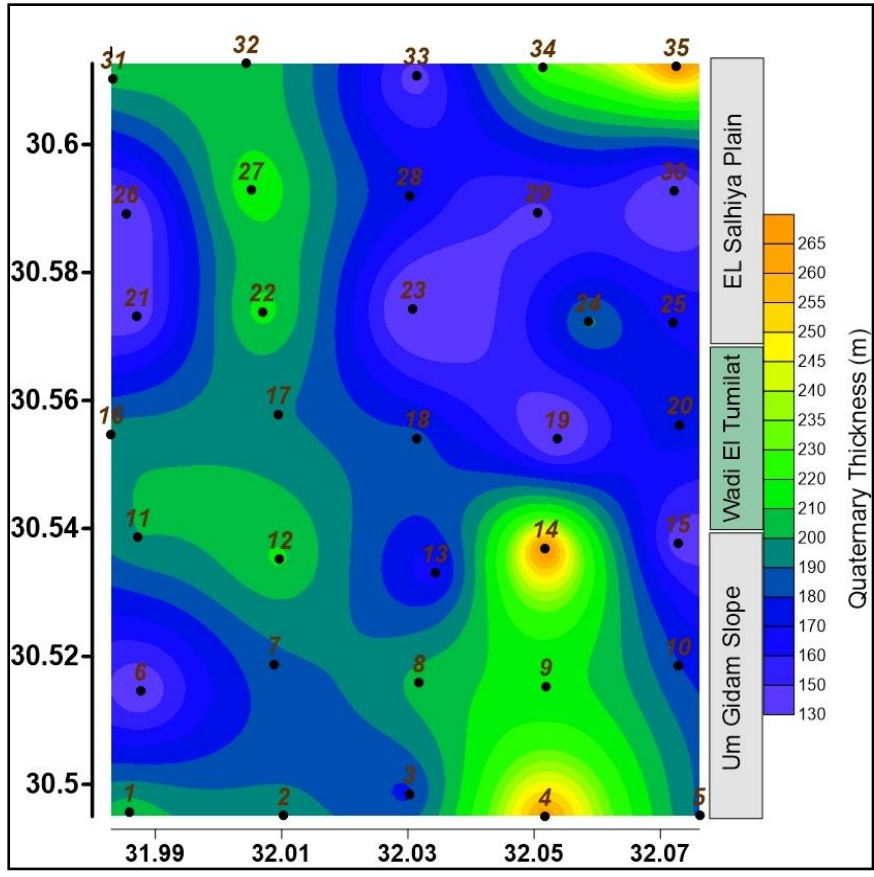
Fig. 4. 14: Thickness variation of the Pleistocene aquifer.

4.8.1.3. *Electrical resistivity distribution*

The resistivity distribution map for the Pleistocene aquifer (Fig. 4.15) reveals relatively low to moderate resistivity values, ranging between 4 Ωm and 95 Ωm. The majority of the resistivites are in the low range, except for Wadi El-Tumilat which is characterized by moderate values of resistivity, as apparent in the resistivity profile in figure 4.16. This reflects of the presence of high salinity water in most of the investigated area, except for the Wadi and this actually agrees with the results we got from hydrochemical analysis performed on water samples from the study area. This is discussed in details in chapter 5.
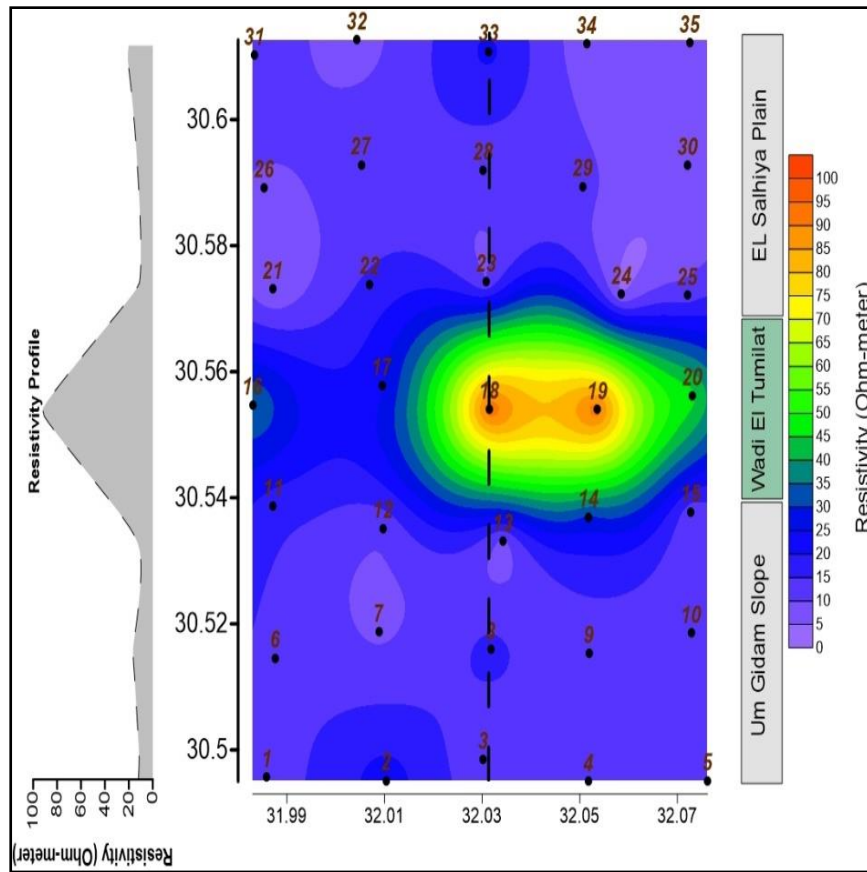
Fig. 4. 15: Resistivity distribution through the Pleistocene aquifer.

4.8.2. Miocene Aquifer

The results obtained from this study are insufficient to provide a detailed characterization of the Miocene aquifer within the study area; we just mapped the depth of its upper surface lying at depth ranging from 130 to 328 m below the ground surface (figure 4.16). The Miocene aquifer is mainly composed of marine marly sandstone and limestone (Fig. 4.12) and it shows relatively low resistivity values ranging from 6 to 22 Ωm. The groundwater within this aquifer is mainly saline. In order to provide a full description for this aquifer, further investigations are required to fully understand its geological, hydrogeological and hydrochemical characteristics and spatial variations.
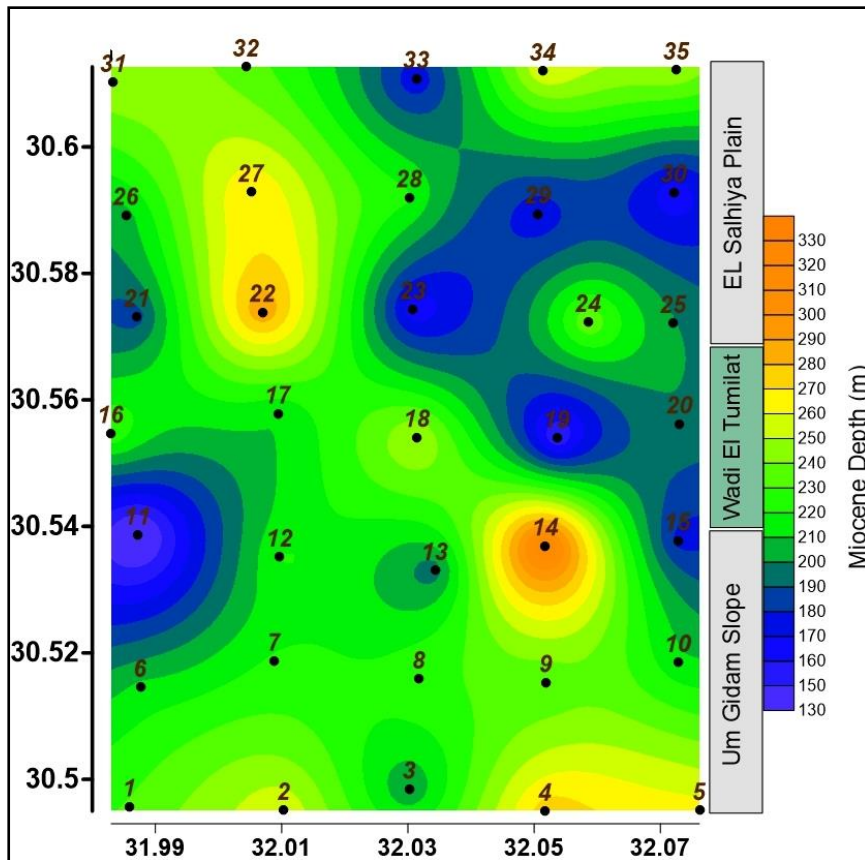
Fig. 4. 16: Depth of the top surface of Miocene aquifer.

Chapter (5)

Investigation of Water Logging Problem Using ERT Method

This chapter is concerned with the challenges and the obstacles which hinder the sustainable development for Ismailia governorate and the surrounding villages. This area is characterized by a great social-economic importance as it is considered the east gate for Egypt to Asia Continent and other Arab countries. It is peculiar for its special geographical location and a very civilized and political history in addition to its high economical importance with its fish wealth and tourism. In addition, it is known by its very high quality agricultural products which grow thank to its groundwater resources and high soil potentialities. This leaded Ismailia to be in the first position for exporting fruits and vegetables which are highly demanded by name. All these sources make Ismailia one of the governorates that attracts investments in different fields either tourism, industrial and agricultural fields. All these reasons motivate the government to pay a great attention for this promising area and give it the priority in the sustainable development plans.

Unfortunately, all these plans are faced with many environmental problems that threat all the exerted efforts and plans for this promising area. We can state here two main problems that have many severe impacts on our area of study. First, the problem of water logging that appears along a large part of the study area, especially in the territories near Wadi El-Tumilat as shown in figure (5.1). Local people are dealing with this issue in many different ways. Some of them adapted with the problem by converting it to blue economy, which is based on fisheries and tried to get benefit from this by converting these lakes into fisheries and recreations zones as testified in figure (5.2). Some others are using the abundant resources of

infertile sand dunes in burying these lakes but this is not the best practice as most of these lakes are continuously recharged. So, after sometime their efforts are dissipated as these lakes are full again.

Second, is the possibility of groundwater contamination and deterioration in its quality due to wastewater percolation from the uncased septic tanks used as a sewage system to the Quaternary aquifer or from the excessive and unmanaged use of fertilizers which filtrates into the subsurface with irrigation water.

So, to study the reasons behind the water logging problem and fully characterize the hydrogeology of the area, Electrical Resistivity Tomography (ERT) technique was selected. Hydrochemical analyses have been carried out on some collected water samples from the available wells taping the quaternary aquifer in the study area to evaluate the current situation of water quality and whether it got polluted or not.

So, in this chapter, we are going to discuss the field set up and measurements, data preparation and quality control analysis, data processing and interpretation for ERT method to come out with the reasons behind water logging problem. Then, we will present and discuss the results of hydrochemical analysis for the collected groundwater samples in chapter five.

Fig. 5. 1: One of the water logging lakes scattered in the study area.

Fig. 5. 2: An example of a water logging lake turned into a fishery near Wadi El-Tumilat.

5.1. ERT Data Acquisition

ERT has became one of the most used geophysical techniques that proved to be very effective in mapping environmental problems as it provides a detailed depiction for the subsurface in both vertical and horizontal directions.

11 profiles of ERT were collected in the study area with constant 5.0 m inter-electrodes spacing. 10 profiles were located at the boarders of some lakes resulting from the water logging while the last one was conducted far away from the area suffering from water logging problem, just to compare the behaviour of ERT in both areas and to study the reason behind water logging problems as shown in figure (5.3). There was no specific trend or direction for arranging ERT profiles except for the accessibility of the area.
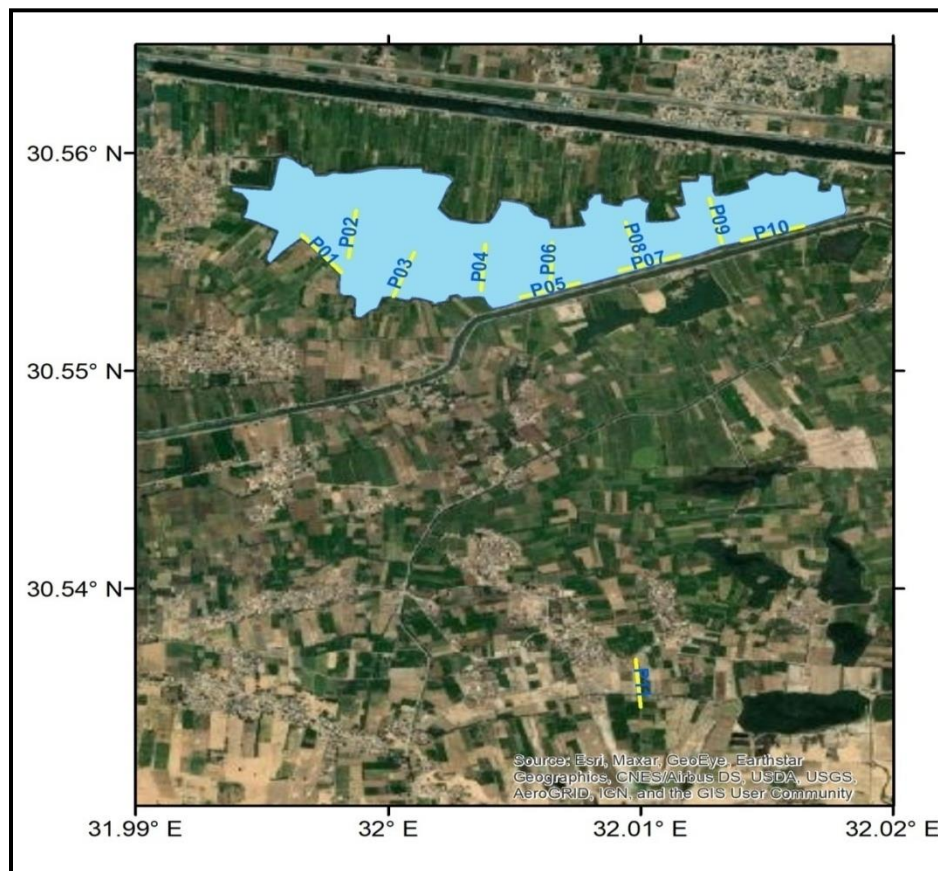
Fig. 5. 3: Location map of ERT profiles collected in the study area.

The total length of each profile is 235 m (48 electrodes * 5 m spacing).The choice of the acquisition array depends on the desired depth of investigation that in turn bases on the target, the sensitivity of the array to horizontal and vertical changes, and the horizontal data coverage. So, the measurements were conducted by applying Wenner - Schlumberger array which is a hybrid between Wenner and Schlumberger arrays (Pazdirek and Blaha, 1996). It has a better horizontal resolution than the normal Wenner array and a better vertical resolution in addition to good signal strength (Loke, 2021) which co-insight with our aims. Based on the applied field acquisition parameters, the maximum investigated depth is about 40 m below the ground surface.

During the measurements, the Induce Polarization (IP) chargeability data were also collected, as IP is known as the best technique for mapping clay layers which we thought that are the reason behind the water logging problem. This hypothesis is based on our literature review to the previous studies and the subsurface geology information we got about the study area. It indicates that clay lenses and intercalations are widely distributed in the study area, but we weren't certain about its existence in the area affected by the water logging.

5.2. ERT data processing

5.2.1. Quality control and analysis of ERT data

It is well known that the quality of measured data and noise contamination level mainly affect the reliability of the obtained results and field work is a crucial step to assure the adequate data quality. To maximize potential benefits of the inversion process, great attention must be paid to the control of observed data quality in fieldwork and during data editing and processing. Also, preventative actions or steps toward minimizing the effects of all kinds of error sources must be taken into consideration. For this reason, it is important to investigate the significant sources

of measured data errors and understand their possible effects on signal-to-noise ratio of the geoelectrical data and in turn of inversion models.

Zhou and Dahlin (2003) have pinpointed that the measurement errors related to electrical resistivity may be simply classified into two kinds, **measurement electrode spacing errors or and observed potential errors**. These are considered as the main two sources of noise or errors in measuring the apparent resistivity for 2D resistivity imaging. However, the resistance between electrodes and ground, as well as the electrical current that actually flows into the ground are additional crucial parameters. **The electrode spacing error** is caused by geometrical errors in electrode positions or inadvertent electrode setting-up, which hopefully is minimized by careful work applied by the data acquisition field team. However, it is not uncommon that some portions of the cables cannot be straightened due to rough terrain, vegetation and logistical obstacles, or the positions are shifted from their theorical location trying to improve electrode contact with the ground. Sometimes electrode positions are measured with a tape, with the associated risk of electrode spacing errors due to measurement inaccuracies, especially on rough topography.

During our measurements in the study area, we took into consideration some precautions in order to mitigate the possible impacts of this type of errors on the final result. Therefore, all the measurements have been carried out along almost flat zones following straight lines as much as possible. Moreover, the conductivity of the shallowest layer was in general very high, so there was a good contact with the used electrodes (i.e. low contact resistance between the electrodes and the ground).

The electrical potential error can arise from many sources e.g. bad electrode contact, cable insulation damage, site background noise (telluric current and power line noise), instrumental problems (not sufficient current injection and picking-up

of noise potentials) and improper instrument setup. Some of these error sources are non-foreseen and occasional incidents. On the other hand, errors may substantially decrease the imaging resolution due to excluded data measurements thus producing an over-smoothed and under-constrained image. Knowledge of the data quality and noise level of data is therefore crucial to the successful application of resistivity technique. Therefore, close attention must be paid to estimate the error levels of data and their effects on inversion results.

In principle, two methods are adopted to increase the data quality. One is to repeat the measurements at the same point multiple times (stacking), in order to take the mean value and evaluate the standard deviation as an affordable estimation for the data precision. However, a low standard deviation does not guarantee always good data quality as some instrumental and coupling problems can't be expressed by standard deviation, especially when coherent noises are present. In other words, data can be very precise, but not accurate. Therefore, validation of measured data and obtained results against previous works and subsurface geology known from well-data is helpful, when available. Fortunately, we found many previous studies for our investigated area, through which the most important is returned back to (Geriesh, 1994) that includes the whole region of Suez Canal comprising our study area.

Controlling data quality is compulsory in order to identify artifacts or anomalies. Geostatistics is particularly well-suited for this task, allowing an independent review of the data quality that can be achieved at any step in the process. Geostatistics enables quantifying the magnitude of artifacts and subsequently the quality of the processing. It also allows a control of spatial coherence of anomalies related to resistivity.

In order to properly estimate the resistivity and chargeability patterns along the deployed profiles for the site of interest showed in figure (5.3), a statistical

procedure was carried out to measure, monitor and evaluate the quality of the data. This may allow a comprehensive understanding of the collected data and choose the proper processing procedures and parameters. Eventually, we come out with conclusions and interpretation that reliably describe the situation and thus we can minimize misinterpretations. Also, this analysis is useful for adequately choose the proper classes and colour scales for the sake of visualization.

In order to achieve such a purpose, ERT profiles shown in figure (5.3) were statistically analyzed in terms of summary of the extreme values, standard deviation, mean, resistivity histogram, chargeability histogram, and box diagrams. Data editing by selective filtering is essential as a first processing (or pre-processing) stage to reduce the uncertainty of the calculated models. Our insight on the data point is constrained by results from previous geophysical studies and lithology from excavated wells.

So, a statistical analysis that allows an approach to the resistive properties in the study area and the ability to discriminate data points that related to real geological structures from outliers that could be resulted from errors during the field survey is presented hereafter.

The minimum and maximum measured resistivity values for the entire set of profiles are 2.5 and 308 Ωm, respectively, while the minimum and maximum IP values are 1.4 and 22 mV/V, respectively (see also the appendix).

Figures 5.4 a, b, and c show the distribution of measured resistivity and chargeability in terms of histograms and box plot for the first profile (p1). Table 5.1 and Fig.5.4 (a and c) indicate that the measured resistivity range is between 3.2 to 239 Ωm and the major part of the data points occur within the range between 2 and 150 Ωm and there are small values of high resistivity outliers between 150 to 240 Ωm. The chargeability data points have also a narrow range from 2 to 14 mV/V.

What is obvious for resistivity profiles, that almost all of them show a bi-modal resistivity distribution indicating two different geoelectrical features while the chargeability ones are unimodal with a sort of Gaussian distribution, indicating just one apparent feature.

5.2.2. ERT and IP data processing and interpretation

The resistivity& chargeability data were processed using RES2DINV software. The same processing steps were applied for both resistivity and chargeability data simultaneously. The measured data were plotted as "Apparent Resistivity Pseudo-sections" to check the data quality and measured point distribution and to eliminate bad data points. Applying "Least Square Approach" (Loke, 2001) the apparent resistivity was inverted to true modelled 2D Resistivity sections. The chosen colour palettes of the sections reflect the value of both calculated resistivity and chargeability. It is worth to mention that for all the inverted models, a constant range for both resistivity and chargeability values was applied for easier comparison.

Figures (5.5-5.10) show the inverted 2-D profiles for both resistivity and chargeability for the area suffering from water logging problem near Wadi El-Tumilat.

The root mean square (RMS) is used to evaluate the accuracy of the inversion process as it measures the difference between the measured and calculated resistivity. This means that each iteration has its RMS value. It is defined as

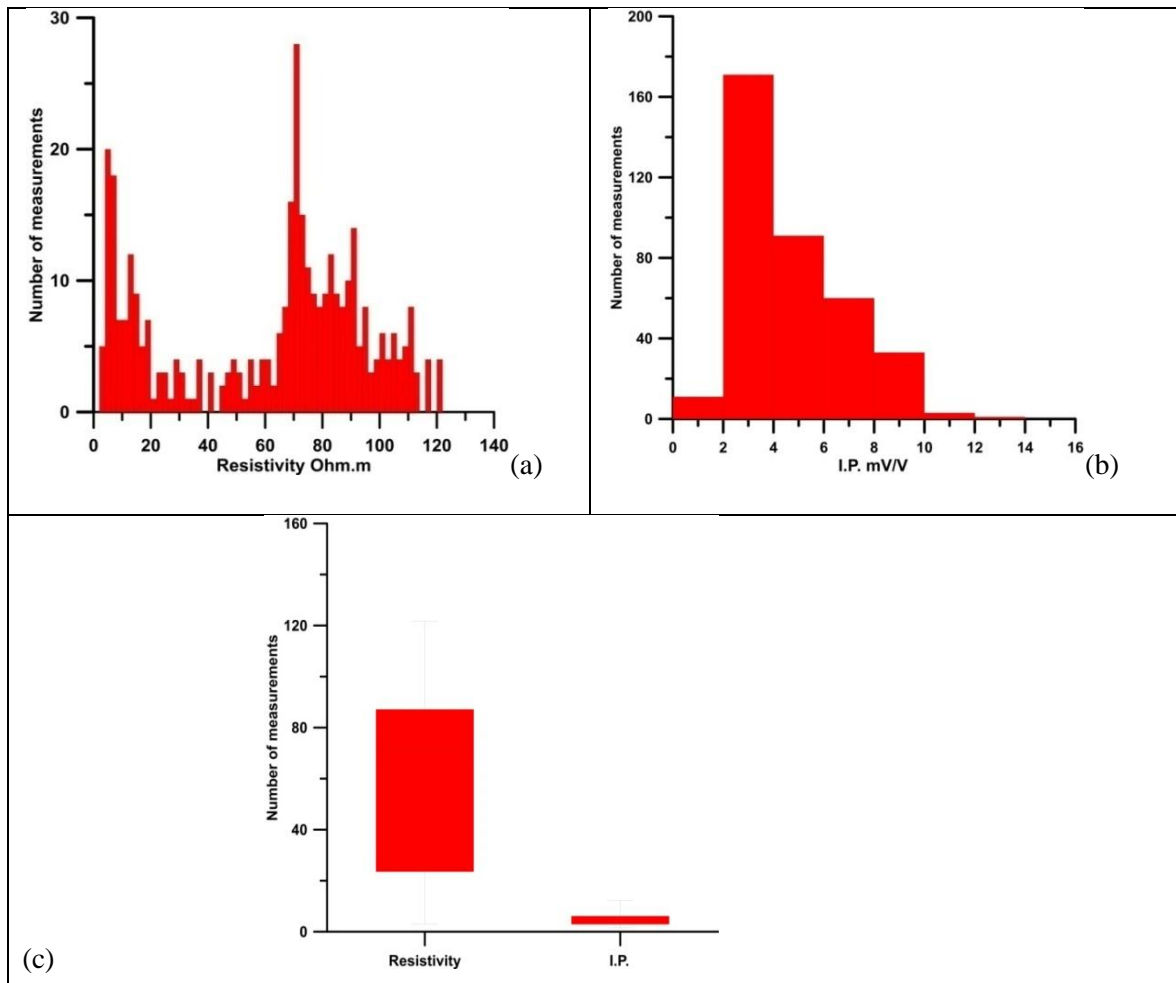$$RMS = \sqrt{\frac{\sum_{i=1}^{N}(d_i - dc_i/d_i)^2}{N}} \times 100$$

Where d_i is data obtained (measured apparent resistivity), and dc is the calculated resistivity by a code or software and N is the number of data points.

The lower the value of RMS, the better the fitting between measured and calculated data. From our experience, this value depends on the accuracy of the measured data, the complexity of the resistivity environment and the chosen algorithm for the interpretation.

For all of our inverted profiles, the RMS value ranges between 1.19 and 7.6% which is accepted from our side. However, in addition to such a parameter, it is always essential to evaluate the geological reliability of the measure, checking for instance if the inverted results have a meaningful resistivity range respect to the expected geological and hydrogeological background.

Table. 5. 1: Summary of data statistics for profile 1.

P1	Resistivity (Ωm)	IP (mV/V)
Data points	343	343
Minimum	3.2	3.4
Maximum	239	15.1
Mean	71	6.7
Standard deviation	39.7	2.2

Fig. 5. 4: Exemplary statistical analyses of the collected resistivity and IP data for profile 1; a) histogram of the resistivity data, b) histogram of the IP data, c) Box plot for both data.
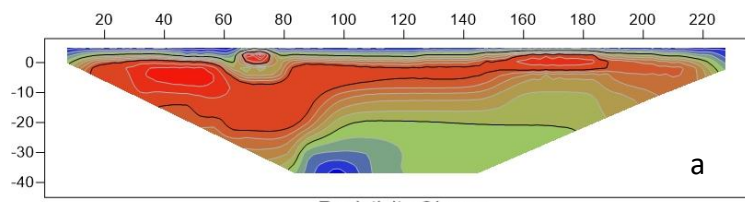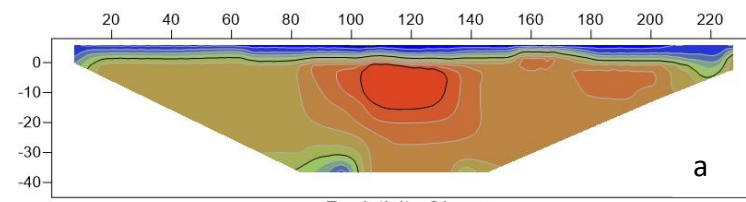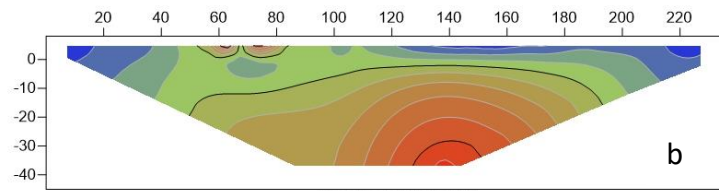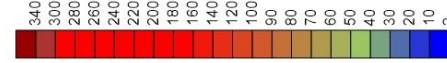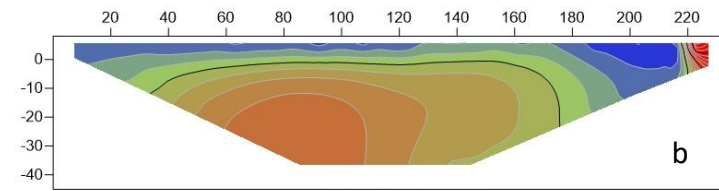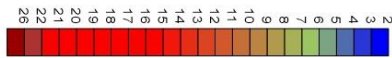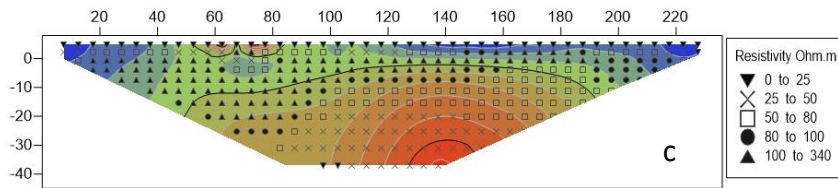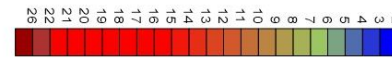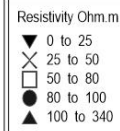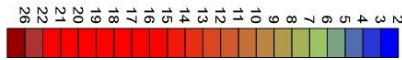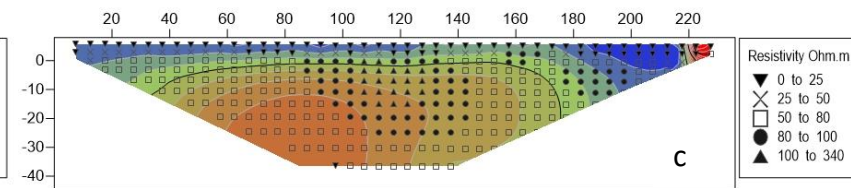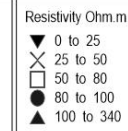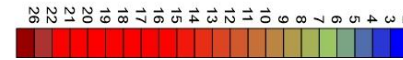
P1   P2

Fig. 5. 5: Inverted geoelectrical sections for profile (P1), left and profile (P2), right; a) 2-D resistivity section, b) 2-D chargeability section, c) aggregated plot for both resistivity and chargeability.
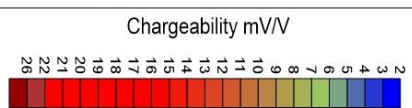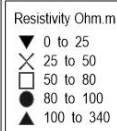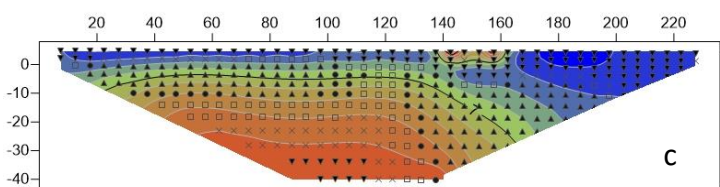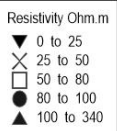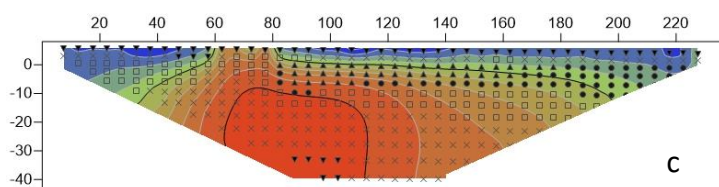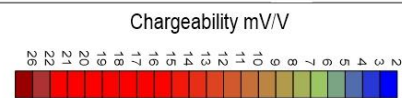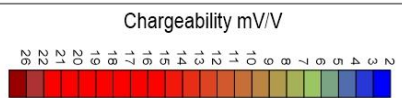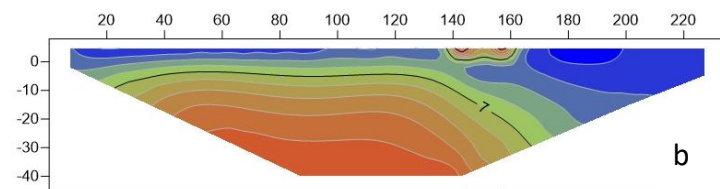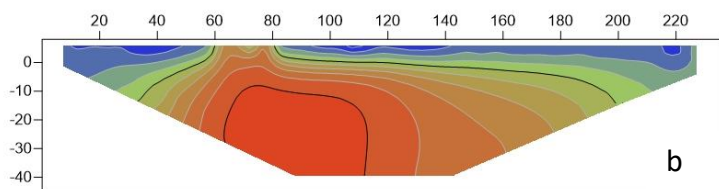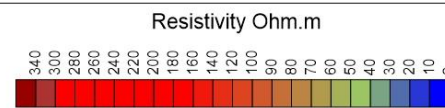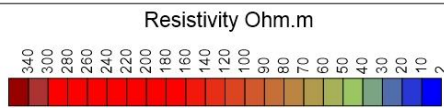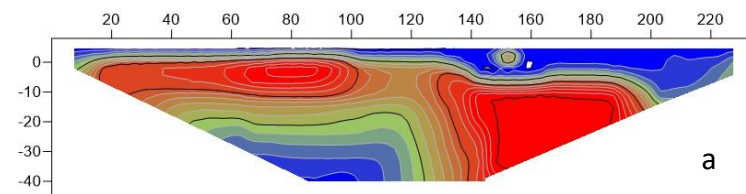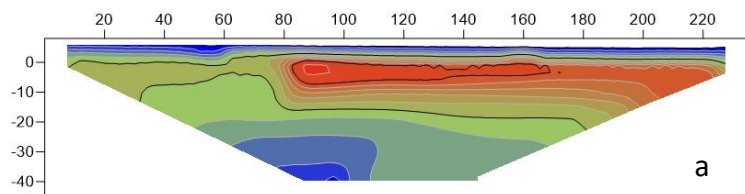
P3

P4

Fig. 5. 6: Inverted geoelectrical sections for profile (P3), left and profile (P4), right; a) 2-D resistivity section, b) 2-D chargeability section, c) aggregated plot for both resistivity and chargeability.

P5
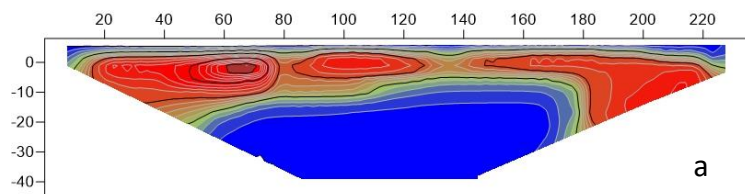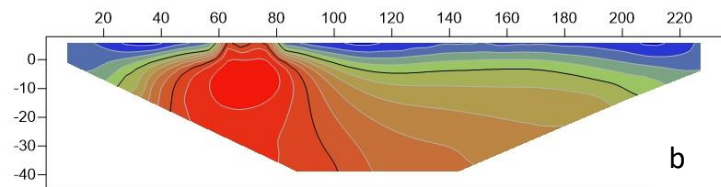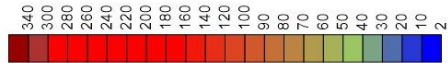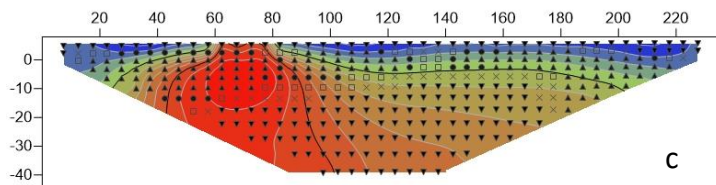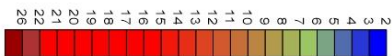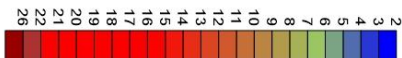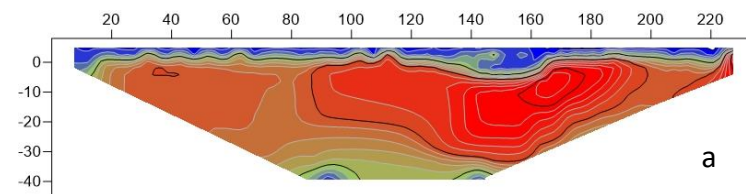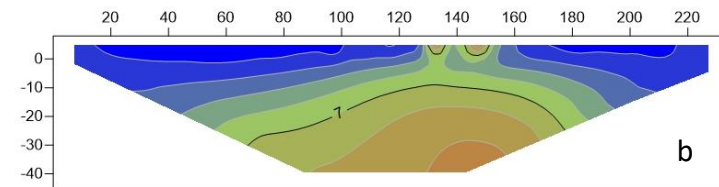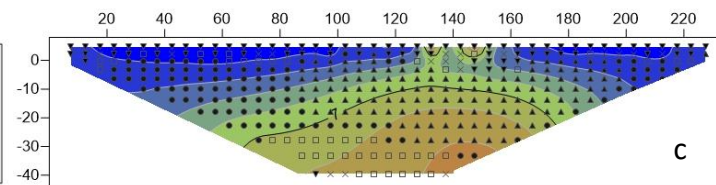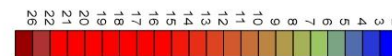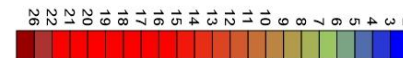
P6

Fig. 5. 7: Inverted geoelectrical sections for profile (P5), left and profile (P6), right; a) 2-D resistivity section, b) 2-D chargeability section, c) aggregated plot for both resistivity and chargeability.
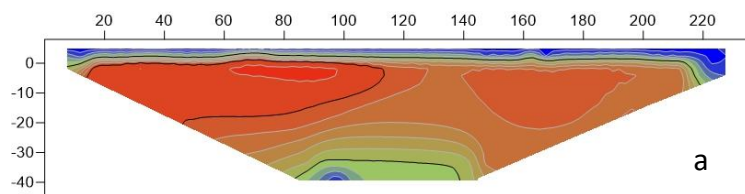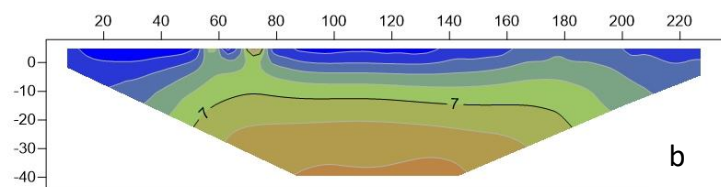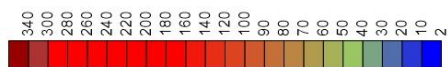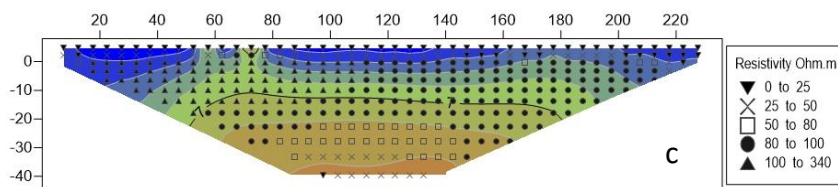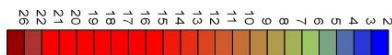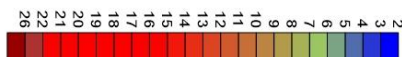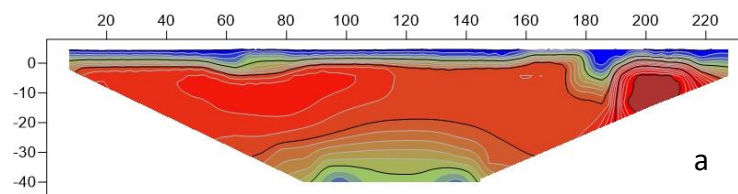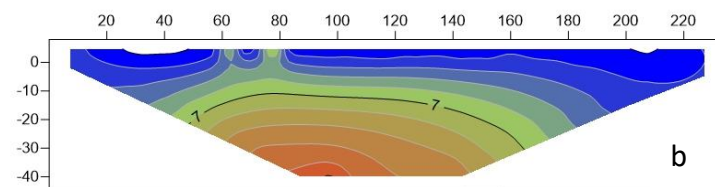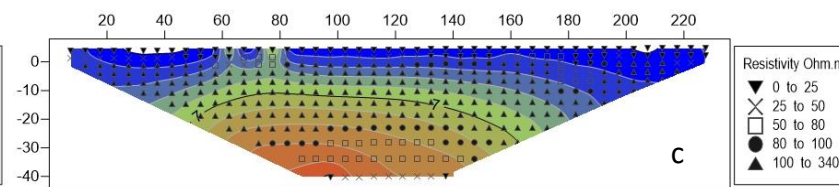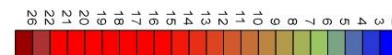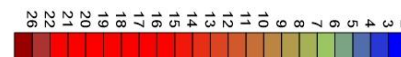
Fig. 5. 8: Inverted geoelectrical sections for profile (P7), left and profile (P8), right; a) 2-D resistivity section, b) 2-D chargeability section, c) aggregated plot for both resistivity and chargeability.

P9
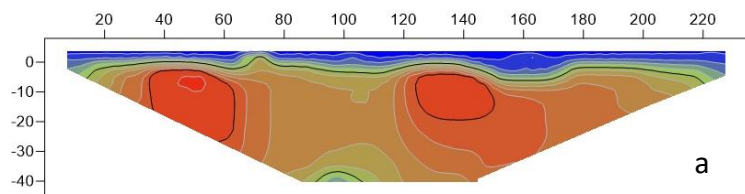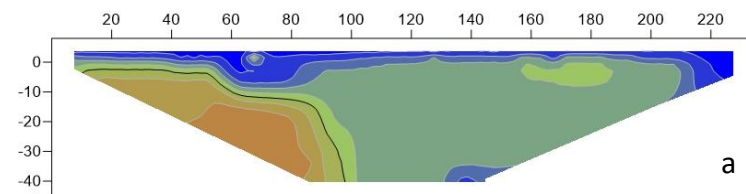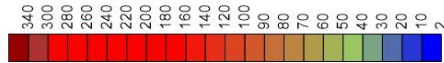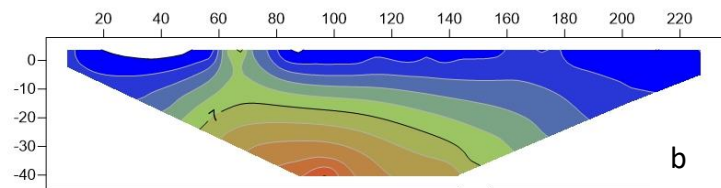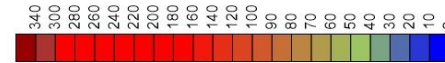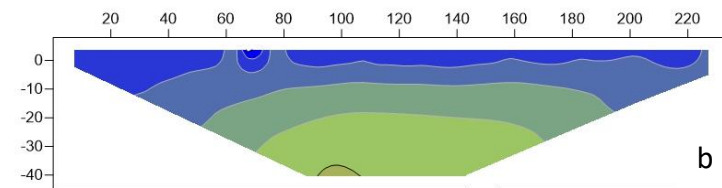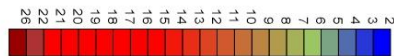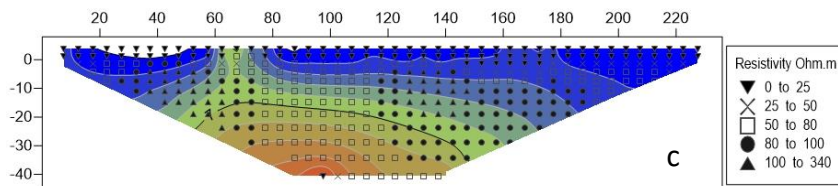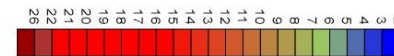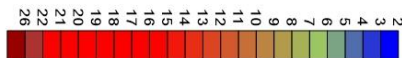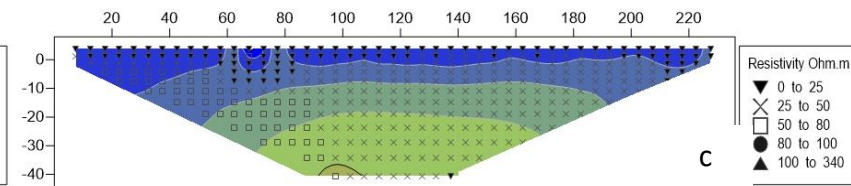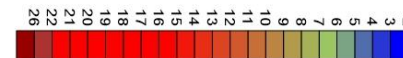
P10

Fig. 5. 9: Inverted geoelectrical sections for profile (P9), left and profile (P10), right; a) 2-D resistivity section, b) 2-D chargeability section, c) aggregated plot for both resistivity and chargeability.
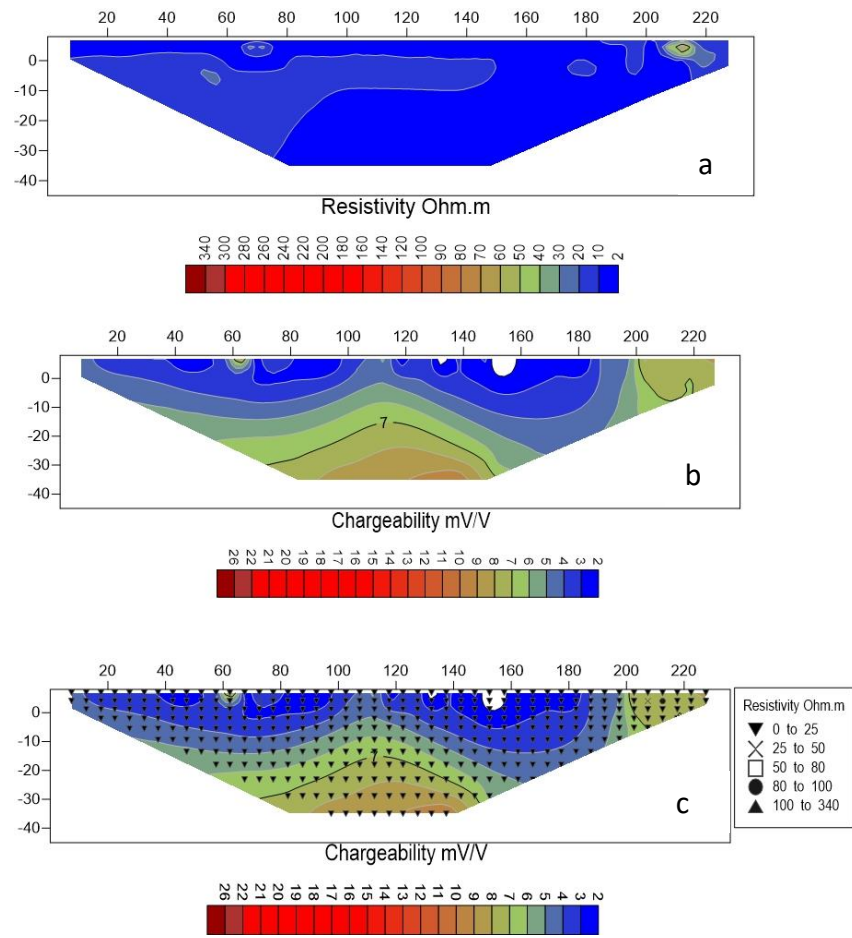
P11

Fig. 5. 10: Inverted geoelectrical sections for profile (P11); a) 2-D resistivity section, b) 2-D chargeability section, c) aggregated plot for both resistivity and chargeability.

5.3. Results and discussion

Investigation for the first 10 profiles located near water logging lakes revealed three main geoelectrical units within a depth of 40 m. Each of these units is characterized by its own geoelectrical properties.

However, in order to provide a comprehensive and holistic representation of our results and to avoid the misinterpretation that may result from visualizing the results of each profile for both methods (ERT & IP) individually, we prepared an aggregated plot for each profile that shows the distribution of both inverted resistivity and chargeability.

Therefore, figs. 5.5 to 5.10, present the inverted 2-D section for each profile with its corresponding aggregated plot for easier interpretation.

- *Upper(shallowest) unit*

It extends from the ground surface to depth not exceeding 10-11 m. The resistivity for this unit ranges between 4-150 Ωm as it represents the surface and near surface medium. It comprises the 2 or 3 small thickness superficial layers which is correlated with the subsurface lithology succession shown in Fig. (5.11) (Geriesh, 1994). These first layers are completely saturated and for this reason the resistivity values are relatively low. As far as the chargeability, it is characterized by low values not exceeding 10 mV/V indicating sandstone and gravels.

- *Middle unit*

It extends from the lower boundary of the above unit and reaches about 30-35 m in many parts along the ERT profiles. One of the peculiar characteristics of this layer is its relatively high chargeability that reaches 25 mV/V in some points along the measured profiles corresponding to relatively high resistivity values (>250 Ωm). This doesn't agree with the electrical properties for clay minerals

109

which are usually characterized by resistivity range between 1 and 100 Ωm and high chargeability in 10-50 mV/V (e.g. Sumi, 1965). Chargeability is controlled by many factors through which the most important are the following:

4. Clay mineral content

5. Grain size

6. Porosity

7. Metallic mineral content

8. Electrolyte composition, as some pollutants can cause the effect of high resistivity, high chargeability (Jones, 2007).

It is relevant that the effect of this unit appears only at these 10 profiles conducted at the water logging area. Comparing these profiles with the profile (P11) conducted far away from the water logging (fig. 5.4) we can see that in this profile this unit is indeed characterized by low resistivity (4-20 Ωm) and low chargeability (2-6 mV/V).

So, going back to the subsurface geology of the study area, we can see that the layer that is found within the same depth of this unit is evaporitic loamy sand as shown in fig. (5.11) that represents E-W geological cross-section along Wadi El-Tumilat and considering the lithology of a well taping the Pleistocene aquifer in the same area (Geriesh, 1994). According to previous geological studies, this layer extends along the Wadi until it turns completely into evaporites near Suez Canal. Actually, this is in accordance with the description of the local farmers in the area as they stated that during digging, at a depth of about 30 m, they reached a "strange layer" (in their description) that looks like gypsum in colour (white colour) and at the same time it has muddy sticky properties. Also, they stated that to reach fresh water they need to dig below it.

So, in our interpretation we think that this layer is responsible for the water logging problem but this can't be confirmed before applying dedicated geochemical analyses for this layer.

- *Lower (deepest) unit*

This unit represents the saturated Pleistocene aquifer and it extends from the lower boundary of the middle unit below the end of all ERT sections (P1-P11). It is characterized by low to medium resistivity values as shown in the figures. It is mainly composed of sand, gravel with local clay intercalations.
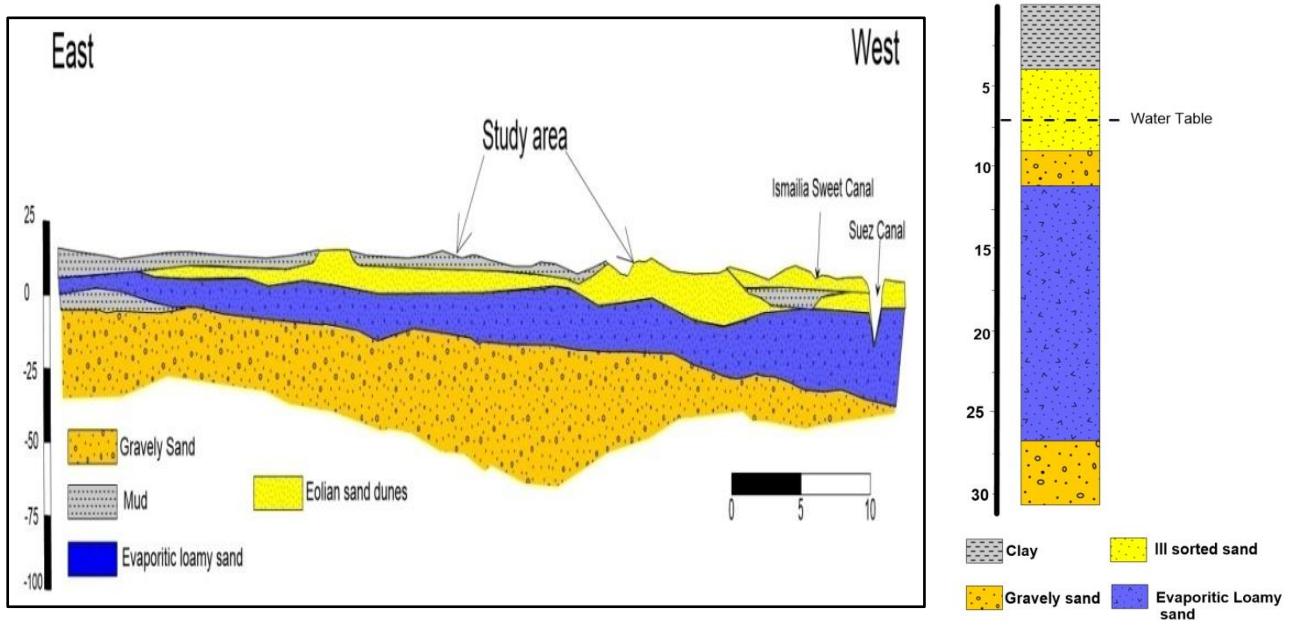
Fig. 5. 11: Geological cross-section along Wadi El-Tumilat E-W and the schematic lithology succession (Geriesh, 1994).

Chapter (6)

Investigation for Groundwater Contamination by Hydrochemical Analysis

Sustainable development for any place depends mainly on the available clean water resources and the way it is managed. As mentioned before, groundwater is definitely the main water resource in our study area. So, understanding the hydrochemical processes that govern groundwater characteristics is the first step needed for sustainable management and exploitation of water resources. The validity of groundwater for drinking, domestic and irrigation purposed can be in fact revealed through dedicated hydrochemical analysis and time monitoring. We can say that quality of groundwater is equally important to its quantity owing to the suitability of water for various purposes as water quality analysis is an important issue in all groundwater studies.

Generally, physical, chemical and biological characteristics of water are defining its quality (Alley, 2007). Hence, any variations in any of these characteristics can affect groundwater quality. These characteristics are mainly controlled by both geological properties and anthropogenic activities (Belkhiri et al., 2010). Therefore, it is affected by natural parameters as geological structure, type of participation, geological processes within the aquifer (Srinivasamoorthy et al., 2012) or by human activities that include disposal of wastes, anthropogenic and agricultural activities, and industrial discharge.

Water supposed to be odourless, colourless and tasteless, so, if any of these properties is different or change the water is said to be polluted or contaminated. So, contamination of water resources happens when there are undesirable changes in the physical, chemical, or biological characteristics of water that can adversely affect the health, survival and activities of humans or other living organisms (Miller, 1994). **The World Health Organization (WHO) says that**

polluted water is water whose composition has been changed to the extent that it is unusable. Which means that toxic water can't be used for drinking or any other purposes like agriculture and irrigation. There is a wide range of pollutants including agricultural chemicals, animal wastes, toxic–hazardous-waste landfills and many other sources of contamination including natural compounds.

6.1. Water sampling

15 samples were collected from the available water wells that are taping the Pleistocene aquifer to investigate whether the groundwater got contaminated by percolation of waste water from the septic tanks used in the study area as sewage system or by heavy agricultural activities that are carried out in most of the investigated zones.

In particular, the samples were collected along two S-N profiles (Fig. 6.1). Each sample was collected duplicate in two-500 ml narrow-mouth, polyethylene pre-washed bottles provided by the "Central Laboratories of the National Water Research Centre (NWRC)".

Fig. 6. 1: Location map of the collected water samples.

6.1.1. Method for water analysis

The methodology used in chemical analysis of the water samples is discussed in the following section according to the guidelines **"Central Laboratories (NWRC)"** in which the water analysis has been conducted. The analyses were carried out according to standard methods and recommendations for examination of water and wastes (APHA, 2012).

Hydrogen ion concentrations (PH)

The pH values of the collected field samples were determined by the use of bench-top pH/ISE meters, ORION model 7l0A equipped with PerpHect Ag/AgCI low maintenance Gel triode electrode, model 9207 BN calibrated using 7 and 10 pH buffers.

Electrical Conductivity (EC)

Electric conductivity of the tested water samples was measured at temperature 25 °C as standard temperature by using ATC bench electric conductivity meters, HANNA, model HI 8820.

Total Dissolved Solids (TDS)

The total dissolved solids in the collected water samples were determined via gravimetric method.

Alkalinity

Alkalinity is a measure of water's capacity to neutralize an acid. It indicates the presence of Carbonates and Bicarbonates, and it is expressed as an equivalent of Calcium Carbonate ($CaCO_3$). Total alkalinity is the summation of CO_3^{-2} and HCO^{3-}. It was measured by titration method using Sulphuric acid 0.02 N with a few drops of phenolphthalein and methyl orange as indicators according to standard method.

Major Anions

Major anions such as sulphate (SO4), nitrate (NO3) were determined in water

by using ion chromatography (IC) (modelDX-600, USA) according to standard methods table (6.1).

Table. 6. 1: IC instruments Detection Limits for Anions

Anions	Detection limit
Nitrate - NO_3	<0.1
Sulphate - SO_4	<0.5

Major and trace elements

Major and trace elements were analyzed using Inductively Coupled Plasma - Emission Spectrometry (ICP-ES) and Ultra Sonic Nebulizer (USN), Model Perkin Elmer Optima-3000, USA table (6.2). The Nebulizer decreases the instrumental detection limits by 10%. Samples were filtered through filtration system via membrane filter of pore size 0.45 um before analyses.

Table. 6. 2:ICP Instrument's detection limits for Heavy Metals

Cations and Metals	Detection limit
Copper – Cu	<0.002
Iron – Fe	<0.010
Manganese –Mn	<0.010
Lead –Pb	<0.005
Zinc – Zn	<0.005
Cadmium – Cd	<0.0005
Nickel – Ni	<0.0001

6.1.2.   Piper Diagram

A Piper diagram is a graphic procedure proposed by Arthur M. Piper in 1944 for presenting water chemistry data to help in understanding the sources of the dissolved constituent salts in water. In other words, it is a graphical representation of the chemistry of a water sample in the form of trilinear diagrams. To create a graph with the major water constituents, Piper (1994)

suggested a combined plot which includes two triangles for cations and anions and a diamond that summarize the two previous plots as shown in figure (6.2). The left triangle represents the cations and the right one is for anions. According to the location of the sample, the hydrochemical facies can be identified. To determine the dominant water type in any sample, first, the concentrations of anions and cations must be located in the lower triangles. Then, we draw two perpendicular lines from the sample point in both cations and anions triangles. Based on the position of the resultant intersection point of both lines, the water type can be determined.
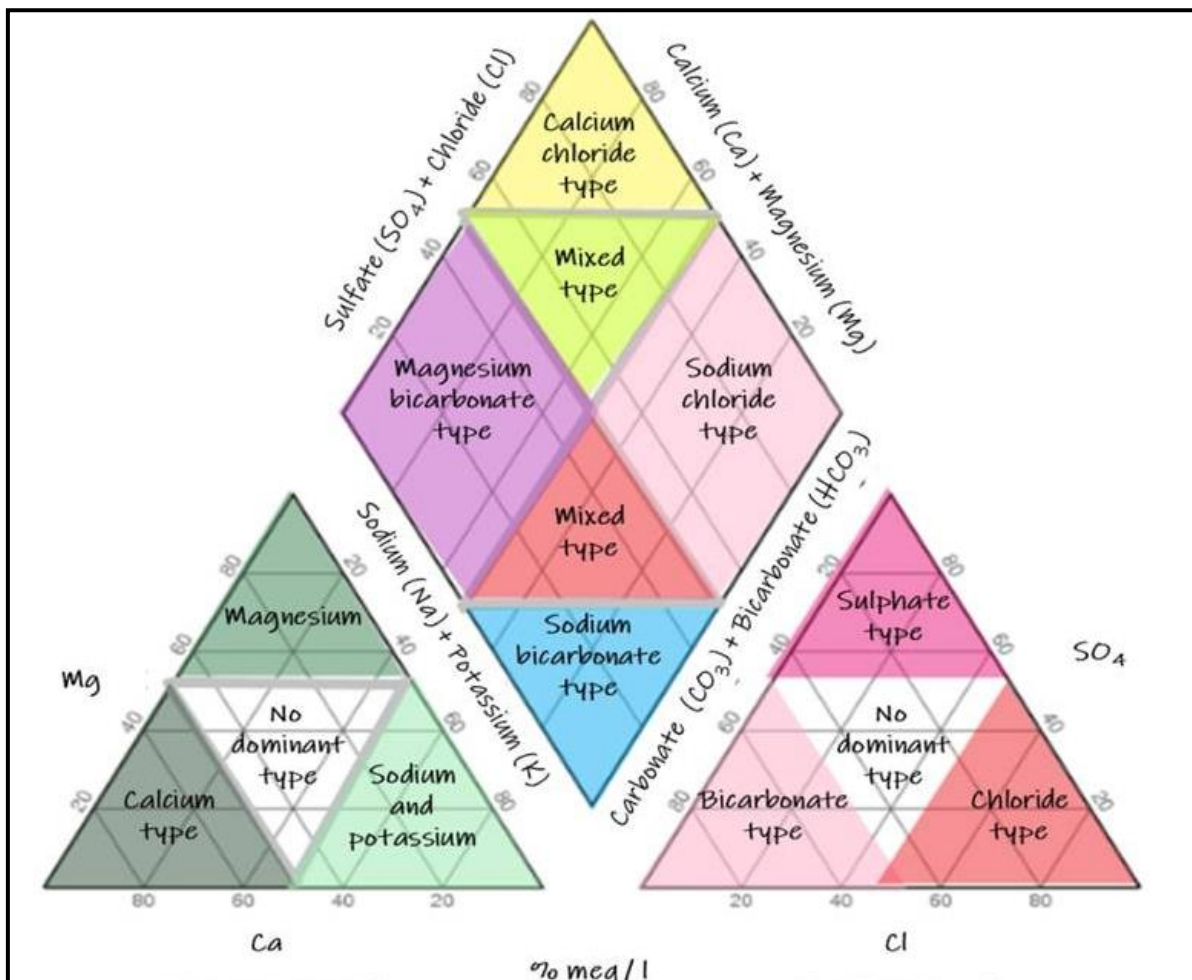
Fig. 6. 2: Hydrochemical facies in Piper Diagram.

6.2. Results

Tables (6.3, 6.4 and 6.5) show the results of hydrochemical analysis of the collected groundwater samples while the admissible levels, given by the World Health Organization (WHO, 1996) and the Egyptian Ministry of Health, law No. 458/2007 (Egyptian Guidelines) for drinking water chemistry, are given in Table (6.6).

6.2.1. Physical parameters

pH Value

One of the most important indicators of water quality is its pH level. pH is a measure of how the water is acid or basic. It is measured on a scale from 0 to 14 where PH with values less than 7 indicate the acidity of water while values higher than 7 indicate its base. The water with value 7 is considered to be neutral, i.e. neither acidic nor basic. The value of the pH is actually a measure of the hydrogen ions in the water. The scale of pH is logarithmic and inversely indicates the concentration of hydrogen ions in the solution as shown in fig. (6. 3). pH level can be affected by groundwater movement through rocks and soil. For example, contact with sandstone results in a nearly neutral pH between 6.5 and 7.5. Limestone, on the other hand, can produce alkaline waters having pH values of about 8.5, or even higher.

The pH values of the collected samples from the study area range between 7.3-7.9, which indicates water of alkaline nature and lying within the limits given by the WHO and Egyptian Guidelines (pH=6.5-8.5) shown in Figure (6.3).

Table. 6. 3: Physical parameters of groundwater samples collected from the studied area.

Sample No.	Depth of drawing (m)	PH	Alkalinity (mg/l)	E.C. (µS/cm)	Resistivity (Ω·m)	TDS (mg/l)
2	70	7.7	536	2560	3.91	1638
4	70-110	7.6	483	6910	1.45	4422
9A	20-30	7.55	585	3200	3.13	2048
9B	70-100	7.45	614	3640	2.75	2329
12	0-15	7.71	761	3510	2.85	2246
14	0-15.5	7.82	488	3620	2.76	2316
15	10-15	7.9	346	827	12.09	529
17	16-20	7.33	219	449	22.27	287
19	20-40	7.42	244	659	15.17	422
22	75-95	7.5	326	7030	1.42	4499
24	75-90	7.61	244	6560	1.52	4198
27	100-135	7.51	273	3660	2.73	2342
29	80-90	7.55	341	4890	2.04	3129
32	80-105	7.61	463	4430	2.26	2835
34	45-120	7.58	390	1632	6.12	1044

Table. 6. 4: Concentration in (mg/l) of major ions of the samples collected from the study area.

Sample No.	Major cations (mg/l)				Major anions (mg/l)			Nutrients (mg/l)		
	Ca^{+2}	Na^+	K^+	Mg^{+2}	Cl^-	Hco_3^-	So_4^-	No_2^-	No_3^-	Po_4^{-3}
2	48.44	350	6	20.5	410.2	536	290.8	<0.2	1.6	<0.2
4	190.87	1200	17.5	40.38	1341.5	483	1145	<0.2	11.7	<0.2
9A	67.2	625	15	34.31	527.6	585	414	<0.2	2.2	<0.2
9B	79.87	700	11	48.3	701.6	614	440.9	<0.2	3.1	<0.2
12	122.06	615	32	36.06	560.2	761	400.6	<0.2	13.2	<0.2
14	213.81	570	32	36.64	600.7	488	608.7	<0.2	8.5	<0.2
15	76.43	70	15	21.76	38.8	346	90.7	<0.2	8	<0.2
17	48.12	29	7	11.27	23	219	27.4	<0.2	0.9	<0.2
19	49.48	71	9	15.45	48.6	244	85.6	<0.2	1.4	<0.2
22	320.8	1150	30	90.06	1400.4	326	1259	<0.2	14.6	<0.2
24	360.49	1090	30	88.31	1250.9	244	1250	<0.2	8.6	<0.2
27	60.63	750	23	29.78	880.6	273	307.3	<0.2	<0.2	<0.2
29	93.19	1000	25	27.11	920.6	341	870.1	<0.2	23.7	<0.2
32	72.66	900	20	33.86	995.2	463	412.1	<0.2	32.2	<0.2
34	43.94	300	6	20.02	217.8	390	186.6	<0.2	13.5	<0.2

Table. 6. 5 (a, b): Concentration (mg/l) of the heavy elements of groundwater samples collected in the study area.

(a)

Sample No.	Al Aluminum	Sb Antimony	As Arsenic	Ba Barium	Cd Cadmium	Cr Chromium	Co Cobalt	Cu Copper
2	<0.007	<0.009	<0.006	0.049	<0.002	0.019	0.004	0.027
4	<0.007	<0.009	<0.006	0.035	<0.002	0.006	0.003	0.028
9A	0.012	<0.009	<0.006	0.096	<0.002	0.003	0.004	0.045
9B	<0.007	<0.009	<0.006	0.061	<0.002	0.003	0.004	0.058
12	<0.007	<0.009	<0.006	0.197	<0.002	0.002	0.005	0.041
14	<0.007	<0.009	<0.006	0.273	<0.002	0.003	0.009	0.048
15	<0.007	<0.009	<0.006	0.178	<0.002	0.003	0.005	0.043
17	<0.007	<0.009	<0.006	0.080	<0.002	0.003	0.005	0.03
19	<0.007	<0.009	<0.006	0.092	<0.002	0.004	0.006	0.021
22	<0.007	<0.009	<0.006	0.032	<0.002	0.003	0.004	0.025
24	<0.007	<0.009	<0.006	0.031	<0.002	0.003	0.004	0.022
27	0.031	<0.009	<0.006	0.069	<0.002	0.005	0.005	0.021
29	<0.007	<0.009	<0.006	0.041	<0.002	0.008	0.007	0.015
32	<0.007	<0.009	<0.006	0.045	<0.002	0.007	0.005	0.017
34	<0.007	<0.009	<0.006	0.059	<0.002	0.002	0.004	0.016

(b)

Sample No.	Fe Iron	Pb Lead	Mn Manganese	Ni Nickel	Se Selenium	Sn Tin	V Vanadium	Zn Zinc
2	0.016	<0.007	0.013	<0.004	<0.007	<0.006	0.018	0.009
4	0.015	<0.007	0.011	<0.004	<0.007	<0.006	0.012	0.011
9A	0.053	<0.007	0.219	<0.004	<0.007	<0.006	0.011	<0.005
9B	0.016	<0.007	0.343	<0.004	<0.007	<0.006	0.023	0.012
12	0.05	<0.007	0.211	0.006	<0.007	<0.006	0.085	<0.005
14	0.061	<0.007	0.53	0.008	<0.007	<0.006	0.064	<0.005
15	0.014	<0.007	0.196	0.004	<0.007	<0.006	0.021	0.017
17	0.093	<0.007	0.436	<0.004	<0.007	<0.006	0.005	0.051
19	0.06	<0.007	0.035	<0.004	<0.007	<0.006	0.009	<0.005
22	0.014	<0.007	0.043	0.007	<0.007	<0.006	0.019	0.011
24	0.021	<0.007	0.008	<0.004	<0.007	<0.006	0.016	0.009
27	0.014	<0.007	0.009	<0.004	<0.007	<0.006	0.014	<0.005
29	0.015	<0.007	0.011	<0.004	<0.007	<0.006	0.016	0.007
32	0.016	<0.007	<0.004	<0.004	<0.007	<0.006	0.017	<0.005
34	0.028	<0.007	0.031	<0.004	<0.007	<0.006	0.022	<0.005

Table. 6. 6: Permissible concentrations of heavy metals in water as set by WHO and Egyptian Guidelines.

Item	Unit	WHO 1996	Egyptian Guidelines 2007
pH	---	6.5 -8.5	6.5 - 8.5
Carbonate (CO_3)	mg/l	----	----
Bicarbonate (HCO_3)	mg/l	----	----
Total Alkalinity	mg/l	----	----
Electrical Conductivity (EC)	µS/cm	----	----
Total Dissolved Solids (TDS)	mg/l	1000	1000
Calcium (Ca)	mg/l	----	----
Potassium (K)	mg/l	----	----
Magnesium (Mg)	mg/l	----	----
Sodium (Na)	mg/l	----	200
Chloride (Cl)	mg/l	250	250
Nitrite (NO_2)	mg/l	3	0.2
Nitrate (NO_3)	mg/l	50	45
Phosphate (PO_4)	mg/l	----	----
Sulfate (SO_4)	mg/l	250	250
Cadmium (Cd)	mg /l	3	3
Barium (Ba)	mg/l	1.3	----
Chromium (Cr)	mg /l	50	50
Copper (Cu)	mg /l	1000	2000
Iron (Fe)	mg /l	300	300
Lead (Pb)	mg /l	10	10
Manganese (Mn)	mg /l	100	400
Nickel (Ni)	mg /l	20	20
Vanadium (V)	mg /l	----	----
Zinc (Zn)	mg /l	3000	3000
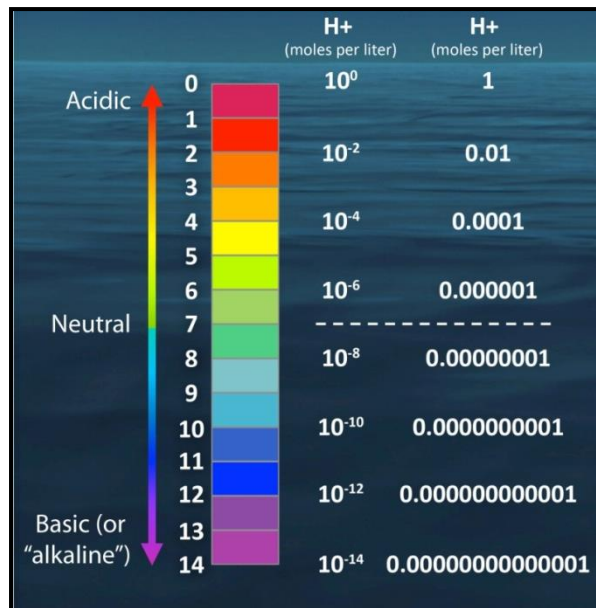
Fig. 6. 3: pH values on a logarithmic scale.

Alkalinity

Alkalinity measures the buffering capacity of the water against changes in pH. In other words, waters with low alkalinity, such as rainwater or distilled water, are very sensitive to changes in pH as alkalinity increases the ability of water to resist to pH changes. Bicarbonates represent the major form of alkalinity in natural waters; its major source is the partitioning of CO_2 from the atmosphere and the weathering of carbonate minerals in rocks and soil. Other salts of weak acids, such as borate, silicates, ammonia, phosphates, and organic bases from natural organic matter, may be present in small amounts. Alkalinity, by convention, is reported as mg/L (refers to carbonates, bicarbonates or calcium carbonates concentrations) since most alkalinity is derived from the weathering of carbonate minerals.

We have to keep in mind that neither alkalinity nor acidity, have any known adverse health effects, but knowledge of these parameters is important for many reasons from which the most important is Bicarbonate (HCO_3^-) and carbonate (CO_3^{2-}) may complex with other elements and compounds, altering their toxicity, transport, and fate in the environment.

In the study area, the alkalinity of the collected water samples ranges from 219 mg/l in sample no. 17 to 761 mg/l in sample no. 12, which is relatively high. We can notice that the bicarbonate anion is the only contributor in the alkalinity value. There are no limits approved by international or local authorities for alkalinity, but we find the highest values in wells No. 9B and 12, which means that there is no specific trend for alkalinity and these high values are due to local sources or concentrations.

EC and TDS and the corresponding resistivity:

TDS and EC are two separate parameters, yet they are somehow connected to each other. EC is the ability of water to conduct electricity while TDS is the sum of the solids dissolved in the water. EC is dependent on temperature and directly related to the type and concentration of salts dissolved in water, (which is related to the total dissolved solids) as salts dissolve into negative and positive charged ions which carry electric current. Yet, the relationship between conductivity and TDS is not directly linear since the conductive mobility of ionic species is variable as univalent ions such as Na^+ and Cl^- are more mobile than multivalent ions such as Ca^{+2}, Al^{+3}, SO_4^{-2} and CO_3^{-2}. Thus, stream water dominant by dissolved Na^+ and Cl^- will have a higher conductivity than the one dominated by Ca^{+2} and SO_4^{-2}, if the pH and electrolyte strength are the same. If the number of ions is very small, in this case the liquid is going to be "resistive" to current flow. We remark that electrical resistivity and conductivity are inversely proportional to each other:

$$\rho = 1/\sigma$$

where

- Resistivity (ρ) measured in Ohm*meters (Ωm),
- Conductivity (σ) is measured in Siemens/m – i.e. ($1/\Omega m$).

The value of electrical conductivity may be an approximate index of the total content of dissolved substance in water. It depends upon temperature, concentration and types of ions present (Hem, 1985). As a rough approximation, the relationship between EC and TDS commonly used is:

[TDS(mg/l) = EC (µS/cm) * 0.67].

EC is widely used for monitoring the mixing of fresh and saline water, for separating stream hydrographs and for geophysical mapping of contaminated groundwater (Hayashi, 2004). According to (Prasanth, et al. 2012), it can be classified into three types; type I, if the enrichments of salts are low (EC < 1,500 µmhos/cm); type II, if the enrichment of salts are medium (EC 1,500 and 3,000 µmhos/cm); and type III, if the enrichments of salts are high (EC > 3,000 µmhos/cm).

According to this classification, more than 75% of our collected samples lie in type III, which indicates high enrichment of salts as shown in table (6.5, 4.6). For a better representation and explanation of our results, we converted the EC values into equivalent resistivity as shown in table (6.4). We can see that resistivity is ranging between 1.4 to 22.3 Ωm which indicates that all the collected water samples have quite high salinity.

This may be evidence of infiltration from the deeper Miocene aquifer or contamination from local sources due to percolation of waste water to the groundwater aquifer from the septic tanks that are used as sanitary system without any cement casing, which allow direct penetration to the underlying aquifer.

Our results confirm that the EC and TDS are linearly related to each other. We can see that the samples taken from the wells near the valley have the lowest values, while moving north or south across the valley the values are very high. This latter condition may indicate water with more pollutants or water with

higher salinity. Also, this agrees with the talk of the local farmers in the area who testified that they get saline water from north and south wells and it occurs even if they dig more than 90 m as given in table (4.4). The use of this water is limited for irrigation purposes and only for some types of plants and cannot be used for drinking or domestic purposes.

Major cations and anions

There are many types of dissolved constituents in groundwater that have a direct effect on its quality. The type and amount of these constituents are controlled by many factors which include the source and chemical composition of recharge water, lithological and hydrological properties of the geologic units, the various chemical processes occurring within the geologic units, and the amount of time through which the water has remained in contact with the geologic units, which is known as Residence Time (Bartos et. al., 2002).

The most abundant measured dissolved constituents are major cations (+ charged) and major anions (- charged). Sodium (Na^+), Potassium (K^+), Calcium (Ca^{2+}) and Magnesium (Mg^{2+}) represent the most popular cations present in water, while chloride (Cl^-), carbonates (CO^{2-}), bicarbonate (HCO_3^-) and sulphates (SO_4^{2-}) are the most abundant anions. So, by measuring the concentration of anions and cations in any water sample, the quality of water is easy to be characterized. In table (6.7) we can see the source of each constituent and its effect on water quality (Bartos et. al., 2002).

Table. 6. 7: source and effect of major cations and anions on water quality.

Constituent	Source	Effect

Na^+ & K^+	Dissolved from many rocks and soil; also in ancient brines, seawater, industrial brines, and sewage.	Large concentrations, in combination with chloride, give a salty taste. Moderate concentrations have little effect on the usefulness of water for most purposes. Sodium salts may cause foaming in steam boilers. A large sodium concentration may limit the use of water for irrigation.
Cl^-	Dissolved from rocks and soil. Present in sewage and found in large concentrations in ancient brines, seawater, and industrial brines.	Large concentrations in combination with sodium, gives salty taste to drinking water. Large concentrations increase the corrosiveness of water towards some metals.
Ca^{2+} & Mg^{2+}	Dissolved from many rocks and soil, but especially from limestone, dolomite, and gypsum. Calcium and magnesium are detected in large quantities in some brines. Magnesium is present in large quantities in seawater.	Causes most of the hardness and scale-forming properties of water; soap consuming due to the hardness of water
SO_4^{2-}	Dissolved from rocks and soil containing gypsum, iron sulfides, and other sulfur compounds. Commonly present in mine water and in some industrial wastes.	Sulfate in water containing calcium forms hard scale in steam boilers. In large concentrations, sulfate in combination with other ions gives bitter taste to water, and may have a laxative effect on some people. Some calcium sulfate is considered beneficial in the brewing process.
HCO_3^- & CO_3^{2-}	Action of carbon dioxide in water on carbonate rocks such as limestone and dolomite.	Bicarbonate and carbonate produce alkalinity. Bicarbonates of calcium and magnesium decompose in steam boilers and hot-water facilities to form scale and release corrosive carbon dioxide gas. In combination with calcium and magnesium, causes carbonate hardness.

The synthesis of chemical characteristics of water samples collected from the study area are hereafter described:

6.2.2. Major cations

The concentration of each cation in the samples collected from the study area is presented in table (6.4) while Fig. (6.3) shows the graphical representation in percentage (%). We can see that the dominance of cations is Na>Ca>Mg>K

where Na is dominant by a percentage of about 82.36% followed by Ca (11.4%), then Mg (4.8%) and finally K (1.4%). Returning back to table (4.4), it is found that Na is exceeding the permissible levels given by the Local authorities in most of the samples except for sample no. 14, 15, and 17 that are taken from the wells near Wadi El-Tumilat. The highest values of Na (>1000) are found in samples no. 4, 22, 24, 29. These high values of Na can limit the use of water for drinking and irrigation purposes. It is remarkable that there is no specific trend for increasing or decreasing direction of the cations which means that the high values are due to local anthropogenic activities and natural processes.
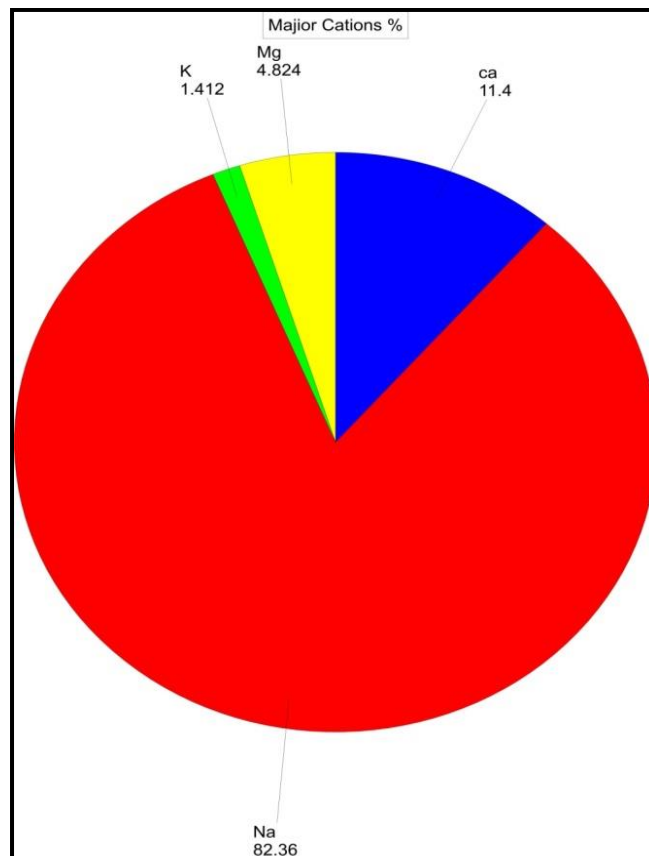
Fig. 6. 4: Cations pie chart for groundwater samples collected from the study area.

6.2.3.   Major Anions

As shown in Fig. (6.4), HCO_3^- is the dominant anion in the whole collected samples (43.3 %) followed by Cl (33.2 %) while SO_4^{2-} is coming at the end

with the least dominance by 23.5 %. There are no permissible limits for HCO_3^- approved by WHO or Egyptian authorities, but it ranges between 219-761 mg/l with the highest concentration in samples 9B, 12 and there is no specific trend for the concentration of HCO_3^- along the path of the collected samples.

The chemical equilibrium equation between bicarbonate and carbonate is: $HCO_3^- = CO_3^{-2} + H^+$. Because bicarbonate and carbonate are on opposite sides of the equilibrium equation, they are not often detected in the same water sample. However, they can occur simultaneously at specific temperatures, pressures and alkaline pH conditions. These conditions can be caused by contamination and leaching from high-pH materials. Carbonate level is zero for whole the collected samples.

Cl^- is ranging from 23 to 1400 mg/l where it exceeds the permissible limits given by WHO and local authorities in all the samples except for sample no. 15, 17, 19 (near Wadi El-Tumilat) and 34 (in the northern parts). Cl comes from many sources, e.g. dissolving from soils and rocks, sewage and industrial brines, sea water. Large concentrations of Cl combined with sodium gives salty taste to water. Returning to table (6.4), we can find that samples with highest concentrations of Na and Cl are no. 4, 22, 24, 29 & 32 which is in accordance with the local inhabitants that said that the water of these wells tastes salty and they don't use for drinking or even for irrigation of many types of plants that can't grow in high levels of salinity. These high concentrations of Cl may result from infiltration of salty water from the deeper Miocene aquifer to the shallow quaternary aquifer.
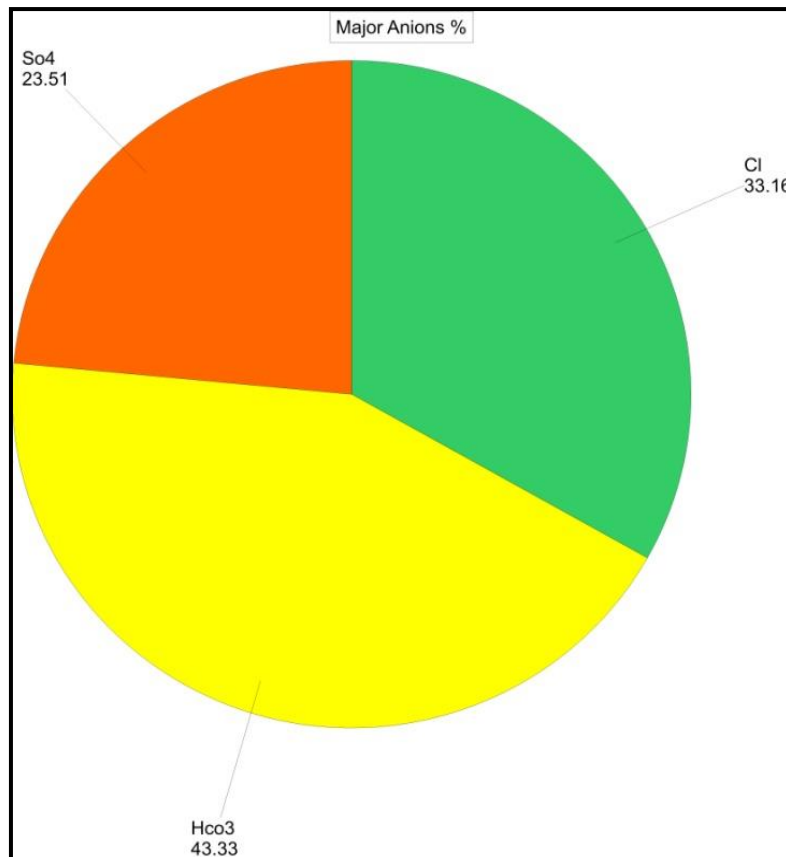
Fig. 6. 5: Anions pie chart for groundwater samples collected from the study area.

For SO_4^{2-} anion, it exceeds the allowed concentrations in all samples (>250 mg/l) except for samples no. 15, 17, 19 &34 while the highest concentrations (>1000) are in samples no. 4, 22 & 24 which may result from industrial wastes and anthropogenic activities.

6.2.4. Nutrients

Concentration of nutrients in groundwater acts as an indicator to identify the influence of agricultural activities on the shallow subsurface environment (Rajmohan et. al., 2005) as excessive use of fertilizers is considered a main reason for increasing the nutrients level in groundwater. The major nutrients resulting from agriculture activities are nitrate, phosphate & potassium. Nitrogen is considered the most important nutrient and it is found in the groundwater in three ionic forms, Nitrate anion (NO_3^-), nitrite anion (NO_2^-) and ammonia cation (NH_4^+).

Nitrate anion is highly mobile and plays the main rule in groundwater pollution resulting from agriculture activities (Nolan et al, 2002). The main sources of nitrates include nitrogenous fertilizers, manure, human and animal wastes. Nitrate is produced through the converting of organic nitrogen that results from plant waste or manures to ammonium ion (NH_4^+) during the ammonification process where the ammonium is subsequently oxidized to nitrate by nitrification (Rajmohan et. al., 2005).

Nitrite is the transition compound as ammonium ions are oxidized to nitrate. With normal oxidative conditions, nitrite is quickly transformed to nitrate, which means that it is found at very low concentrations in groundwater.

Phosphate is normally found in low concentrations in groundwater because it tends to be sobbed into the soil and the aquifer sediments rather than transported into groundwater (Holman et. al., 2008).

In the study area, both nitrite and phosphate are undetected in the analysed samples, where both of them are found at a level that is below detection level (BDL) of the analyser.

Nitrites, in all the samples, lie within the permissible standards (<45 mg/l) that are approved by international or local authorities as shown in fig. (6.5). The highest concentrations are found in sample no. 32 (32.2 mg/l) which lies in the northern part of the study area (El-Salhyia) and this may be due to the agriculture activities and excessive use of fertilizers.
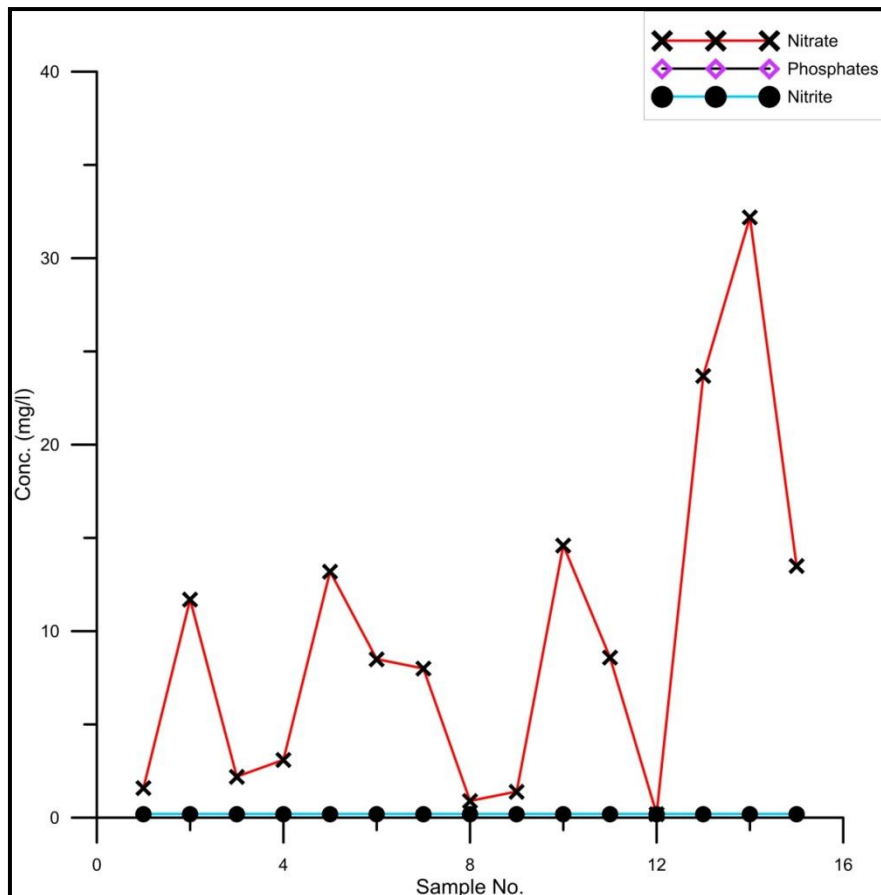
Fig. 6. 6: Graphical display of nutrients concentration in the collected groundwater samples.

6.2.5. Heavy metals

Heavy metals are found naturally in groundwater at permissible levels that are useful for the human health as they are dissolved from sediments and rocks during groundwater movement. Increasing these limits, they can be toxic and cause huge damage to the human body, depending by they own characteristics. So, the presence of these metals in drinking water must be monitored all the time to be kept under control and not to exceed the limits that are approved by WHO. Contamination by heavy metals is also reported in small concentrations around industrial areas and landfills (Lu. et al., 2018). The other important contamination route is through excessive application of agrochemicals that are retained in the unsaturated zone and reach groundwater through irrigation return flow. Accumulation of the bio-toxic heavy metals in crops and subsequent transport in the food chain pose potential risk to human health. Hence, several

130

studies have been conducted on these lines **(Karbassi et al., 2008; Wongsasuluk et al., 2014; Lu et al., 2018)**.

In the study area, most of the present wells are of private property which means that they were dug by local inhabitants and are used directly for drinking and domestic purposes or for irrigation without any controlling or monitoring for heavy metals (and other chemical compounds), which subject local people to high threat for getting diseases that are related to contaminated water and water of overall poor quality.

Concentrations of the heavy metals: Al, Sb, As, Ba, Cd, Cr, Co, Cu, Fe, Pb, Mn, Ni, Se, Sn, Zn and V in the water samples collected from the study area are shown in Table (6.4a, 6.4b), while their allowable concentrations provided by the WHO and Egyptian Guidelines are presented in Table (6.5). Fig. (6.6) shows the graphical representation of these elements. As shown in the table, their order in dominance is as following: Ba>Cu>Cr>V>Fe>Mn>Zn>Sb>Al>Se>Pb>Sn>As>Co>Ni>Cd.
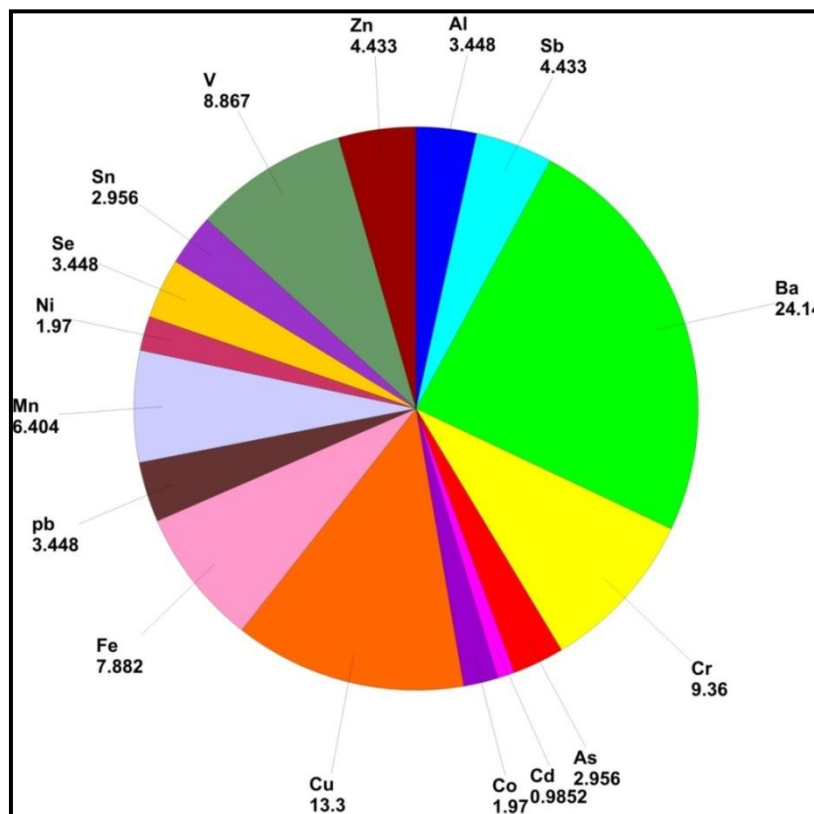
Fig. 6. 7: Pie plot of heavy metals concentrations in the collected groundwater samples.

131

It is significance that all the heavy and trace elements are found in very little concentrations and never exceed the permissible limits.

Barium is the most dominant element in all samples. It is found in many compounds in the environment either normally or from human activities. It is found naturally in most of rocks and sediments and can inter groundwater by leaching and eroding of sedimentary rocks (Contruvo 2018). It is also used in manufacturing of many products like plastics, paints, rubber, etc. High concentrations of Barium in drinking water can affect the blood pressure and kidneys of both humans and animals. In the study area, Barium is found within the allowed limits approved by WHO and Egyptian authorities as it does never exceed 0.5 mg/l.

Copper naturally occurs in soil, rocks, water and plants and it is also basic component in many industries like electrical wiring and household pluming materials like pipes and faucets. In addition, copper components are used in agricultural pesticides and fertilizers. Copper is important for the human and animal bodies but at very limited amounts, exceeding this amount can cause severe danger to the human health. Copper is found naturally in groundwater at very low levels. High levels may result from mining, farming and manufacturing operations. Also, it can enter the drinking water through the corrosion of the copper pipes. In the study area copper is found at very low concentrations which are much lower than the permissible limits given by the WHO (1000 mg/l).

Chromium is widely present in soil, plants and in natural deposits of ores with other elements and it may occur naturally in groundwater. It is found in many industries like stainless steel, magnetic tapes, paints, cement, etc. It can enter the environment as a contaminant through leaching from hazardous waste sites, discharges of dye and paint pigments or burning fossil fuels. It can cause cancer when it is inhaled and also can irritate the lungs. That's why the world

Health Organization had set its allowed limits to 50 mg/l. In the study area, chromium is found with very little trace (>0.1 mg/l) which means that it has no significance effect on the groundwater quality.

Vanadium enters the environment mainly from the burning of fossil fuels, such as residual oils and coal, and from production of steel and manufacture of pigments and paints. Vanadium in the collected samples from the study area shows very low levels than the limits approved by WHO.

Iron and Manganese are metallic elements that can be found in many types of rocks and they are essential elements for all living organisms, but with very small concentrations. It is noticed that concentrations of Fe and Mn in groundwater are higher than those in surface water. Fe and Mn can be either naturally occurring at groundwater through weathering of iron and manganese bearing minerals and rocks or due to anthropogenic resources as industrial effluent, acid-mine drainage, leaching from sewage and landfills. Other sources including well casing, pump parts and piping and storage tanks can be contributing sources for Fe and Mn in groundwater (https://novascotia.ca/nse/water).

Normally, Iron and Manganese are not considered as a health risk at the concentrations they are found in most natural waters. High concentration of iron or manganese may cause the staining of plumbing fixtures or laundry. Also, Mn solids may form deposits within pipes and break off as black particles that give water an unpleasant appearance and taste. Similarly, iron particles can gather together and block pipes or fixtures and produce color, taste and rust flakes in water.

From the collected samples of the study are, we can see that that both iron and manganese are found in very small concentrations where Fe concentration is <0.1 mg/l for all samples and Mn is <1 mg/l. These levels are much lower than those approved by WHO and the Egyptian authorities as given in table (6.5).

Lead is one of the heavy metals that have no known benefit for the human body. On the contrary it is very toxic and has damage effects when it enters the human body even with very low concentration (Saha et al., 2017) as too much lead can cause damage to some body organs like kidneys, nervous and reproductive systems (Todd et al., 1996). For this reason, the WHO approved the permissible limits of lead in drinking water not to be more than 10 mg/l. Lead is used in many manufactures as gasoline, paints, batteries and metallic products. It can enter groundwater through natural or manmade resources as it can leach into drinking water through contact with lead-containing materials such as pipes, fixtures, or solder.

In the study area, as shown in table (6.4b), lead concentration is lower than the detection limit (BDL) of the analyzer in all the collected samples (<0.007 mg/l).

6.3. Water quality by Piper diagram

The Piper diagram for the collected water samples is shown in figure 6.7. Na is the dominant cation, while Cl is the dominant anion. The prevailing water type is Na-Cl, followed by the Na-HCO$_3$ type. The water of Na-Cl type is known to be salty and excessive amounts of dissolved salts in water can affect agriculture, drinking water supplies and the whole ecosystem health. Beside the water usage constraints and limitations, high levels of salinity in water and soil may cause:

- Poor health or death of native vegetation, which in turn alters the ecosystem structure.
- Reduction in crop yields.
- Corrosion of machinery and infrastructure.
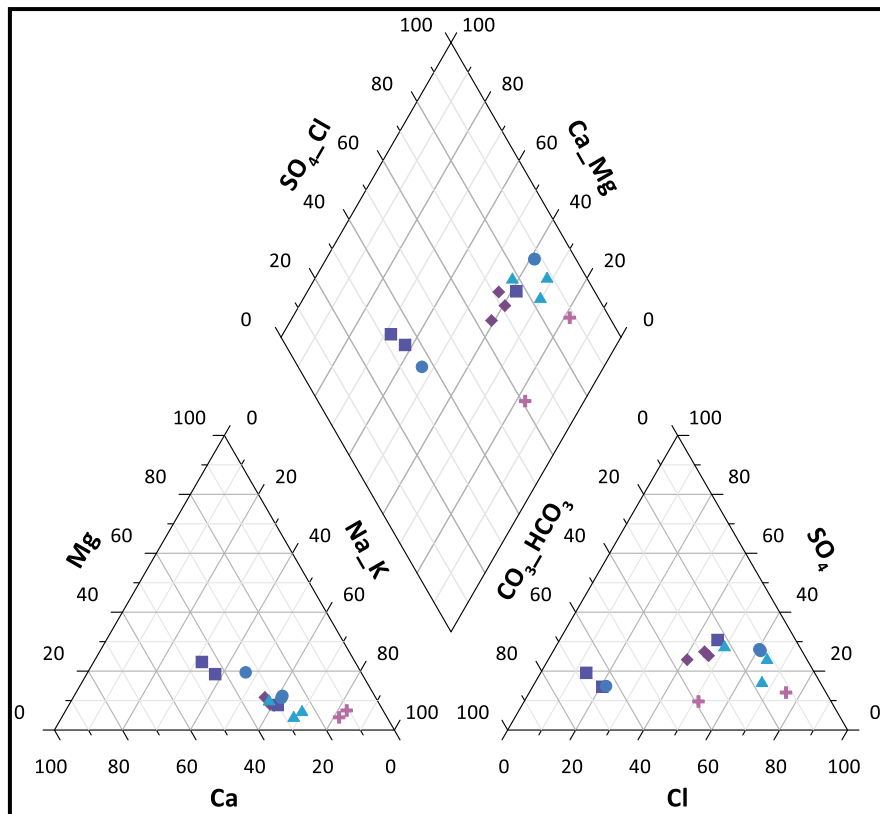
Fig. 6. 8: Piper diagram of groundwater samples from the studied area.

6.4. Conclusions

- From the ERT results, we can conclude that clay is not responsible for the water logging as we expected at first. In fact the geoelectrical properties of the low resistivity unit are not in accordance with those of clay, in particular considering the IP values. Considering the geology of the study area we found that there is a layer of evaporitic loamy sand that agrees with our results and with the description of the local farmers in the area.

- Sediments of this layer need to be geochemically analyzed to study their properties and in turn assessing how much they affect the water logging problem. Unfortunately, due to our limited financial support we couldn't do this up to now.

- Hydrochemical analyses were performed for the collected samples from the study area to explore whether wastewater that percolates from the buried

135

septic tanks used as a sewage system to the underlying groundwater aquifer has affected the water quality or not. No clear evidence indicates that the percolated waste water is the main controller of the ionic levels and distribution or that it has affected the water quality in the investigated area.In fact, the ionic levels randomly vary along the sampling line, and no specific trend could be obtained for their behaviour.

- The detailed hydrochemical analysis revealed that trace and heavy metals are present in very low concentrations in all samples collected from the study area and have no effect on groundwater quality.

- About 75% of the collected samples are characterized by high TDS (>3000) thus exceeding the allowed limits approved by WHO and local authorities, except the samples collected from Wadi El-Tumilat. This may be due to the continuing recharge for the quaternary aquifer from Ismailia Canal. This high salinity may be evidence to the infiltration of the deeper Miocene saline water to the quaternary aquifer or leakage from the sewage. As a result of this high salinity, this water isn't suitable for drinking or domestic uses. In addition, it put some restrictions to the agricultural activities and the growing crops in the study area as many plants can't grow properly in conditions of high salinity, which causes many economic challenges to the agricultural activities dependent community.

- The quality of water should be re-evaluated and monitored from time to time to detect any changes in salinity and water chemistry which may affect the present and future uses of water.

Summary of Achievements

River Nile is the main source of water in Egypt and it is the life artery that provides necessary water for most parts of the country. However, in the last few years, the demand for water in Egypt has increased by a very fast rate due to the significant growth of Egypt's population and to the country aspirations to augment the food through advanced technology-based reclamation.

It is clear that Egypt is suffering from lack in its water resources due to two main reasons. First, its water share of the River Nile is limited, controlled by international agreements, and may be reduced in the future due to developments along the Nile River roots, until the southern Egyptian borders with Sudan (e.g. dams, building new cities, agricultural projects). Second, the River Nile is subjected to violations and contamination due to unmanaged liquid and solid waste disposals in the river itself, which in turn affect the water quality and make the purification process harder and more expensive. As a result, the Egyptian government followed the policy of constructing many water plants in the cities or parts suffering from shortage in water resources in order to provide them with the water needed for various uses (i.e. drinking, domestic, industrial and agricultural).

In this study, the area west to Ismailia city was chosen to test the effectiveness of a combined geophysical and geochemical approach to characterize the aquifers and better planning their future exploitation. Ismailia governorate and its vicinities are characterized by a great social-economic importance as it is considered the east gate for Egypt to Asia Continent and other Arab countries. In addition, it is known by its very high-quality agricultural products which grow thank to its good groundwater resources and high soil potentialities.

However, further developments in this vital part are somehow threatened by shortage in clean surface water supplies and depend mainly on groundwater

resources. Also, this area is facing two main environmental challenges. At first, groundwater is subjected to contamination and deterioration in its quality due to leakage from the poorly developed sewage system of the villages or excessive use of fertilizers. The second problem is water logging that constitutes the major threat for the green economy of this very productive area.

Objectives

- Identification and characterization of groundwater aquifers in the area of interest, which is achieved by integrated geophysical methods including Vertical Electrical Sounding (VES), Electrical Resistivity Tomography (ERT) and Time Domain Electromagnetic (TEM).

- Investigate the possible sources of contamination and deterioration in water quality by hydrochemical analysis of some water samples collected from the available water wells in the study area. By this step we can check the possibility to use groundwaters for drinking and other uses.

- Study the reasons for the water logging problem by applying ERT near some lakes resulted from previous water logging activities.

- Based on the results of fore-mentioned approaches we were able to describe the present situation of groundwater aquifers, to identify the proper locations for drilling new water wells, and to assess the suitability of groundwater for drinking and other purposes.

- Finally, we can implement a Geographic Information System (GIS) database that incorporates all results and information obtained from this study that may boost the sustainable development plans of the considered cities and is a relevant outcome for monitoring and future studies.

Data acquisition and field set up

The first field survey was performed in September 2020 in Egypt with the help of my colleagues and professors of NRIAG. The main purpose of this survey was to perform the regional geophysical data acquisition to characterize and map the groundwater aquifers using (VES) and (TEM) techniques. The study area is about 10x14 km with inter-spacing between stations about 2 km. It includes the desert part, the reclaimed part and the area suffering from the problem of water logging.

In this concern, 35 VES and TEM locations were surveyed to make suitable joint data inversion. The resistivity measurements were performed using the SyscalR2 equipment by applying the standard Schlumberger-electrode configuration with current electrodes (AB) spacing varying logarithmically from 2 to 1000 meters. TEM measurements were conducted using the SIROTEM MK3 instrument where the common single-squared loop configuration with a loop side length of 50 m has been employed and used for both transmitting and receiving the signals.

The second field survey was performed in July 2021 with the aim of studying the environmental problems (specifically water logging and groundwater contamination) within the study area by applying ERT and Hydrochemical analysis. So, 11 ERT profiles were collected: 10 profiles were established in the area that is mainly affected by water logging problem, while one profile was done far away from that area, just to compare the behaviour of ERT in both areas and to understand the reason for water logging. For studying the groundwater quality, 15 water samples were collected from the available water wells that are taping the Pleistocene aquifer.

Data processing and interpretation

- The inversion of the VES and TEM data, individually, give a general view about the electrical properties within the study area. The VES data were inverted using *IPI2WIN 1-D* while TEM data were inverted using *TEMIX Xl 4*. The VES and TEM models were used to construct three geoelectrical cross sections (A-A', B-B' and C-C'). It was revealed that VES inversion includes five geoelectrical layers in most of the built models and six layers in some points, while TEM inversion models are made of six layers in most of the locations with only a few having only five layers. This step was performed to critically evaluate differences and similarities between both methods. The second step was establishing the *1-DJoint Inversion* between VES and TEM data to obtain one multi-layer model at each station that satisfies both data sets. The VES -TEM data have been jointly inverted in a 1-D scheme using the Curupira algorithm.

- The VES-TEM joint models were used to construct three geoelectrical cross sections (A-A', B-B' and C-C'). From these cross-sections six geoelectrical layers were defined in the area. These layers can be grouped in four composite units based on the available geological information of the area. The first unit is made up of the upper most two geoelectric layers and it represents the surface layers that are subjected to different weathering conditions. The second unit comprises the third geoelectrical layer which is representative for Quaternary sand and gravel. Layers No. 4 and 5 represent the Pleistocene aquifer. The last unit is the deepest detected layer and represents the Miocene aquifer that is mainly made of limestone.

- ERT data were processed using RES2DINV program package. The measured data were plotted as "apparent resistivity pseudo-sections" to

check the data quality and measured point distribution. By applying a Least Square Approach, the apparent resistivity was inverted in order to obtain 2D resistivity sections with the real resistivity values. The integration and comparison of the 10 profiles located near water logging lakes revealed three main geoelectrical units within a depth of 40 m. The upper unit extends from the ground surface to depth not exceeding 10-11 m with resistivity between 4-150 Ωm. The middle unit reaches about 30-35 m in many parts along the ERT profiles. One of the peculiar characteristics of this layer is its relatively high chargeability that reaches about 25 mV/V in some points along the measured profiles corresponding to relatively high resistivity values (>250 Ωm). Considering the subsurface geology of the study area, we assumed that evaporitic loamy sand is the layer that corresponds with this geoelectrical feature. According to previous geological studies, this layer extends along the Wadi until it turns completely into evaporates near Suez Canal. So, in our interpretation we think that this layer is responsible for the water logging problem but this could be confirmed only with dedicated geochemical analyses focused on this layer. The lower unit is representing the saturated Pleistocene aquifer. It is characterized by low to medium resistivity values as. It is mainly composed of sand, gravel with local clay intercalations.

- Hydrochemical analyses were performed for 15 water samples collected from the study area to explore whether wastewater that percolates from the buried septic tanks used as a sewage system in most of the study area has affected the water quality or not.

- The detailed hydrochemical analyses revealed that trace and heavy metals are present in very low concentrations in all samples collected from the study area and have no effect on groundwater quality. About 75% of the collected samples are characterized by high TDS (>3000) that exceeds the

allowed limits approved by WHO and local authorities except the samples collected from Wadi El-Tumilat which may be due to the continuing recharge for the quaternary aquifer from Ismailia Canal.

Conclusions

- The geophysical survey conducted at the area shows two distinct aquifer systems, namely: the shallow aquifer of Pleistocene age and the deeper aquifer of Miocene age.

- The Pleistocene deposits are the main water-bearing sediments in the study area and its vicinities. It consists of successive layers of sand and gravel with many clay lenses. The upper surface of this aquifer could be detected at depth from 10 to 83 m below the ground surface with a total thickness ranging from 129 m at station no. 23 and 273 m at station No. 14. Its resistivity ranges between 4 to 95 Ωm.

- The depth to the Quaternary aquifer is mainly affected by the subsurface structural complexity. This causes the infiltration of the deeper saline groundwater belongs to the Miocene aquifer to the Quaternary aquifer in many parts of the investigated area.

- Low resistivity values of this aquifer may be due to presence of clay or infiltration of saline water from the deeper Miocene aquifer along the fault lines.

- For the Miocene aquifer, the results obtained from this work are insufficient to provide detailed information about it. It is mainly made of marly marine sandstone and limestone. Its upper surface is detected at depths ranging from 130 to 328 m with resistivity ranging between 6 and 22 Ωm.

- It was revealed from ERT data inversion and interpretation that the middle unit that is mainly composed by evaporitic loamy sand is responsible for the problem of water logging that threats the study area.

- As a result of high salinity, this water isn't suitable for drinking or domestic uses according to the limits allowed by WHO or Egyptian authorities, which are supposed to be less than1000 mg/l. In addition, it put some restrictions to the agricultural activities and the growing crops in the study area as many plants can't grow properly in conditions of high salinity which cause many economic challenges to the communities highly dependent by agriculture.

At the end of our study we can recommend the following:

- Applying dedicated geochemical analysis for the evaporitic loamy sand layer that we think to be responsible for water logging in order to give verify some working hypotheses with new data
- The quality of water should be re-evaluated from time to time to detect any changes in salinity and water chemistry which may affect the present and future uses of water.
- This study needs to be replicated for areas with similar concerns in eastern parts of Ismailia in order to characterize a wider area and better define possible future mitigation strategies and develop an optimised water exploitation strategy.

References

Abd El-Gawad, A. (1997). Shallow geophysical exploration for defining the water occurrences in the area east of the Nile Delta (Doctoral dissertation, PhD Thesis, University of Ain Shams, Cairo, Egypt).

Albouy, Y., Andrieux, P., Rakotondrasoa, G., Ritz, M., Descloitres, M., Join, J. L. & Rasolomanana, E. (2001). Mapping coastal aquifers by joint inversion of DC and TEM soundings-three case histories. Groundwater, 39(1), 87-97.

Abd El Hamid, A. T., El Mahmoudi, A. S. & El-Haddad, I. M. (2005). Geoelectrical Exploration for Groundwater Around The New Communities, East Nile Delta. In 18th EEGS Symposium on the Application of Geophysics to Engineering and Environmental Problems (pp. cp-183). European Association of Geoscientists & Engineers.

Alley, E. R. (2007). Water quality control handbook. McGraw-Hill Education.

APHA, (2012): Standard methods for the examination of water and wastewater, 22nd edition edited by E. W. Rice, R. B. Baird, A. D. Eaton and L. S. Clesceri. American Public Health Association (APHA), American Water Works Association (AWWA) and Water Environment Federation (WEF), Washington, D.C., USA.

Bartos, T. T., & Ogle, K. M. (2002). Water quality and environmental isotopic analyses of ground-water samples collected from the Wasatch and Fort Union formations in areas of coalbed methane development: implications to recharge and ground-water flow, eastern Powder River Basin, Wyoming (No. 2). US Department of the Interior, US Geological Survey.

Bayoumy, M. R. (1971). Pedological studies on agricultural expansion areas west of the Suez Canal (Doctoral dissertation, M. Sc. Thesis, Fac. Agric., Cairo Univ., Egypt, 85p).

Belkhiri, L., Boudoukha, A., Mouni, L., & Baouz, T. (2010). Application of multivariate statistical methods and inverse geochemical modeling for characterization of groundwater—a case study: Ain Azel plain (Algeria). Geoderma, 159(3-4), 390-398.

Bortolozo, C. A. (2011). Inversão conjunta 1D de dados de SEV e TDEM: aplicações em hidrogeologia (Doctoral dissertation, Universidade de São Paulo).

Bortolozo, C. A., Porsani, J. L., dos Santos, F. A. M. & Almeida, E. R. (2015). VES/TEM 1D joint inversion by using Controlled Random Search (CRS) algorithm. Journal of Applied Geophysics, 112, 157-174.

Bortolozo, C. A. & Porsani, J. L. (2012). Curupira v1. 0. Software de inversão conjunta 1D de sondagens SEV/TDEM. Registro de Software no. 12988-1. Revista da Propriedade Industrial, 2165(090), 145.

Christensen, N. B. and Sørensen, K. I., (1998). Surface and borehole electric and electromagnetic methods for hydrogeological investigations. European Journal of Environmental and Engineering Geophysics 3.

Cotruvo, J. (2018). Drinking water quality and contaminants guidebook. CRC Press.

Dahab, K. A., Omran, A. A., Abdalall, G. Z. & Alkilany, S. M. (2009). Hydrochemical studies of the quaternary groundwater aquifer in El-Salhiya area and its vicinities, East Nile Delta, Egypt. Journal of the Faculty of Science Menoufia University, 23, 171-193.

El-Fayoumy, I. F. (1968). Geology of groundwater supplies in the region east of the Nile Delta. Unpublished Ph. D. Thesis, Fac. of Sci., Geology Department, Cairo Univ., Egypt.

El-Shamy, I. Z. & Geriesh, M. H. (1992). Hydrogeology of west Ismailia area, Egypt. The Desert Institute Bulletin (Egypt).

El Haddad, I. M. (2002). Hydrogeological studies and their environmental impact on future management and sustainable development of the new communities and their surroundings, east of the Nile Delta, Egypt. Unpublished doctoral dissertation). Mansoura University, Mansoura, Egypt.

El-Dairy, M. D. (1980). Hydrogeological studies on the eastern part of Nile Delta using isotope techniques. A master thesis submitted to Zagazig Uni., Egypt.

Ezz El-Deen, H. M. (1993). Sedimentological and geophysical studies of Heliopolis Basin, Cairo-Ismailia Desert Road and their applications, Egypt (Doctoral dissertation, M. Sc. Thesis, Ain Shams University, Cairo, Egypt).

El Shazly, E. M., Abdel Hady, M. A., El Shazly, M. M., El Ghawabby, M. A., El Kassas, L. A., Salman, A. B. & Morsi, M. A. (1975). Geological and groundwater potential studies of El-Ismailia master plan study area remote sensing research project. Academy of scientific research and technology, Cairo, Egypt.

Eltarabily, M. G. A. & Negm, A. M. (2017). Groundwater management for sustainable development east of the Nile delta aquifer. Groundwater in the Nile Delta, 687-708.

El-Rayes, A. E., Shendi, E. H., Geriesh, M. H. & Afify, H. F. (2004). Contamination and treatment model of domestic water supplies of Ismailia

District, Ismailia, Egypt. In Proceedings of the 7th Conference on Geology of Sinai for Development Ismailia, Egypt (pp. 69-80).

El Shazly, E. M., Abdel Hady, M. A., El Shazly, M. M., El Ghawabby, M. A., El Kassas, L. A., Salman, A. B. & Morsi, M. A. (1975). Geological and groundwater potential studies of El-Ismailia master plan study area remote sensing research project. Academy of scientific research and technology, Cairo, Egypt.

Embaby, A., Beheary, M. & Rizk, S. (2017). Groundwater quality assessment for drinking and irrigation purposes in El-Salhia plain East Nile Delta Egypt. Int. J. Eng. Technol. Sci, 12, 51-73.

Farag, I. A. M. & Sadek, A. (1966). Stratigraphy of Gebel Homeira area, Cairo-Suez district. J. Geol. UAR, 10(2), 107-123.

Fitterman, D. V. & Stewart, M. T. (1986). Transient electromagnetic sounding for groundwater. Geophysics, 51(4), 995-1005.

Gad, M. I. (1995). Hydrogeological studies for groundwater reservoirs, east of Tenth of Ramadan City and vicinities. Unpublished M. Sc. Thesis, Ain Shams Univ.

Gad, M. I., El-Kammar, M. M. & Ismail, H. M. G. (2015). Groundwater vulnerability assessment using different overlay and index methods for quaternary aquifer of Wadi El-Tumilat, East Delta, Egypt. Asian Review of Environmental and Earth Sciences, 2(1), 9-22.

Geriesh, M. H. (1994). Hydrogeological and hydrogeochemical evaluation for the groundwater resources in the Suez Canal region, Egypt (Doctoral dissertation, Fac. Sci., Suez Canal Univ).

Hayashi, M., (2004).Temperature-electrical conductivity relation of water for environmental monitoring and geophysical data inversion. Environmental Monitoring and Assessment 96:119–128.

Hem, J. D. (1985). Study and interpretation of the chemical characteristics of natural water (Vol. 2254). Department of the Interior, US Geological Survey.

Holman, I. P., Whelan, M. J., Howden, N. J., Bellamy, P. H., Willby, N. J., Rivas-Casado, M., & McConvey, P. (2008). Phosphorus in groundwater—an overlooked contributor to eutrophication?. Hydrological Processes: An International Journal, 22(26), 5121-5127.

Jupp, D. L. B. and Vozoff, K., (1975). Joint inversion of geophysical data. Geophysical Journal of the Royal Astronomical Society, V. 42, pp. 977-991.

Karbassi, A. R., Monavari, S. M., Nabi Bidhendi, G. R., Nouri, J., & Nematpour, K. (2008). Metal pollution assessment of sediment and water in the Shur River. Environmental monitoring and assessment, 147(1), 107-116.

Khalil, M. A., Abbas, A. M., Santos, F., Massoud, U. and Salah, H., (2012). Application of VES and TDEM techniques to investigate sea water intrusion in Sidi Abdel Rahman area, northwestern coast of Egypt. Arab J Geosci DOI 10.1007/s12517-012-0564-z.

Klein, J., and Lajoie, J., (1980). Electromagnetic Prospecting for Minerals. Practical Geophysics for the Exploration Geologist, Northwest Mining Association, Spokane, WA.

Kunetz, G., (1966). Principles of direct current resistivity prospecting. Gebrüder-Borntraeger, Germany.

IPI2Win-1D Program, (2000). Programs set for 1D VES data interpretation, Dept. of Geophysics, Geological faculty, Moscow University, Russia.

Loke, M. H., (1999). Time-lapse resistivity imaging inversion. Proceedings of the 5th Meeting of the Environmental and Engineering Geophysical Society European Section, Em1.

Loke, M. H., (2001). 2-D and 3-D electrical imaging surveys (Tutorial).

Lu, H., & Yu, S. (2018). Spatio-temporal variational characteristics analysis of heavy metals pollution in water of the typical northern rivers, China. Journal of Hydrology, 559, 787-793.

Massoud, U., Santos, F., El Qady, G., Atya, M. and Soliman, M., (2010). Identification of the shallow subsurface succession and investigation of the seawater invasion to the Quaternary aquifer at the northern part of El Qaa plain, Southern Sinai, Egypt by transient electromagnetic data. Geophysical Prospecting, 2010,58, 267–277

Massoud, U., (2005). Geophysical studies for groundwater exploration in El-Bruk area, north central Sinai, Egypt. Ph.D. Thesis, Fac. Of Sciences, Minufiya Univ., Egypt.

Meju, M. A. (2005). Simple relative space–time scaling of electrical and electromagnetic depth sounding arrays: implications for electrical static shift removal and joint DC-TEM data inversion with the most-squares criterion. Geophysical prospecting, 53(4), 463-479.

Metwaly, M., Elawadi, E., Sayed, S. R. and Al-Arifi, M., (2014). Combined Inversion of Electrical Resistivity and Transient Electromagnetic Soundings for Mapping Groundwater Contamination Plumes in Al Quwy'yia Area, Saudi Arabia. JEEG, March 2014, V. 19, Issue 1, pp. 45–52.

Miller, K. D., (1994). A Model for the Development of Simple Cell Receptive Fields and Orientation Columns Through Activity-Dependent Competition Between ON- and OFF-Center Inputs. Journal of Neuroscience 14, 409-441.

Nabighian, M. N., (1979). Quasistatic transient response of a conducting half-space. An approximate representation, Geophysics, 44, 1700-1705.

Nolan, B. T., Hitt, K. J., & Ruddy, B. C. (2002). Probability of nitrate contamination of recently recharged groundwaters in the conterminous United States. Environmental science & technology, 36(10), 2138-2145.

Parasnis, D. S., (1997). Principles of Applied Geophysics, 5th edition,Chapman & Hall, London.

Pazdirek, O., & Blaha, V. (1996). Examples of resistivity imaging using ME-100 resistivity field acquisition system. In 58th EAGE Conference and Exhibition (pp. cp-48). European Association of Geoscientists & Engineers.

Piper, A. M. (1944). A graphic procedure in the geochemical interpretation of water-analyses. Eos, Transactions American Geophysical Union, 25(6), 914-928.

Price, W. L. (1977). A controlled random search procedure for global optimisation. The Computer Journal, 20(4), 367-370.

Prasanth, S. V., Magesh, N. S., Jitheshlal, K. V., Chandrasekar, N., & Gangadhar, K. J. A. W. S. (2012). Evaluation of groundwater quality and its suitability for drinking and agricultural use in the coastal stretch of Alappuzha District, Kerala, India. Applied Water Science, 2(3), 165-175.

Raiche, A. P., Jupp, D. L. B., Rutter, H. & Vozoff, K. (1985). The joint use of coincident loop transient electromagnetic and Schlumberger sounding to resolve layered structures. Geophysics, 50(10), 1618-1627.

Rajmohan, N., & Elango, L. (2005). Nutrient chemistry of groundwater in an intensively irrigated region of southern India. Environmental Geology, 47(6), 820-830.

Reynolds, J. M., (1997). An introduction to applied and environmental geophysics, PDF, West Sussex, PO19 IUD, England.

Saha, S., Saha, B. N., Pati, S., Pal, B., & Hazra, G. C. (2017). Agricultural use of sewage sludge in India: benefits and potential risk of heavy metals contamination and possible remediation options–a review. International Journal of Environmental Technology and Management, 20(3-4), 183-199.

Said, R. & Beheri, S. (1961). Quantitative geomorphology of the area east of Cairo. Bull Soc Geogr Egypt, 34, 125-150.

Salem, Z. E. S., Fathy, M. S., Helal, A. F. I., Afifi, S. Y. & Attiah, A. M. (2021). Groundwater Quality for Irrigation as an Aspect of Sustainable Development Approaches: A Case Study of Semi-Arid Area Around Ismailia Canal, Eastern Nile Delta, Egypt. In Groundwater in Egypt's Deserts (pp. 295-326). Springer, Cham.

Schmutz, M., Albouy, Y., Guérin, R., Maquaire, O., Vassal, J., Schott, J. J. & Descloîtres, M. (2000). Joint electrical and time domain electromagnetism (TDEM) data inversion applied to the Super Sauze earthflow (France). Surveys in Geophysics, 21(4), 371-390.

Shata, A. & El Fayoumy, I. (1970). Remarks on the regional geological structure of the Nile Delta.

Shukri, N. M. & El Ayouty, M. K. (1956). The geology of Gebel Iweibid-Gafra area, Cairo-Suez district. Bull. Soc. Geogr. Egypt, 29, 67-109.

Sørensen, K. I., Auken, E., Christensen, N. B. and Pellerin, L., (2005). An Integrated Approach for Hydrogeophysical Investigations: New Technologies and a Case History. In Butler DK (ed.) Near-Surface Geophysics 2, Investigations in Geophysics 13: 585–603. Society of Exploration Geophysics.

Srinivasamoorthy, K., Vasanthavigar, M., Chidambaram, S., Anandhan, P., Manivannan, R. and Rajivgandhi, R., (2012). Hydrochemistry of groundwater from Sarabanga Minor Basin, Tamilnadu, India. Proceedings of the International Academy of Ecology and Environmental Sciences, 2012, 2(3):193-203.

Swift, R., (1990). Transient electromagnetic soundings in complex geological environments. Ph. D. Thesis, Leicester Univ., UK.

Todd, A. C., Wetmur, J. G., Moline, J. M., Godbold, J. H., Levin, S. M., & Landrigan, P. J. (1996). Unraveling the chronic toxicity of lead: an essential priority for environmental health. Environmental Health Perspectives, 104(suppl 1), 141-146.2

Ward, S. H. and Hohmann, G.W., (1987). Electromagnetic theory for geophysical application. In: Electromagnetic Methods in Applied Geophysics (ed. M. N. Nabighian), pp. 131–312. SEG.

WHO (1996). World Health Organization: Guidelines for drinking 640 water quality. In Health criteria and other supporting information- 641, vol. 2, Geneva.

Wongsasuluk, P., Chotpantarat, S., Siriwong, W., & Robson, M. (2014). Heavy metal contamination and human health risk assessment in drinking water from shallow groundwater wells in an agricultural area in Ubon Ratchathani province, Thailand. Environmental geochemistry and health, 36(1), 169-182.

Zaghloul, Z. M., Taha, A. A., Hegab, O. & El Fawal, F. (1977). The Neogene-Quaternary sedimentary basins of the Nile delta. Egyptian Journal of Geology, 21(1), 1-19.

Zhou, B., & Dahlin, T. (2003). Properties and effects of measurement errors on 2D resistivity imaging surveying. Near surface geophysics, 1(3), 105-117.

Zohdy, A. A. R., Anderson, L. A. and Muffler, L. J. P., (1973). Resistivity, self-potential and induced polarization surveys of a vapor-dominated geothermal system. Geophysics, V. 38, pp. 1130-1144.

Appendix A:

FIELD SURVEY, DATA PROCESSING AND INTERPRETATION

Table (1): Geoelectrical parameters obtained from VES data.

St.	ρ1	ρ 2	ρ3	ρ4	ρ5	ρ6	H1	H2	H3	H4	H5
1	22.34	46.1	16.11	10.85	22.04		0.746	6.16	43.69	103	
2	48.6	96.2	37.7	12.6	4.95		0.614	12	29.7	108	
3	250	59	13	18.3	4.08		0.536	8.71	27	109	
4	195	53	149	28.25	14	6.25	0.4	1.09	3.41	25.5	118
5	87	174	17.98	30.92	3.25		0.776	3.728	44.99	84.6	
6	25.6	61.5	9.8	16.9	4.08		0.115	2.46	38	93	
7	49.5	20.6	36.3	15.05	9.43		1.62	4.06	24.1	113	
8	78.3	16.3	6.38	22.3	3.63		0.98	1.48	23.5	96.7	
9	33.76	62.44	140.5	22.6	10.4	4.18	0.6745	0.63	2.82	19.8	119
10	7.76	30.8	9.43	19.8	2.5		0.557	2.61	24.6	86.5	
11	9.07	5.9	12.4	20.5	8.65		0.525	3.97	39.1	96	
12	3.35	8.9	2.934	17.48	10.28	5.566	0.495	0.72	4.36	30	109
13	32.9	8.2	20.8	13.5	4.8		0.441	4.36	19.5	102	
14	36.3	97.7	27.5	16	6.43		1.6	3.9	28.7	109	
15	37	7.57	44.3	15.2	3.42		0.742	1.6	22.6	102	
16	32.2	11.2	74.3	32.2	15.9		0.84	2.79	40.5	90.4	
17	18	10.6	33.5	21	16		0.59	3.41	43.2	97.7	
18	26.67	11.3	68.28	20.59	49.9	15.2	0.564	2	4.69	26.9	95.2
19	80.5	235	53	149	37.5	11.7	1.34	1.47	11.8	19.7	109
20	8.89	32.9	11	27	7.28		0.562	1.6	23.5	115	
21	14.5	71.2	157	66.4	14.2	8.39	0.467	1.47	16.7	40	98
22	5.959	21.45	6	12.9	21.16		0.749	6.9	58.84	101.4	
23	12.6	113	65.9	31	17.9		2.4	9.1	33.9	109	
24	28.6	74.2	124.9	32.89	17.6		0.888	5.84	38.5	110	
25	18.5	104	29.2	10.4	5.5		1.32	7.92	34	94.3	
26	79.3	124	349	202	24	12.2	0.6	2.56	8	61.9	95.9
27	7.5	66.45	35.5	18.72	11.5		1.7	24.3	41.5	109	
28	11.7	80.4	181	100	25.9	6.9	0.853	3.67	19.9	18	109
29	20	244	122	31.6	12.3		1.58	13.3	28.6	111	
30	18.3	118.5	75.7	18.9	4.7		1.666	11.49	33.5	93.4	
31	8.72	54.2	218	33.5	12.6		0.823	3.67	70	85.1	
32	19.23	200.3	70.71	26.67	10		1.26	14.43	38.9	120.2	
33	31.6	119.4	52	17.97	8.04		2.31	12.14	24.6	115.6	
34	25.9	286	90.6	17.4	6.9		1.55	5.3	32.5	95.3	
35	17.55	97.42	68.43	22.8	4.682		1.442	13	31.5	96.8	

Table (2):Geoelectrical parameters obtained from TEM data

St.	ρ1	ρ 2	ρ3	ρ4	ρ5	ρ6	H1	H2	H3	H4	H5
1	17.2	5.93	26.3	13.6	3.4	1.5	20	30	43.8	76.2	136.7
2	34.5	11.9	5.5	20.4	8.9	1.2	15.6	24.2	53.3	57	105
3	42.8	3.7	16.5	5.8	1.7	1	14.7	22	63.4	52	124.6
4	84	36.8	5.4	24	6.9	1.4	16	16.4	34.3	70.8	117.9
5	164.5	35	2.375	22.65	11.35	2	38.3	14.7	39.7	55.69	102.46
6	87.3	3.5	15	10.64	4.88	1.5	17.39	22.79	52.4	45.73	77.65
7	84.2	31	4.3	15.3	5.45	1.1	20.3	12.4	30.34	77.64	77.78
8	112.5	44.9	7.4	18	9.3	1.3	15.8	10.3	31.8	66	110.7
9	10	14.2	25	18.5	7.4	0.774	13	15.3	43.2	60.4	113.6
10	42.9	3.67	14.5	9.7	6.53	1.77	15.4	14.4	39.9	61	120.3
11	49.5	6.2	25.8	10.3	4	1.5	19.7	29.6	43.4	56.4	77.9
12	24.5	3	26.4	3.2	1.23		30.69	32	78	92.3	
13	6	15.9	7.8	4.4	0.8		30	35.4	58.2	96.6	
14	174.5	80.68	15	59.58	30.35	6	34	34.6	62.7	75.75	137.9
15	69.58	7.3	39.9	6	1.4		26.85	64	70.3	137.57	
16	23.5	76.6	37.8	13.4	2	1.1	14.4	26.54	42.67	43	106.5
17	165.68	67	15.4	6.55	1.3		43.78	38.64	76.2	66	
18	140	102.2	59.2	29.1	5		34.3	52.8	42.6	156.3	
19	48.64	129.5	14.9	2.24	1.1		9.4	25.2	104.97	78.2	
20	32.55	61	35.4	12.56	2.74		24	45	67.4	86	
21	24.7	22.4	10	5	2.5	1.5	21.7	18	21.7	96.359	88
22	25.69	4.7	14.7	5.8	2	1.5	25.6	35	42.5	55.5	90.9
23	27.2	2.7	9.6	3.7	1.7	1.1	31	19.2	64.4	44.6	96.3
24	55	22	9.24	5.7	1.95	1.27	34.3	10.4	30.6	72.8	101.4
25	28	5.1	10.3	2.9	1.3		22	23.5	106.4	108.6	
26	14.9	40.2	9	1.5	0.64		23.5	45.5	102.7	49.96	
27	9.6	34.6	14.5	6.8	0.467		38	32.56	106.3	96.6	
28	37.4	3.2	16.3	4.5	1.7		25.1	20.5	106.7	98	
29	43.2	5.5	15.5	7	2	0.675	29.2	19.8	61.7	47	52.9
30	88.8	4.76	8.85	3.83	2		24	22.3	96	100	
31	23	38	19	6	0.12		8.58	60.2	92.2	103.4	
32	51.2	21	12.4	4.7	2	0.84	22.4	29.5	64.54	51.5	54.3
33	40.4	15.8	8.5	1.9	0.8		7.6	29.6	113	70.6	
34	67.8	34.95	12.59	1.98	0.587		14	28.3	83.87	96.3	
35	64.88	39	7.2	1.65	1		17.3	25.2	104.8	87.2	

Table (3): Geoelectrical parameters obtained from VES-TEM joint inversion.

St.	ρ1	ρ 2	ρ3	ρ4	ρ5	ρ6	H1	H2	H3	H4	H5
1	21.8	52.4	18	8	16	2.2	1.6	2.4	19	75	133
2	42	82.7	4.8	36.4	9.3	1.5	0.5	22.2	40.8	27.5	167.8
3	139	34	2.4	12.5	9.9	1.6	0.6	11.2	11.3	89	87.8
4	254.3	77.5	87.7	9	14	2.8	0.3	1.4	8.9	70	196
5	53.7	118	12.5	2	19.8	2	1.1	3.1	72.5	30.6	156.7
6	17.6	42.6	7	21	7.9	1.5	0.11	2.5	73	19.9	117.4
7	53	27	71	5.2	13	0.8	1	20.4	13	50	137
8	80.9	20	7.2	21.8	12.2	1.7	1	1.3	20.7	64	141.2
9	53.3	260	37	8.7	17.4	1.5	1	2.3	26.4	38.8	164
10	5.1	21	5.5	15.8	9	2.8	0.4	4	27.3	54.7	125.8
11	6.3	4.8	11.3	30.2	4.2	1.5	0.8	5.4	12	51.8	60
12	1.3	12.6	2.8	14.6	7	1.4	0.2	0.2	7.8	28.2	184.4
13	27	6	17.4	5.5	10.9	1.4	0.4	6	24.4	51	111.2
14	75	176.8	56.8	13.3	44.3	8.5	1.5	4.8	48.3	43.5	229.4
15	36.2	7.8	42.6	7.9	14.7	3	0.9	1.7	31.4	35.5	106.5
16	25.7	10.7	62.2	16.8	55.3	1.9	0.6	4.9	28.6	109.5	86.4
17	33	16	55.2	38	9.4	2.6	0.4	4.8	14.7	120.7	70
18	28.7	69.2	39.4	149	40.6	7.5	2.4	17.5	49.2	62	121.7
19	38.4	63.8	22.7	172	15.8	2.4	0.8	4.2	12.2	9.8	120.6
20	18.1	59.5	20.8	29.7	63.9	3.3	0.7	1.5	19.3	77	101.3
21	9.5	57.6	41.4	5.3	4.5	3	1.1	17.7	24.7	96.6	44.4
22	9.7	28.5	6.8	29.7	2.6	22	1.2	6.2	67.4	64.2	151.7
23	3.7	99	4.4	14.5	5.5	1.7	3.8	6.4	21.8	52	77
24	8.9	25	43.7	6.8	2	1.7	1	10.5	35	102.3	91.7
25	15.4	80	3.7	18	7.2	2	1.5	13.9	18	44.8	122.5
26	32	134.2	76.9	4.7	13.8	0.8	2.3	3.7	67	56.7	76.4
27	5.5	45	54	4.5	23	0.8	1.7	30.6	18.3	29.8	190
28	4.6	62.4	2	13	12	1.6	1.4	33	14	64.6	108.8
29	5.3	53.8	101	7.6	17	1.8	1.4	13	11	55.3	91.3
30	9	45.3	75.5	4.5	11.6	3.3	1.4	10.2	18	41.2	90.3
31	1.2	52.9	334.2	14.9	12	1.6	0.2	8.9	35.4	101.4	102.3
32	8.9	95	84.5	12	2.4	1	1.4	3.6	20	124.3	85.2
33	16.8	57	50.7	35.4	7.4	1.9	2.2	10.4	16	2.9	139.4
34	16.2	171.2	76.5	11.6	1.8	0.7	1.5	4	27	117.7	110.6
35	7.6	40.8	94	8.5	2.3	4	1.4	24.5	5	115.9	103.2

Appendix B:

ELECTRICAL RESISTIVITY TOMOGRAPHY (ERT)

Table (1): summary of data statistics for profile 1.

| P1	Resistivity (Ωm)	IP (mV/V)
Data points	343	343
Minimum	3.2	3.4
Maximum	239	15.1
Mean	71	6.7
Standard deviation	39.7	2.2

a)

b)

c)
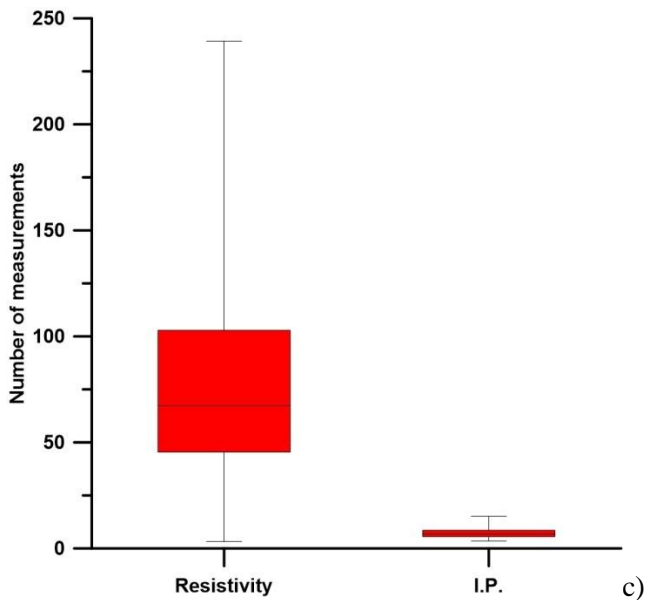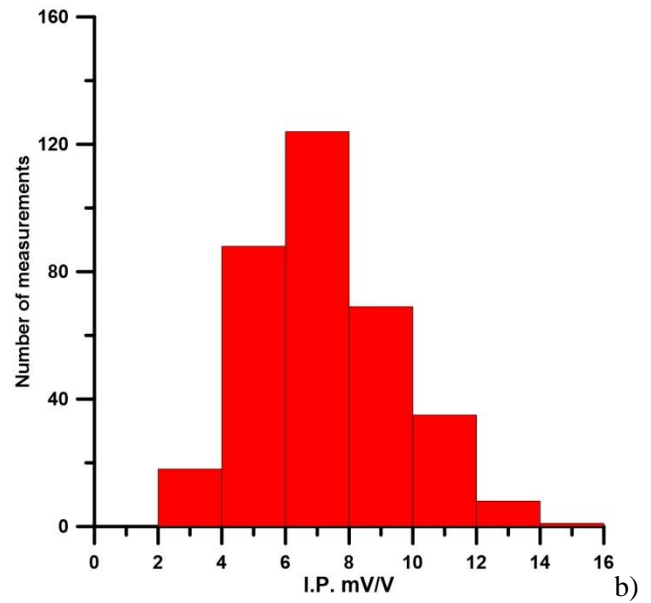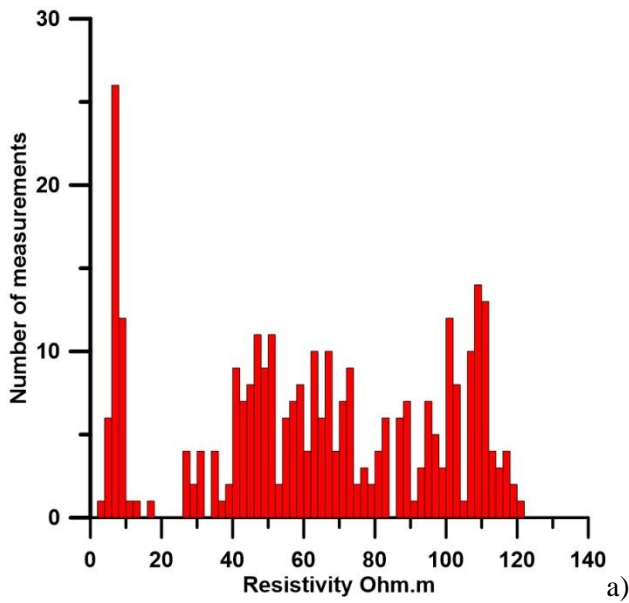
Fig. (1): Statistical representation of the collected resistivity and IP data for profile 2; a) histogram of the resistivity data, b) histogram of the IP data, c) Box plot for both data.

Table (2): summary of data statistics for profile 2.

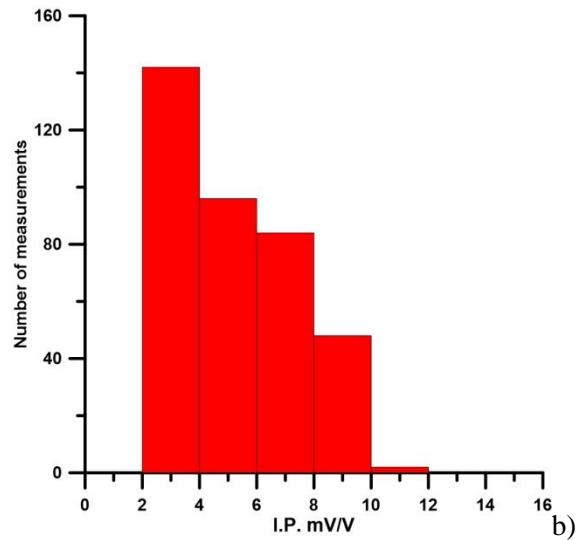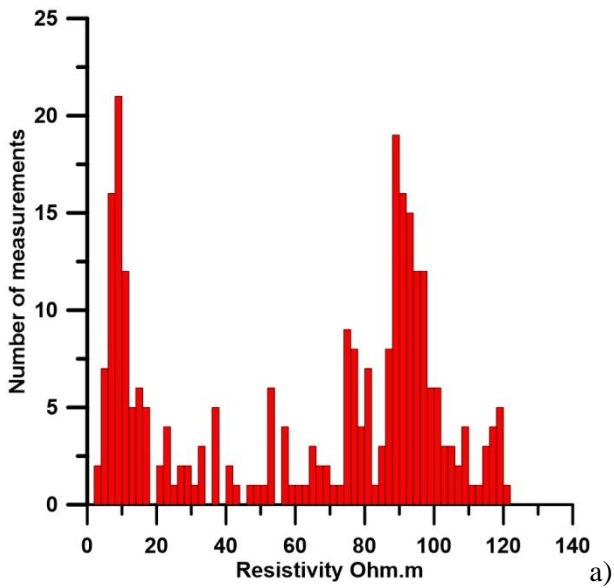| P2	Resistivity (Ωm)	IP (mV/V)
Number of Values	343	343
Minimum	3.8	2.8
Maximum	116.7	21.6
Mean	61.7	7.1
Standard deviation	29.2	2.4
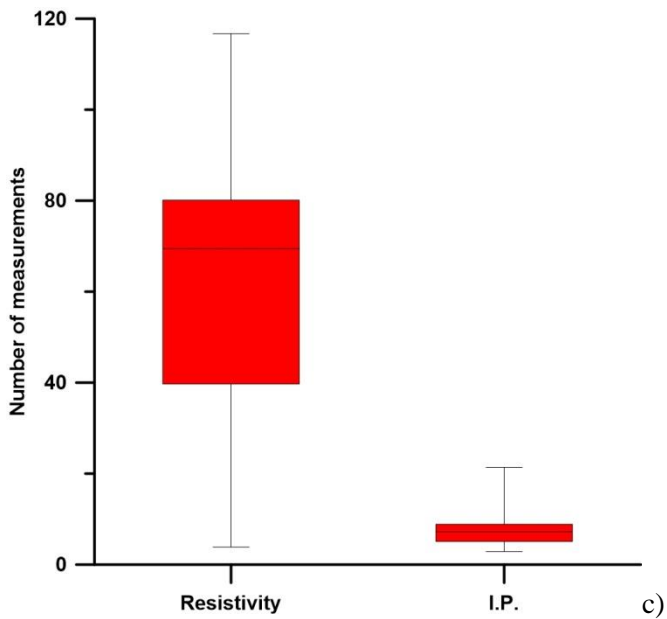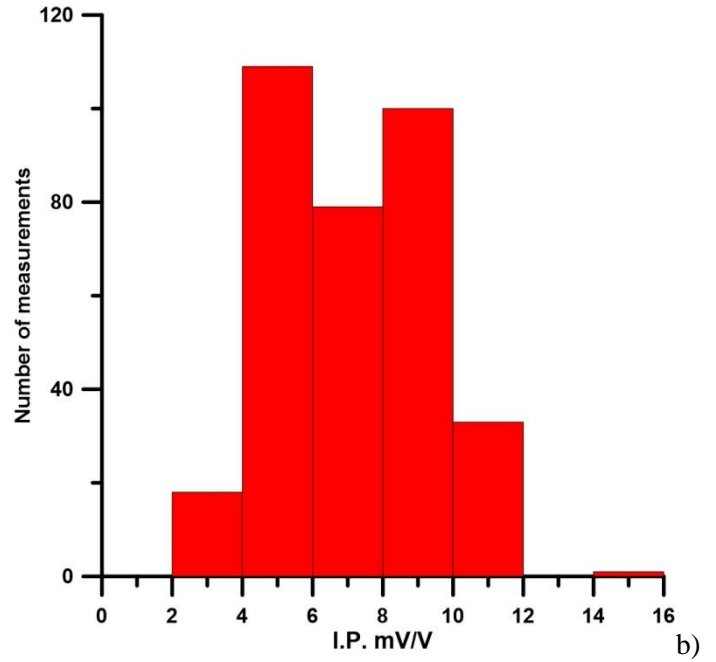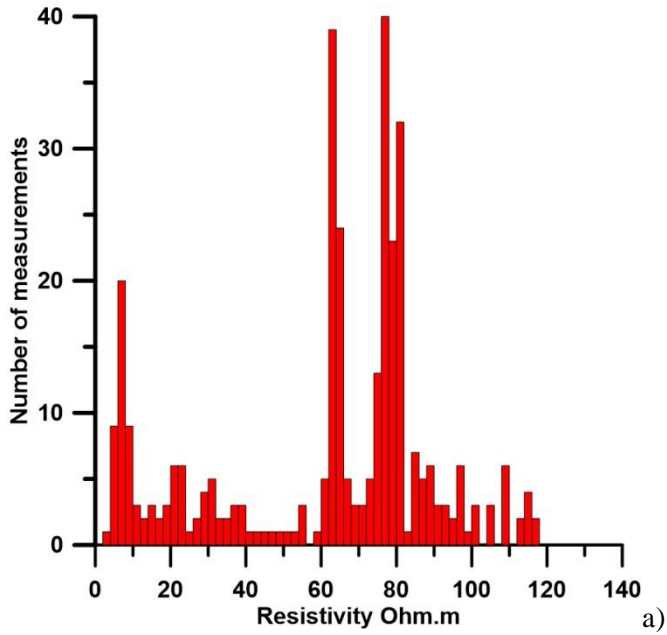
Fig. (2): Statistical representation of the collected resistivity and IP data for profile 2; a) histogram of the resistivity data, b) histogram of the IP data, c) Box plot for both data.

Table (3): summary of data statistics for profile 3

| P3	Resistivity (Ωm)	IP (mV/V)
Number of Values	343	343
Minimum	3.4	2.9
Maximum	124.8	12.8
Mean	54	8.6
Standard deviation	30.8	3

a)

b)

c)
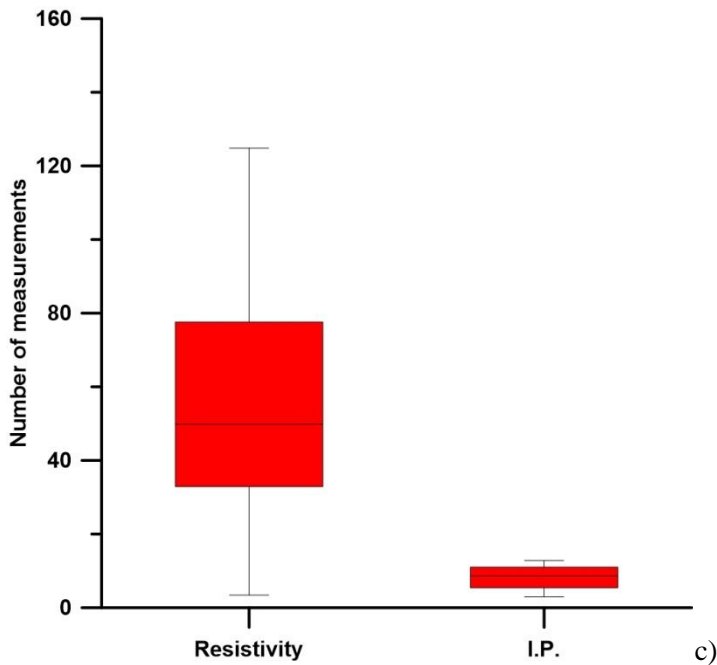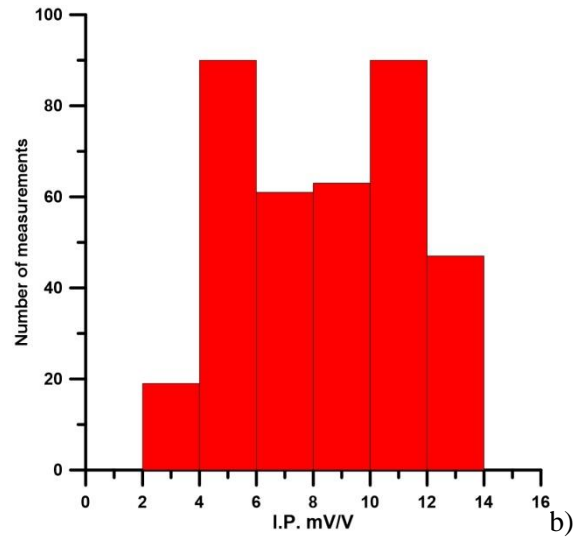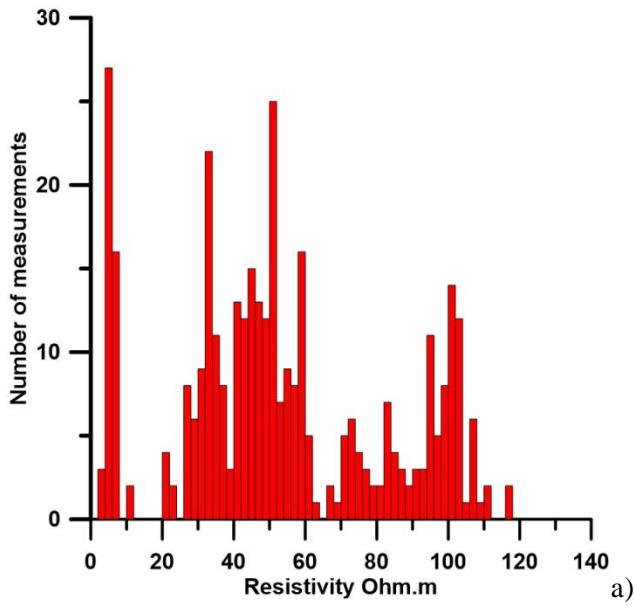
Fig. (3): Statistical representation of the collected resistivity and IP data for profile 2; a) histogram of the resistivity data, b) histogram of the IP data, c) Box plot for both data.

Table (4): summary of data statistics for profile 4.

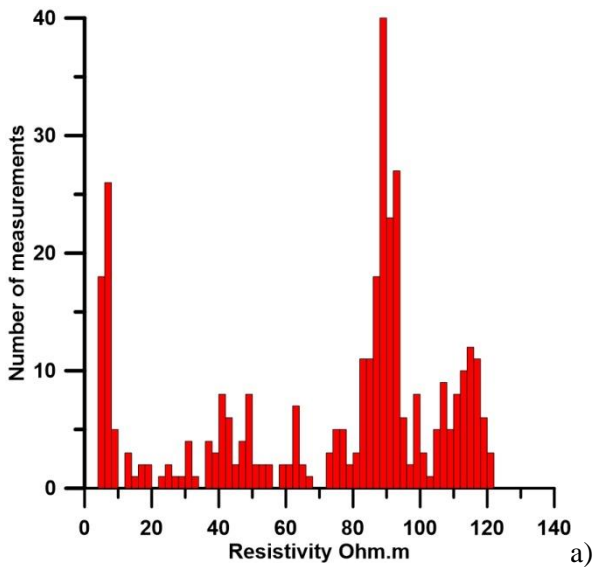| P4	Resistivity (Ωm)	IP (mV/V)
Number of Values	370	370
Minimum	2.5	2.5
Maximum	215	15.7
Mean	75.8	6.6
Standard deviation	64.6	2.7
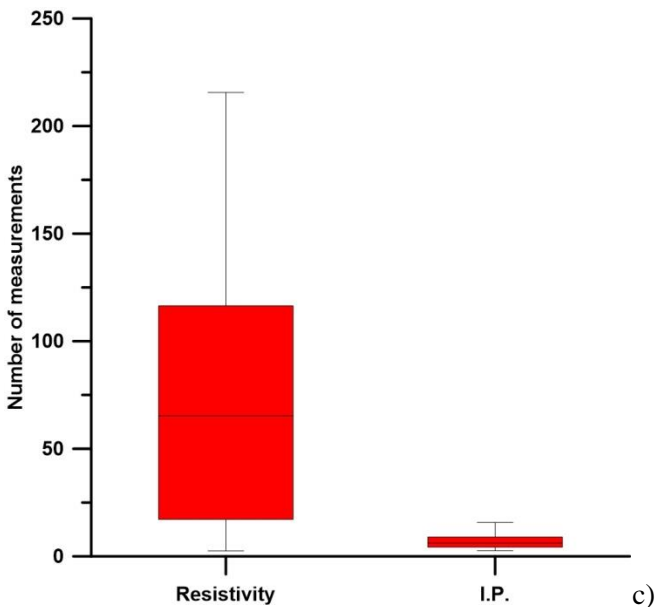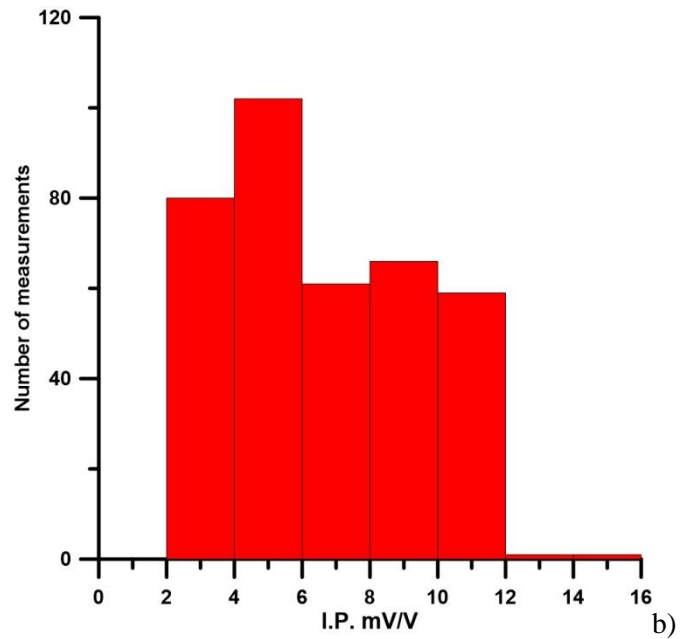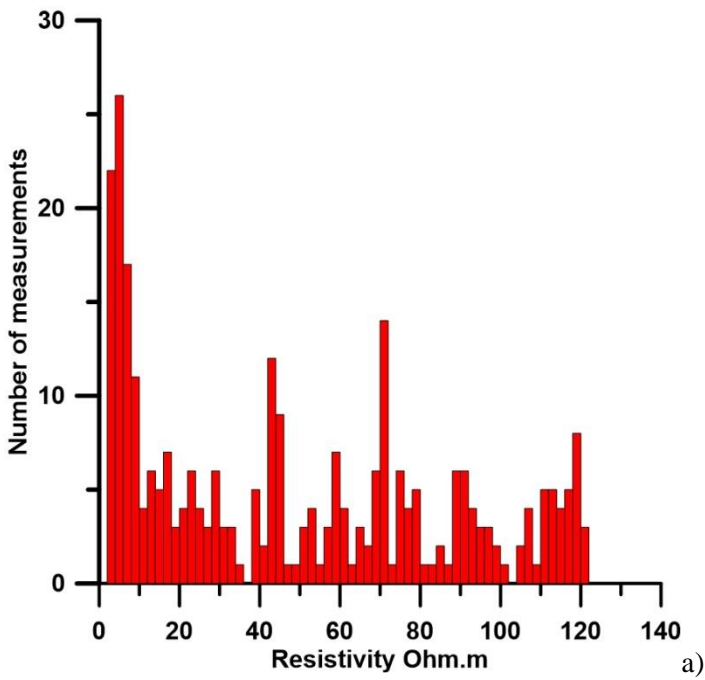
Fig. (4): Statistical representation of the collected resistivity and IP data for profile 2; a) histogram of the resistivity data, b) histogram of the IP data, c) Box plot for both data.

Table 5: summary of data statistics for profile 5.

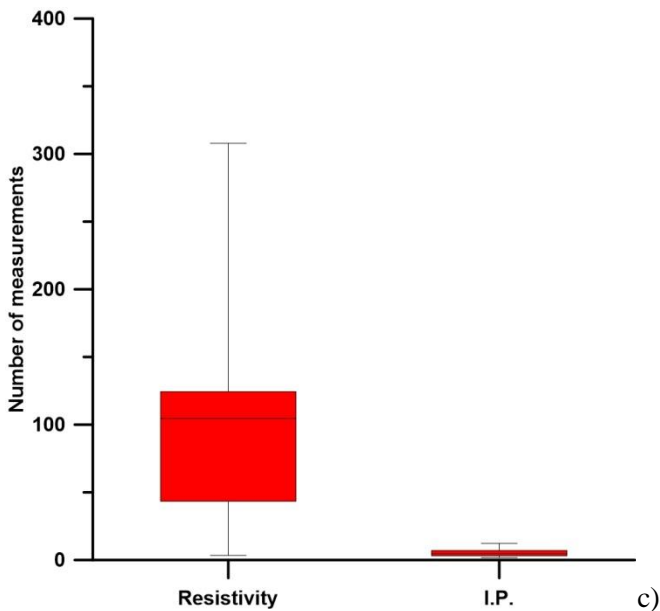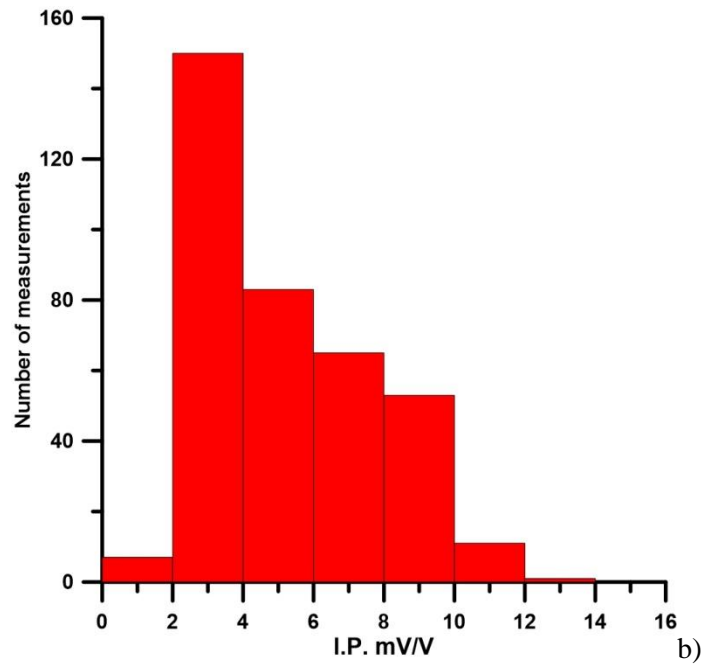| P5	Resistivity (Ωm)	IP (mV/V)
Number of Values	370	370
Minimum	4.7	2.8
Maximum	334	14.7
Mean	65.9	8.1
Standard deviation	66.5	3.3

a)

b)

c)
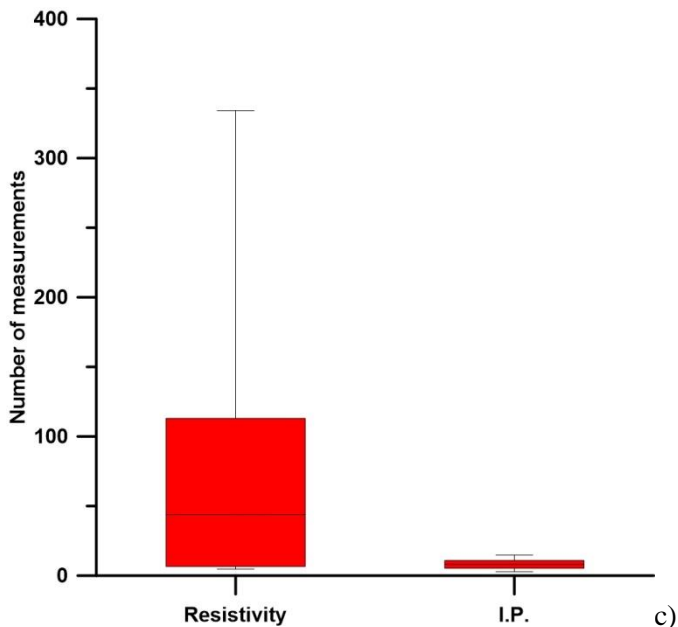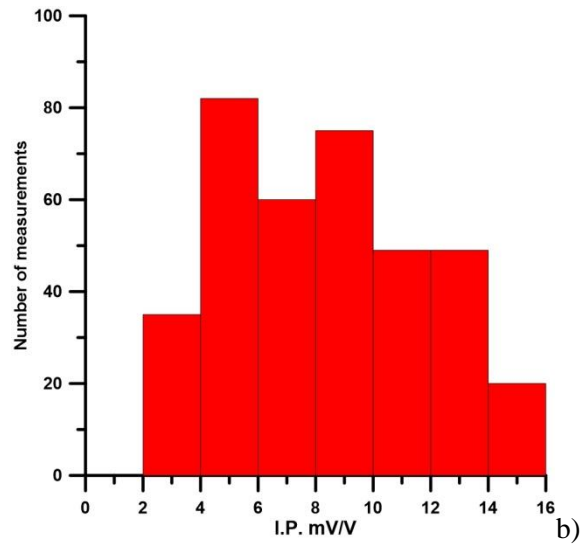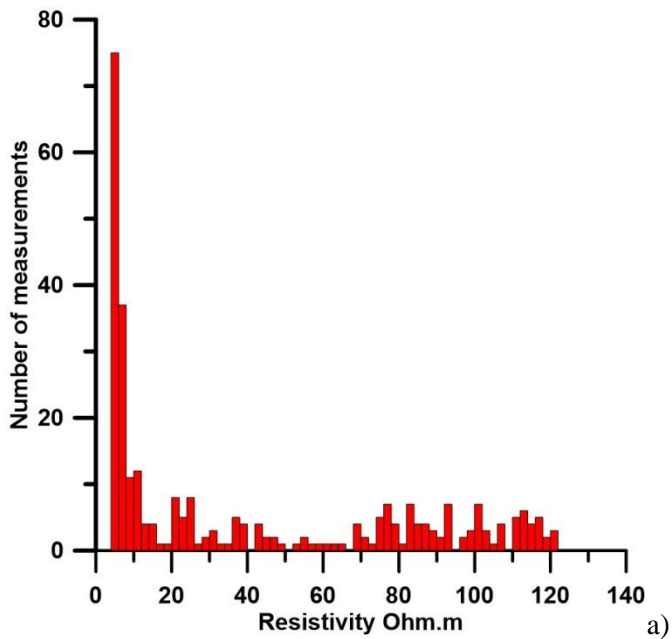
Fig. (5): Statistical representation of the collected resistivity and IP data for profile 2; a) histogram of the resistivity data, b) histogram of the IP data, c) Box plot for both data.

Table (6): summary of data statistics for profile 6.

| P6	Resistivity (Ωm)	IP (mV/V)
Number of Values	372	372
Minimum	3.9	2.15
Maximum	260.5	10.3
Mean	87.5	5.2
Standard deviation	56	2

a)

b)

c)
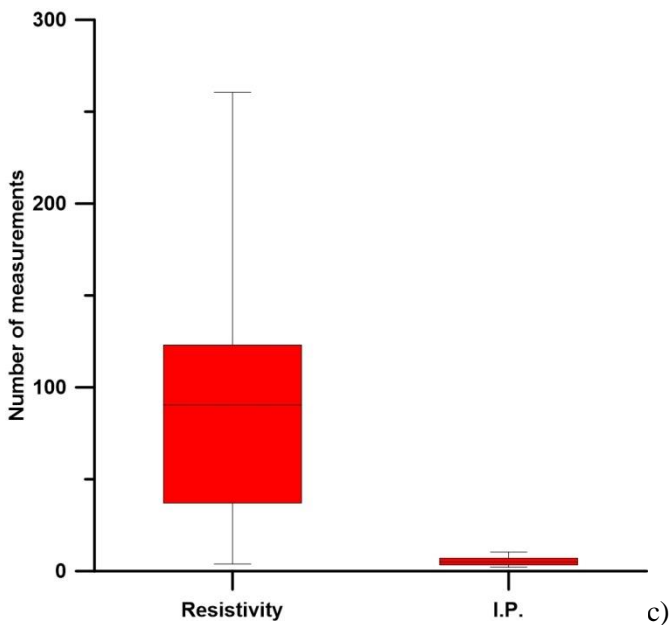
Fig. (6): Statistical representation of the collected resistivity and IP data for profile 2; a) histogram of the resistivity data, b) histogram of the IP data, c) Box plot for both data.

Table (7): summary of data statistics for profile 7.

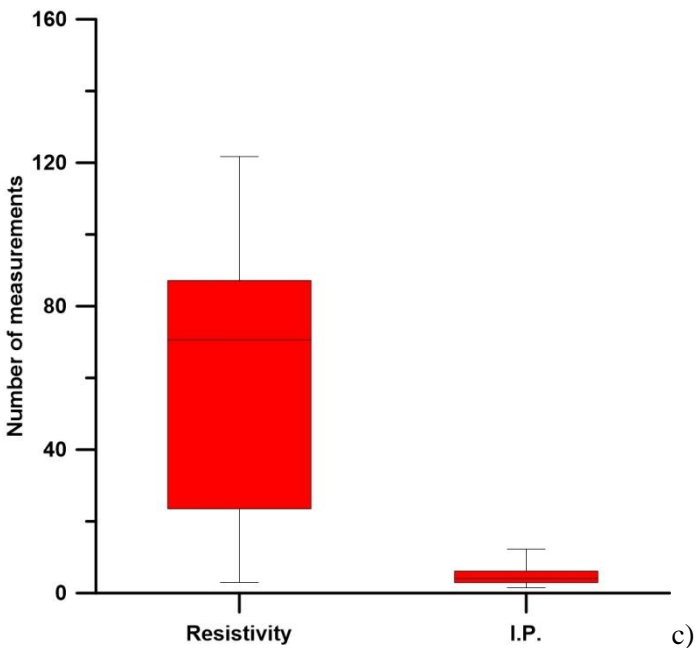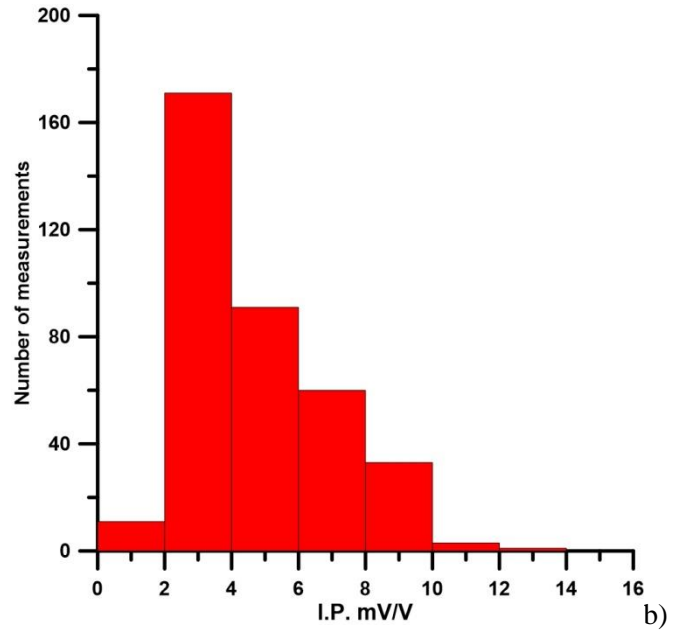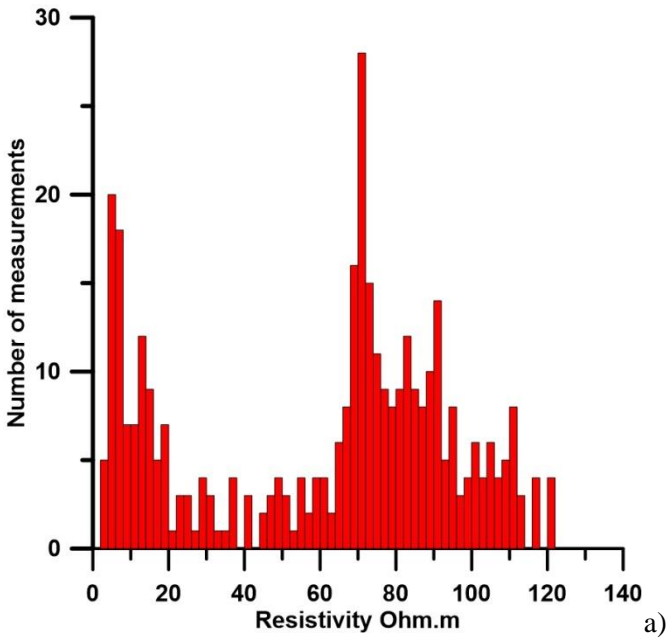| P7	Resistivity (Ωm)	IP (mV/V)
Number of Values	369	369
Minimum	4.1	2.2
Maximum	126.6	10.8
Mean	74.2	5.7
Standard deviation	36	1.8
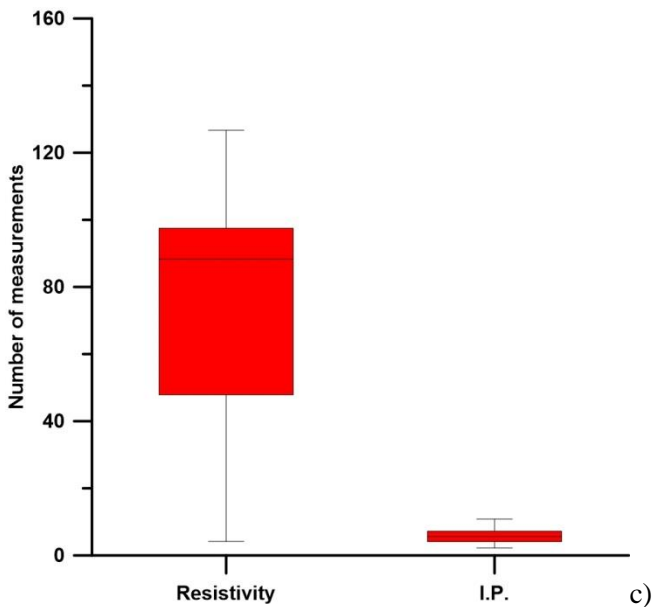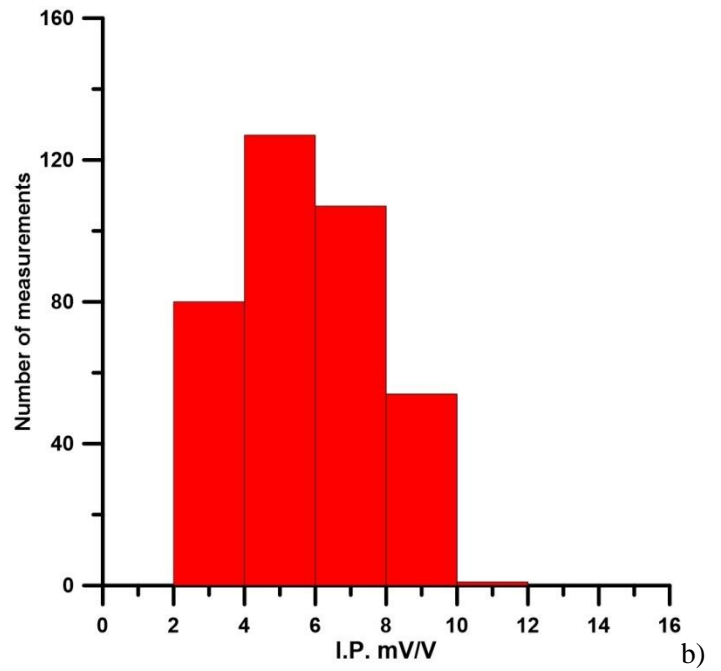
Fig. (7): Statistical representation of the collected resistivity and IP data for profile 2; a) histogram of the resistivity data, b) histogram of the IP data, c) Box plot for both data.

Table (8): summary of data statistics for profile 8.

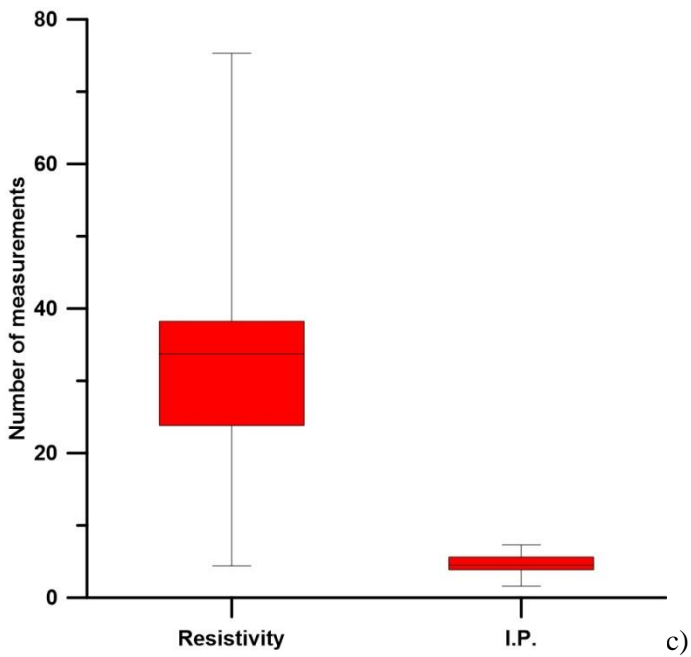| P8	Resistivity (Ωm)	IP (mV/V)
Number of Values	370	370
Minimum	3.4	1.7
Maximum	307.8	12.2
Mean	92.5	5.2
Standard deviation	61.1	2.4
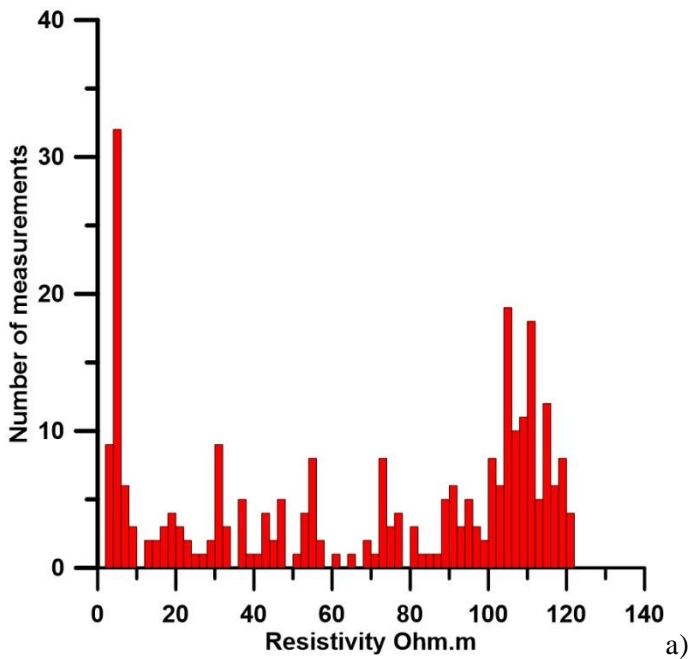
Fig. (8): Statistical representation of the collected resistivity and IP data for profile 2; a) histogram of the resistivity data, b) histogram of the IP data, c) Box plot for both data.

Table (9): summary of data statistics for profile 9.

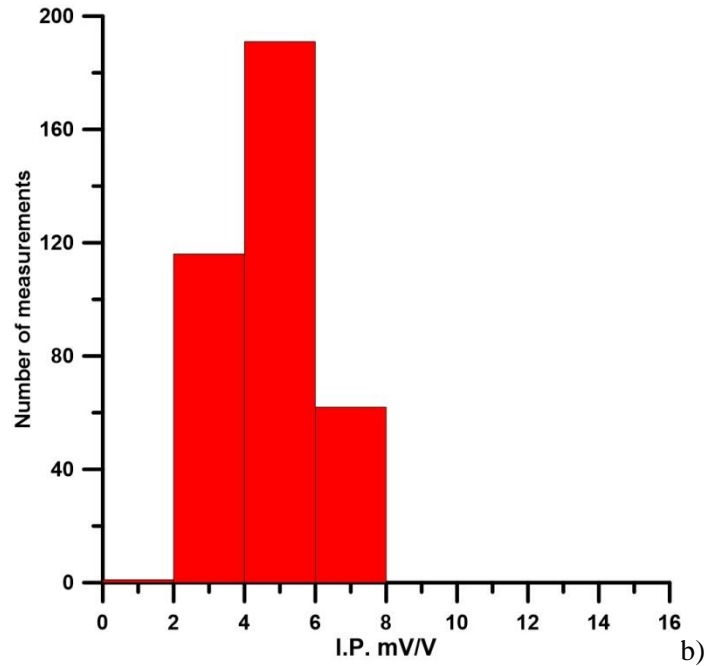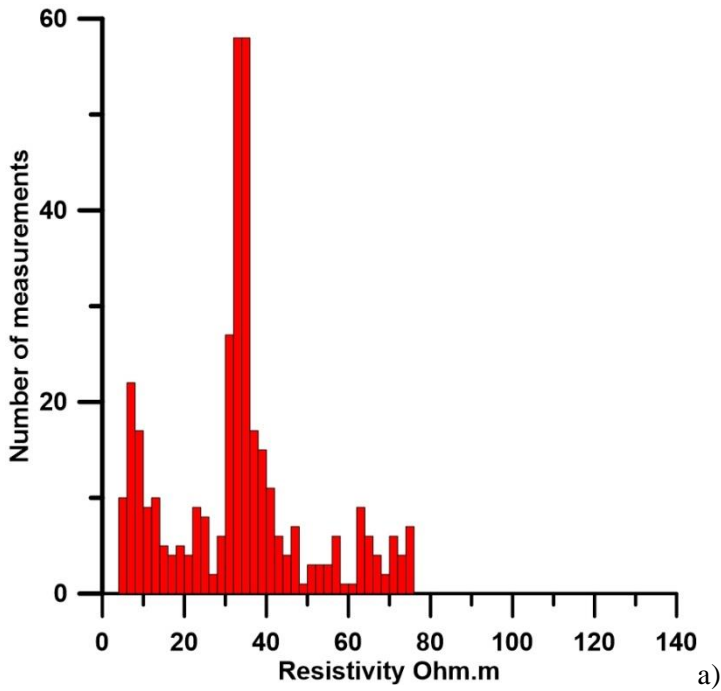| P9	Resistivity (Ωm)	IP (mV/V)
Number of Values	370	370
Minimum	3	1.4
Maximum	121.7	12.3
Mean	61	4.6
Standard deviation	34.6	2.1

a)

b)

c)

Fig. (9): Statistical representation of the collected resistivity and IP data for profile 2; a) histogram of the resistivity data, b) histogram of the IP data, c) Box plot for both data.

Table (10): summary of data statistics for profile 10.

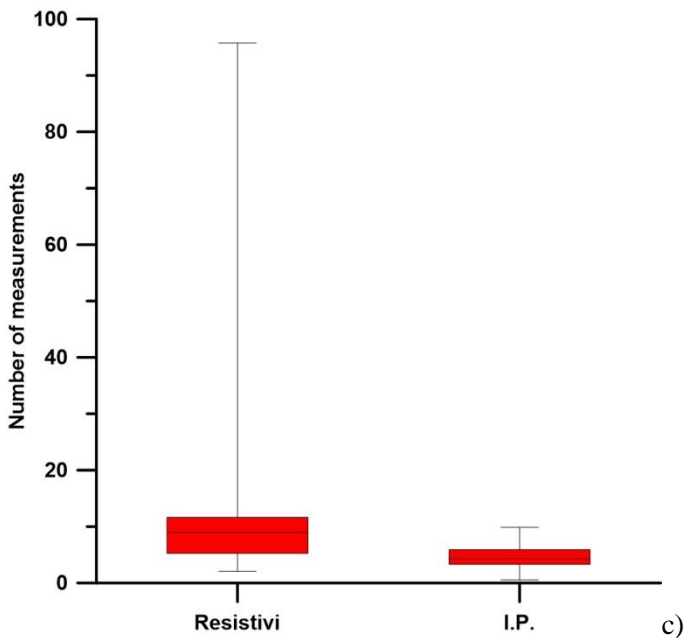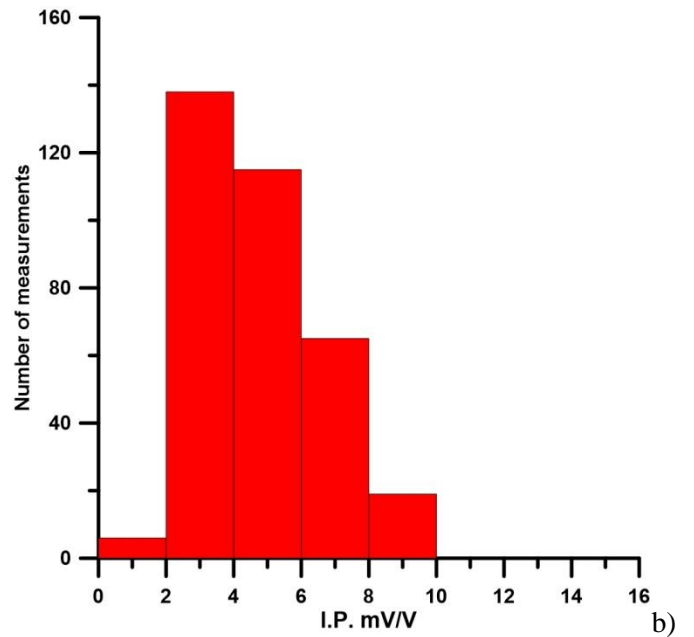| P10	Resistivity (Ωm)	IP (mV/V)
Number of Values	370	370
Minimum	4.3	1.6
Maximum	75.3	7.3
Mean	33.3	4.7
Standard deviation	17.1	1

Fig. (10): Statistical representation of the collected resistivity and IP data for profile 2; a) histogram of the resistivity data, b) histogram of the IP data, c) Box plot for both data.

Table (10): summary of data statistics for profile 11.

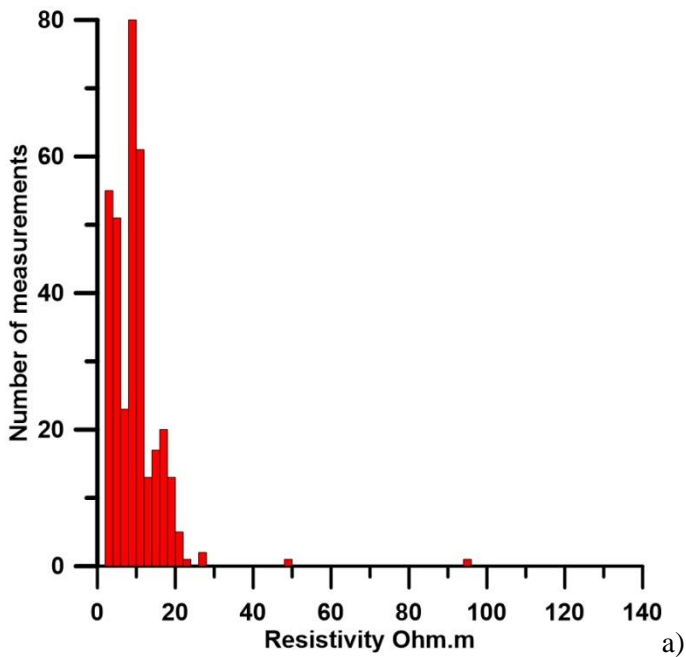| P11	Resistivity (Ωm)	IP (mV/V)
Number of Values	370	370
Minimum	2.08	0.5
Maximum	95.74	9.8
Mean	9.6	4.7
Standard deviation	17.1	1

Fig. (11): Statistical representation of the collected resistivity and IP data for profile 2; a) histogram of the resistivity data, b) histogram of the IP data, c) Box plot for both data.